UNIVERSIDAD MICHOACANA DE SAN NICOLÁS DE HIDALGO

INSTITUTO DE FÍSICA Y MATEMÁTICAS

Relativistic Kinetic Theory with Applications in Astrophysics.

Tesis

que para obtener el título de

Doctor en Ciencias en el área de Física

Presenta:

Paola Carolina Rioseco Yáñez

Bajo la asesoría de:

Dr. Olivier Charles-Albert Sarbach

Instituto de Física y Matemáticas, UMSNH

Morelia, Michoacán. Febrero de 2019.

To the memory of my parents.

Acknowledgements

First, I would like to express my sincere gratitude to my advisor Olivier Sarbach for his patience and guidance, who during my stay in Mexico has constantly supported and encouraged me with the research including during the completion of this thesis. I thank him for supporting me in the attendance of conferences and meetings, and encouraging me to work harder, as well as for the infinite corrections to improve the language in use during the writing of manuscripts.

I would also like to thank the remainder of the members of my thesis committee thesis Francisco Astorga, Ulises Nucamendi, Darío Núñez and Thomas Zannias for their support and comments about my research and thesis.

Next, I want to thank Luis Lehner for supporting me during my research stay in autumn 2018, as those many discussions on physics we had motivated me for doing research. Also, I convey my gratitude to the staff and faculty at Perimeter Institute for Theoretical Physics (PI).

Moreover, I thank Håkan Andréasson and David Fajman for their hospitality during my visit to Chalmers University of Technology and University of Vienna and Jéremié Joudioux and the Erwin Schrödinger International Institute for Mathematics and Physics for support to participate in the workshop *Geometric Transport Equations in General Relativity* (February 2017).

I also thank Yuri Bonder, Juan Carlos Degollado, Ana Laura García, Tanja Hinderer, Claudia Moreno, Darío Núñez, Oscar Reula and Roberto Sussman for their interest in my research and useful comments regarding my work. At the Institute for Physics and Mathematics I am grateful to Adnan Bashir, Ulises Nucamendi, Christian Schubert for advice and fruitful discussions about physics, and to Alejandra Ayala and Esperanza Jaramillo for being remarkably helpful in bureaucratic matters.

For their moral support and friendship, I would like to thank James Edwards (especially during my research and applications for postdoctoral posi-

tions), Rubén Cardenas and Gabriela García. From Chile, thanks go to Elvira Benites and Fabrizzio Merello for their patience and great support to Hanne Van Den Bosch for many discussions about physics and to M.J Gúzman for supporting me.

During my PhD I obtained financial support from CONACyT, from the thematic Network "Agujeros Negros y Ondas Gravitatorias" and from PI for a research stay during fall 2018.

Paola Rioseco.

February, 2019

Contents

Abstract

This thesis is based on a description of processes of accretion of matter towards black holes. The matter model that is used is a relativistic kinetic gas, which is based on a description through the one-particle distribution function on the phase space and whose dynamics is given by the relativistic Liouville equation (i.e. the collisionless Boltzmann equation). We formulate the kinetic theory mathematically on the cotangent bundle of the spacetime manifold. Then, we focus on solving the Liouville equation over a fixed spacetime without any assumptions about the symmetries on the distribution of gas particles. To solve it, we use tools from the theory of integrable Hamiltonian systems; thanks to these tools we are able to solve the problem by trivializing the Liouville vector field by expressing it in terms of action-angle variables. This allows us to find the most general solution that describes a distribution of collisionless particles over this geometry.

For accretion models where the matter falls into a Schwarzschild black hole, we calculate the physical observables such as the current density and energy-momentum tensor. For the particular case of a distribution that is spherically symmetric and static, assuming that at infinity it corresponds to a distribution in thermodynamic equilibrium, the accretion rate in the low temperature limit is computed and shown to coincide with the value found previously through a Newtonian approximation by Shapiro and Teukolsky. However, with our work we obtain more details about the gas' behavior from the analysis of the principal pressures at the horizon. We find that the radial pressure is about ten times smaller than the tangential one, providing a partial explanation for the low accretion rate in those models. Furthermore, we obtain a stability result where we consider an arbitrary initial condition (i.e. without symmetry assumptions) whose distribution in the asymptotic region depends only on energy. We show that the time evolution of this distribution function relaxes to a steady-state, spherically symmetric configuration.

In the second part of this thesis work, we describe disk-like configurations, consisting of bound trajectories confined to the equatorial plane of a Kerr black hole. Interestingly, in this case the configuration still undergoes a relaxation in time, even though collisions are neglected. In fact, we prove a theorem showing that (in a certain mathematical sense made precise in this work) the gas cloud converges in time to a stationary and axisymmetric configuration. The underlying mechanism for this process is phase space mixing, which implies that although the distribution is quasi-periodic in time, the physical observables (computed from averages over f) converge in time. Further, we find that the final state of the gas is described by an effective distribution function that only depends on the constants of motion, which is determined from an appropriate average over the initial distribution function.

Keywords:

Relativistic Kinetic Theory, Cotangent Bundle, Mixing phenomenon,
Accretion, Black Hole.

Resumen

Esta tesis se basa en una descripción de procesos de acreción de materia hacia agujeros negros. El modelo de materia que se utiliza es conocido como teoría cinética relativista de los gases, la cual se basa en una descripción a través de una función de distribución de una partícula en el espacio de fase y cuya dinámica está dada por la ecuacioón de Liouville relativista (Boltzmann sin colisiones). Nosotros formularemos matemáticamente la teoría cinética sobre el espacio cotangente asociado a la variedad. Luego, nos enfocamos en resolver la ecuación de Liouville sobre un espacio tiempo fijo sin asumir ninguna simetría sobre la distribución del gas. Para resolverla usamos herramientas provenientes de los sistemas Hamiltonianos integrables, gracias a lo cual, se logra trivializar el campo vectorial de Liouville descrito en términos de las variables de acción-angulo y con ello se encuentra la solución más general que describe a una distribución de partículas sobre esta geometría.

En el caso de un modelo de acreción donde la materia cae hacia un agujero negro tipo Schwarzschild, nosotros calculamos los observables fisicos como la corriente y el tensor de energía impulso. A partir de esto y asumiendo que la distribución es esfericamente simétrica y estática, además que en el infinito, la distribución corresponde a una distribución en equilibrio termodiámico, se reprodujo el valor para la tasa de acreción en el límite de temperaturas bajas, la cual coincide con valores conocidos previamente a partir de calculos basados en la teoría Newtoniana discutidos por Shapiro y Teukolsky. Sin embargo, en nuestro trabajo podemos obtener mas detalles sobre el comportamiento del gas a partir del análisis de las presiones principales en el horizonte. Nosotros, encontramos que la presión radial es cerca de diez veces mas pequeña que la presión radial, lo cual da una explicación parcial a la baja tasa de acreción en estos modelos. Además obtuvimos un resultado de estabilidad, donde se considera un dato inicial arbitrario (sin asumir simetrias) y una distribución que solo depende de la energía en la región asintótica. Nosotros mostramos que la evolución temporal de esta distribución se relaja a una configuración estacionaria y esféricamente simétrica.

En la segunda parte de este trabajo, describimos una configuración tipo disco, que consiste en trayectorias acotadas confinadas en el plano ecuatorial del agujero negro de Kerr. Curiosamente, en este caso la configuración de gas experimenta un proceso de relajación en el tiempo, aunque no se consideren colisiones entre las partículas. En concreto, nosotros demostramos (de manera mas precisa en la formulación matemática de este trabajo) mediante un teorema que la nube de gas converge en el tiempo a una configuración estacionaria y axial-simétrica. Detrás de este proceso de relajación, existe un mecanismo conocido como el fenómeno de mezcla, que tiene lugar en el espacio de fase

el cual implica que aunque la función de distribución de una partícula es dependiente del tiempo, los observables a nivel macroscópico (pueden obtenerse a través de promedios sobre la función de distribución f) convergen en el tiempo. Entonces, nosotros encontramos que el estado final del gas está descrito por una función de distribución efectiva la cual solo depende de las constantes de movimiento del sistema, y el cual está determinado a partir de un apropiado promedio sobre la función de distribución inicial.

Palabras claves:

Teoría Cinética Relativista, Espacio cotangente, Acreción, fenómeno de mezcla, Agujeros Negros.

Part I

Introduction

Chapter 1

Motivation

This thesis is based upon two papers that show the applications of a collisionless relativistic kinetic gas over a fixed black hole spacetime background in accretion models.

Kinetic theory is used for modeling the time evolution of a set of particles through the Boltzmann equation under the assumption that the gas is sufficiently diluted such that the molecular chaos hypothesis is justified. There are several regimes of kinetic theory that can be considered, depending on the physical situation at hand, collisions might be relevant (for example, in the hydrodynamic limit) or may be neglected (such as in Landau-damping of plasmas, or in a galaxy), in which case it is sufficient to solve the Liouville equation (i.e. the Boltzmann equation without the collision term). Kinetic theory can also be described from the Newtonian point of view [1], (when the gravitational field is weak and most of the gas particles have velocities much smaller than the speed of light), from special relativistic point of view [2] (weak gravitational field and large velocities), or from a fully (general) relativistic point of view [3] (presence of strong gravitational fields and curvature, such as in the vicinity of a black hole or in the very early universe). At the microscopic level, kinetic theory can describe different objects, such as atoms, electrons in a plasma or ions of a neutral gas. Alternatively, from a galactic dynamics point of view, the particles can be considered to be stars, galaxies or clusters of galaxies, depending on the physical situation under consideration, see for example the book [4]. Finally, the gas particle could be modeled as classical particles or quantum particles, depending on the relation between the mean free path and the de Broglie wave length of the particles.

The time evolution of the distribution function depends on the physical interaction. For example, in the case where the particles collide at high speed on a flat spacetime, the dynamics is given by the special relativistic Boltzmann equation. If the particles have electric charge (i.e. electrons or ions) and their collisions can be neglected, the evolution is described by the Maxwell-Vlasov

system of equation. In galactic dynamics or cosmological scenario, the evolution of stars or galaxies can be described by the Einstein-Liouville equation. In addition, several effects can overlap, e.g. the description of a set of charged particles around a black hole, in which case their dynamical evolution is governed by the Einstein-Maxwell-Liouville system.

Solving these types of systems can be very complicated. In particular, this is the case where we consider strong gravity scenarios, in which case the Einstein-Liouville system must be solved. Some of the strategies to solve this system are based on symmetry assumptions to reduce the system to a lower-dimensional one, based on perturbative schemes, on numerical methods or a combination of these strategies. See for instance [5, 6, 7, 8] for numerical work with various symmetry assumptions for solving these kinds of systems. For a recent review about the current state of the art for solving the Einstein-Liouville system see [9], and for examples where solutions are presented based on assumptions like staticity, see for instance [10, 11, 12, 13, 5], or where is included the charge of particles in the system solving Einstein-Maxwell-Vlasov with additional assumptions, see [14].

In this work, we focus on physical scenarios for which the self-gravity of the gas can be neglected in first-order approximation, such that we concentrate on solving the Liouville equation over a fixed black hole geometry. Although the influence of back reaction in this work is not studied, we are interested in extending our work to examples where self-gravity is included, such as in stability problems, or cosmic censorship. The main achievement in this work is to solve the Liouville equation (collisionless) over a fixed and strongly curved spacetime background, for which we will introduce analytical tools based on action-angle variables in terms of which the Liouville equation can be solved analytically.

Our work is partially motivated from recent and future observations [15] of supermassive black holes at the center of galaxies (such as the $SgrA^*$ or $M87$), at scales smaller than their gravitational radius. These observations requiere more specific models to describe the plasma and matter that is presented in the neighborhood of black holes. There exists a broad spectrum of black hole accretion models in the literature [16], based on hydrodynamics see for instance [17] review. We are interested in modeling accretion processes with relativistic kinetic theory, and see if this model can offer some advantage with respect to others models of matter. In particular, we focus on understanding accretion rates in the case that matter is absorbed by a black hole and compare this with the known results in the book by Shapiro and Teukolsky [16]. In the case of disk configurations, we are interested the dynamical behavior of matter for large times.

Other potential applications of our study to astrophysics are related to the description of distribution of stars around supermassive black holes [18], and for modeling of dark matter inhomogeneities (see [19] for a treatment based on

N-body simulations and [20] for a direct simulation of the Vlasov equation in the newtonian limit).

Chapter 2

Summary of main results

In this section, we provide a brief summary of the main results of this thesis. More details will be provided in subsequent sections, starting with some examples about a mathematical description on the cotangent bundle in Chapter 3, continuing with a perturbative description of the Einstein-Liouville system in Chapter. 4 and analytic tools from the Hamiltonian formalism in Chapter 5. Finally, in the last Chapter 6 of this introduction some examples and applications of the main results related to Papers I and II appended will be presented.

In Paper I, we assume that the relativistic kinetic gas is sufficiently diluted, such that its self-gravity can be neglected. We assume that the black hole is stationary and described by a Kerr black hole family of solutions that are characterized by their mass and total angular momentum[1]. However, for simplicity we assume that the rotation is zero in this first work. With this, the space-time background is Schwarzschild. In addition, as was mentioned before, we assume in the entire thesis that the gas is collisionless. Therefore, the gas in our model is described by a one-particle distribution function that satisfies the Liouville equation on the Schwarzschild geometry.

In a first step we find the most general solution of the distribution function that solves the Liouville equation. Here, we use ideas from the theory of integrable Hamiltonian systems that are described in Chapter 5. We compute the space-time observables in horizon penetrating coordinates such that the physical quantities measured on the horizon cannot diverge due to a bad choice of the coordinates. Likewise, in the case of particles that fall in the black hole, we discriminate between the trajectories of the particles, eliminating from our analysis the case of bound trajectories, which is not relevant for the calculation of observables on the horizon. Although the space-time has symmetries (spherically symmetric and static), this does not mean that the distribution of kinetic gas particles needs to inherit them. In particular, we find the most general solution

[1]Due to the assumption of vacuum and stationarity, one may invoke the no-hair theorem to calculate that the black hole is described by the Kerr family, see for instance [21]

of the Liouville equation without symmetry assumption. Hence, the corresponding gas configuration is, in general, non-spherical and time-dependent.

To analyze its physical contents, we start with a distribution assumed to be both spherically and static. In the asymptotic region, we assume the presence of a reservoir of particles at some specific temperature T, such that the distribution is assumed to be isotropic and in thermodynamic equilibrium, finding explicitly the accretion and compression rates of the gas in the limit of low temperatures ($k_B T \ll mc^2$ is much smaller than the rest energy mc^2). We found that our result agrees with the corresponding Newtonian calculation [16]. Nevertheless, a relevant new result found in Paper I are the values on the horizon for the radial and tangential pressures; in particular, we found that the radial pressure is around 10 times smaller than the tangential pressure, giving a possible explanation to the fact that the accretion rate for a collisionless gas is much smaller compared to the Bondi-Michel accretion in the hydrodynamic case of an isotropic perfect fluid, see [16].

Finally, Paper I presents an analysis on the nonlinear stability of the static and spherically symmetric solution. To this end, the symmetry assumption on the distribution function is relaxed, and initial conditions for the distribution function on a constant time slice are specified (this initial distribution function is not required to be spherically symmetric). The essential hypothesis is that the initial distribution function is bound by an equilibrium distribution function and secondly that in the asymptotic region it converges to some function $f_\infty(E)$ that depend only on the energy E of the particles. With these assumptions, we prove that outside of the horizon the observables converge along the world line of static observers to the corresponding observables associated with the stationary spherical flow described by $f_\infty(E)$. The physical explanation of this stability result is that almost all the gas particles disperse or fall into a black hole such that after an infinite time only the particles that come from the reservoir in the asymptotic region described by $f_\infty(E)$ are seen by the observer.

In the second paper, Paper II [22], we focus our research on studying the mixing phenomenon. The mixing phenomenon appears in a collisionless system of kinetic gas particles[2] and can be roughly described as a "relaxation in time of certain observables" in which the properties of the phase flow induce a homogenization and stretching of the distribution function in phase space. Phase space mixing transfers the energy contribution from each nonzero spatial frequency to large velocity frequencies implying that, in frequency space, the distribution function decays rapidly to its zero spatial frequency contribution. This implies that observables such as the current and the energy-momentum tensor (i.e. the outcome of integrating the distribution function over a test function) converge in time to the corresponding quantity with zero spatial frequency.

[2]The mixing phenomenon will be presented in Section 6.2, based on a simple one-dimensional Newtonian model, and will be extended to the relativistic case in Paper II.

Phase space mixing plays an important role in different areas of physics, including galactic dynamics, plasma physics and in quantum physics. In the context of galactic dynamics, phase space mixing was introduced by Lynden-Bell (1967) in the articles [23, 24, 25]. The phase space mixing acts as a mechanism responsible for carrying the one-particle distribution function that describes certain configuration (e.g. stellar distribution on a galaxy) to a state where the gas configuration relaxes to a configuration that only depends on the conserved quantities. Here, one refers to the final state as the "relaxed" state or equilibrium state, which is very different to a state of "thermodynamic equilibrium" (which is driven by the collisions of the particles, whereas for phase space mixing collisions are not taken into account) see [26, 27] for more details. In the context of plasma physics, mixing is the mechanism underlying "Landau damping", the relaxation of a charged collisionless gas to a homogenous configuration. In 2012 the work of the mathematicians Mouhot and Villani (2012) [28] gave a rigorous proof of this phenomenon in a Newtonian setting. Mouhot and Villani's proof shows that mixing occurs in the full nonlinear coupled Vlasov-Poisson system, describing a configuration of charged particles in a box with periodic boundary conditions. For generalizations to special relativistic plasmas, see [29, 30]. For results in other areas, such as quantum physics, particularly for Bose-Einstein condensates, see e.g. [31].

In the scenario considered in Paper II, we focus on a relativistic kinetic gas whose particles follow bound trajectories confined to the equatorial plane of Kerr black hole, thus considering the complementary sector of paper I, where only unbound trajectories were considered. Therefore, we now shift the focus on the behavior of a relativistic kinetic gas forming a disk (thin or thick)[3], and find the final state of the gas configuration. Therefore the situation considered assumes that the particles of the relativistic kinetic gas are trapped in the equatorial plane of the Kerr black hole potential that constitute a thin disk where its self-gravity can be neglected and where there is no influence of electro-magnetics fields. In this setting, we extend the mixing ideas[4] for a collisionless relativistic kinetic gas configuration and analyze the effects of the phase mixing on the dynamical behavior of observables.

To analyze this scenario, we proceed as follow. First, using techniques of Hamiltonian dynamics we find the action-angle variable representation for the Liouville equation, over the Kerr background. The action-angle variables can be analytically represented using elliptic integrals. Through these variables, we trivialize the Liouville vector field and find the solution for the most general solution that describes the collisionless relativistic kinetic gas of a thin disk in a Kerr geometry. By means of this solution for the distribution we compute the current density, and we show that the particle density measured by a sta-

[3]Paper II only discusses "thin" disk configuration, where all the gas particles are confined to the equatorial plane. A future paper will address the more general case of thick disk.

[4]Through the formulation of a theorem and by numerical examples.

tionary observer (fixed spatial point, i.e. one that follows a Killing trajectory), converges in time to a constant value. Here we give an intuitive explanation for this convergence capturing the behavior of the distribution function on a cut of the phase space where we can observe that the distribution stretches in time over the phase space, illustrating the mixing idea (see figure 5 in Paper II).

In addition, we formulate rigorously the mathematical theorem for the mixing property in this specific case. To do this, we define a generic observable denoted by N_φ, which is obtained by integrating the distribution function multiplied with a test function φ over the relativistic phase space. Here the time behavior of the observable is obtained by the transport of the test function φ along the flow generated by the time translation symmetry of the spacetime. We formulate a theorem showing that under a certain determinant condition on the support of φ, the time translated observable N_{φ_t} converges when $t \to \infty$ to the same observable with the distribution f replaced by the initial distribution function which is averaged over the angle variables. Using this theorem, we are able to predict the final state of the gas configuration. We also explore the validity of the determinant condition that allows the theorem to be applied and we analyze a couple of examples about distributions of special orbits including those where the determinant conditions is violated, and show that mixing occurs in all cases considered. The main application of the theorem is that the gas relaxes in time to a stationary, axisymmetric configuration described by a distribution function depending only on constants of motion. Our numerical examples reveal that this relaxation process is quite fast, taking only a few thousands light-crossing times corresponding to the gravitational radius.

Chapter 3

A brief mathematical description of relativistic kinetic theory on the cotangent bundle.

In our work, the relativistic Boltzmann equation is solved in the collisionless case on a fixed geometry. In that case it is relevant to study both the geometrical and mathematical structure that describe the dynamical behavior of the kinetic gas. In our case we use the formalism on the cotangent bundle that is useful for a Hamiltonian description. For an equivalent description formulated on the tangent bundle, see [32] and [33], and reference therein.

This Chapter offers an overview of the following topics: first in Section 3.1 presents a formal geometric description of the relativistic Liouville equation. Next, in the Section 3.2 we introduce the Sasaki metric on the cotangent bundle. With this metric, we define in Section 3.3 the volume form induced on the cotangent bundle, and finally in subsection 3.4 is presented the definition of observables on the cotangent bundle.

A simple kinetic gas consists of a set of identical particles with rest mass m, assumed to be positive. For the definitions we assume that the manifold $(\mathcal{M}, g)$ is C^∞ Lorentz manifold of dimension $n = 4$ with signature convention $(-1, 1, 1, 1)$, following we denote by ∇ the associated Levi-Civita connection.

The kinetic gas particles will be described by a one-particle distribution function f where $f : \Gamma \to \mathbb{R}$, is a function on the phase space, which is a certain

subset of the cotangent bundle. $T^*\mathcal{M}$ is defined as

$$T^*\mathcal{M} := \{(x,p) : x \in \mathcal{M} \wedge p \in T^*_x\mathcal{M}\}^1. \tag{3.1}$$

$T^*\mathcal{M}$ is a 8-dimensional orientable manifold, see Paper I for the sketch of a proof. Thus the elements of $T^*\mathcal{M}$ consist of points (x,p), where x is an event and p any covector at this event (playing the role of the canonical momentum of the particle).

For the following we use the fact that $T^*\mathcal{M}$ can be locally described by *adapted local coordinates* (x^μ, p_μ), where x^μ are local coordinates over $\mathcal{M}$, and $p \in T^*_x\mathcal{M}$ is expanded in terms of the basis dx^μ_x, $\mu = 0 \ldots 3$.

Define the subspace $\Gamma := \{(x,p) \in T^*\mathcal{M} : g^{-1}(p) \quad future \quad directed.\}$ Due to the fact that the gas particles have fixed mass $m > 0$, their momentum p satisfy $g^{-1}(p,p) = -m^2$, and hence we restrict ourselves to the mass shell, defined as follows.

$$\Gamma_m := \{(x,p) \in T^*\mathcal{M} : g_x^{-1}(p,p) = -m^2, \quad g^{-1}p \quad future \quad directed\}. \tag{3.2}$$

Γ_m plays the role of the relativistic phase space, 7-dim.

3.1 Symplectic structure and Liouville vector field.

In this section we define different structures will allow us to define the Liouville vector field

Proyection Map: π where $\pi : \ T^*\mathcal{M} \to \mathcal{M}, \quad (x,p) \mapsto x$, that projects points over the cotangent bundle $T^*\mathcal{M}$ on $\mathcal{M}$ and let the "push forward" of π (the differential map) at the point (x,p) be the map

$$\pi_{*(x,p)} = d\pi_{(x,p)} : T_{(x,p)}(T^*\mathcal{M}) \to T_x\mathcal{M},$$

that carries tangent vectors defined on the tangent space of the manifold $T^*\mathcal{M}$ to the tangent plane on $\mathcal{M}$, defined in the following invariant way:

$$\pi_{*(x,p)}(Z)(h) = \left. Z[h \circ \pi]\right|_{(x,p)},$$

with the function $h : \mathcal{M} \to \mathbb{R}$ and the tangent vector and the tangent vector $Z \in T^*_{(x,p)}(T^*\mathcal{M})$. In terms of adapted local coordinates,

$$Z_{(x,p)} = \left. X^\mu \frac{\partial}{\partial x^\mu}\right|_{(x,p)} + \left. Y_\lambda \frac{\partial}{\partial p_\lambda}\right|_{(x,p)}, \tag{3.3}$$

we have

$$\pi_{*(x,p)}(Z) = \left. X^\mu_{(x,p)} \frac{\partial}{\partial x^\mu}\right|_x \in T_x\mathcal{M}.$$

[1] Assuming too that $\mathcal{M}$ have associated a Levi-civita connection, ∇

Next, we define the **Poincaré one-form** as one-form Θ on T^*M which map a tangent vector $Z_{(x,p)} \in T_{(x,p)}(T^*\mathcal{M})$ at $(x,p) \in T^*_x\mathcal{M}$ on

$$\Theta_{(x,p)}\left(Z_{(x,p)}\right) := p\left(\pi_{*(x,p)}\left(Z_{(x,p)}\right)\right) \in \mathbb{R}, \tag{3.4}$$

that is, it takes a vector defined in the tangent space of the manifold $T^*\mathcal{M}$ and turns it into a real. This map is linear; hence Θ defines a one form over $T^*\mathcal{M}$. In terms of *adapted local coordinates* using 3.3, we have

$$\Theta_{(x,p)}\left(Z_{(x,p)}\right) = p\left(X^\mu \frac{\partial}{\partial x^\mu}\bigg|_x\right) = X^\mu p_\mu = p_\mu dx^\mu_{(x,p)}\left(Z_{(x,p)}\right). \tag{3.5}$$

Therefore, the Poincaré one-form in terms of these coordinates reads

$$\Theta_{(x,p)} = p_\mu dx^\mu_{(x,p)}. \tag{3.6}$$

The next object to define is the **symplectic form** $\Omega_{(x,p)} : T_{(x,p)}(T^*\mathcal{M}) \times T_{(x,p)}(T^*\mathcal{M}) \to \mathbb{R}$, which is the differential of the Poincaré one-form. The symplectic form satisfies $\Omega_{(x,p)}(X,Y) = 0 \;\forall\; Y \in T_{(x,p)}(T^*\mathcal{M})$, implies that $X = 0, \quad X \in T_{(x,p)}(T^*\mathcal{M})$, which means that it is a bilinear, antisymmetric and non-degenerated form on $T^*\mathcal{M}$.
Explicitly, in *adapted local coordinates*, we obtain from (3.6),

$$\Omega = d\left(p_\mu dx^\mu\right) = dp_\mu \wedge dx^\mu \equiv dp_\mu \otimes dx^\mu - dx^\mu \otimes dp_\mu. \tag{3.7}$$

This symplectic structure allows us to assign to each smooth function $H : T^*\mathcal{M} \to \mathbb{R}$ known as the **Hamiltonian function** a vectorial field called the **associated Hamiltonian vector field** X_H through the differential $dH_{(x,p)} \in T^*_{(x,p)}(T^*M)$, such that

$$dH_{(x,p)} = \Omega_{(x,p)}\left(\cdot, X_H\right). \tag{3.8}$$

Explicitly, in *adapted local coordinates*, we can expand

$$dH = \frac{\partial H}{\partial x^\mu}dx^\mu + \frac{\partial H}{\partial p_\lambda}dp_\lambda, \quad X_H = X^\mu\frac{\partial}{\partial x^\mu} + Y_\mu\frac{\partial}{\partial p_\mu}, \tag{3.9}$$

where (X^μ, Y_μ) are the yet unknown components of X_H. To find them, we apply the definition (3.8) to an arbitrary vectorial field

$$Z = Z^\mu\frac{\partial}{\partial x^\mu} + W_\lambda\frac{\partial}{\partial p_\lambda}$$

and compute

$$dH(Z) = \Omega\left(Z, X_H\right) = \left(dp_\mu \otimes dx^\mu - dx^\mu \otimes dp_\mu\right)\left(Z, X_H\right).$$

Hence,

$$\frac{\partial H}{\partial x^\mu} Z^\mu + \frac{\partial H}{\partial p_\mu} W_\mu = X^\mu W_\mu - Y_\mu Z^\mu.$$

Comparing the coefficients, we find $X^\mu = \frac{\partial H}{\partial p_\mu}$ and $Y_\mu = -\frac{\partial H}{\partial x^\mu}$.
With this, finally, the Hamiltonian vector field X_H is

$$X_H = \frac{\partial H}{\partial p_\mu}\frac{\partial}{\partial x^\mu} - \frac{\partial H}{\partial x^\mu}\frac{\partial}{\partial p_\mu}. \tag{3.10}$$

Note that, the integral curves $\gamma(\lambda) = (x^\mu(\lambda), p_\mu(\lambda))$ to X_H, satisfy the Hamiltonian equations

$$\dot{x}^\mu(\lambda) = \frac{dx^\mu}{d\lambda}(\lambda) = \frac{\partial H}{\partial p_\mu}(\gamma(\lambda)), \tag{3.11}$$

$$\dot{p}_\mu(\lambda) = \frac{dp_\mu}{d\lambda}(\lambda) = -\frac{\partial H}{\partial x^\mu}(\gamma(\lambda)). \tag{3.12}$$

We define the **Poisson bracket**, between two smooth functions. $F, H : T^*\mathcal{M} \to \mathbb{R}$, as

$$\{F, H\} := \Omega(X_F, X_H) = -dF(X_H) = -\Omega(X_H, X_F) = dH(X_F). \tag{3.13}$$

In *adapted local coordinates*, using $X_H = \frac{\partial H}{\partial p_\mu}\frac{\partial}{\partial x^\mu} - \frac{\partial H}{\partial x^\mu}\frac{\partial}{\partial p_\mu}$ and X_F defined in the same way, we obtain

$$\begin{aligned}\{F, H\} = \Omega(X_F, X_H) &= (dp_\mu \wedge dx^\mu \equiv dp_\mu \otimes dx^\mu - dx^\mu \otimes dp_\mu)(X_F, X_H) \\ &= \frac{\partial F}{\partial p_\mu}\frac{\partial H}{\partial x^\mu} - \frac{\partial F}{\partial x^\mu}\frac{\partial H}{\partial p_\mu}.\end{aligned}$$

From Eq. (3.13), is easy to see that $\{F, H\} = 0$ if and only if, F is constant along the Hamiltonian flow, that is, if and only if F is a conserved quantity.

For the following, we focus on the Hamiltonian describing free-particle motion,

$$H(x, p) := \frac{1}{2} g_x^{-1}(p, p) = \frac{1}{2} g^{\mu\nu}(x) p_\mu p_\nu. \tag{3.14}$$

The associated Hamiltonian vector field is called the Liouville vector field, and we find $L := X_H = \{\cdot, H\}$. Where the explicit components of the Liouville vector field

$$\frac{\partial H}{\partial p_\mu} = g^{\mu\nu}(x) p_\nu, \qquad \frac{\partial H}{\partial x_\mu} = \frac{1}{2} p_\alpha p_\beta \frac{\partial g^{\alpha\beta}}{\partial x^\mu}.$$

Then we find that

$$L := g^{\mu\nu}(x) p_\nu \frac{\partial}{\partial x^\mu} - \frac{1}{2} p_\alpha p_\beta \frac{\partial g^{\alpha\beta}}{\partial x^\mu}\frac{\partial}{\partial p_\mu}. \tag{3.15}$$

Note that in this case the integral curves of X_H, when projected onto $\mathcal{M}$, describe geodesic motion, and hence in particular the trajectories of gas particles between collisions.

3.2 Sasaki metric on the cotangent bundle.

We want to define a volume form on the cotangent space to be able to integrate over $\mathcal{T}^*\mathcal{M}$, to do this we define a metric over the cotangent bundle named Sasaki metric. Sasaki metric $\hat{g}$ was introducing in [34] in the context of Riemannian geometries, so first applied to kinetic theory [35]. See [33] for more details on its role for the formulation of the general relativistic kinetic theory on the tangent bundle associated with the spacetime manifold.
The Sasaki metric is interesting because L is a geodesic vector field associated with the dynamics of the particles in $(T\mathcal{M}, \hat{g})$ [36]. This means that, such as a free particle on $\mathcal{M}$ follows geodesics on g, on the tangent bundle $T\mathcal{M}$ the dynamics of particles follow geodesics of $\hat{g}$ given by the flow of the Liouville vector field.

In order to introduce the Sasaki metric, we first define a decomposition on the cotangent bundle using the following subspaces.

The **Vertical subspace** $V_{(x,p)}$ in $T_{(x,p)}(T^*M)$ is defined as the set

$$V_{(x,p)} := \ker\left[\pi_{*(x,p)}\right] = \{Z \in T_{(x,p)}(T^*M) : \pi_{*(x,p)}(Z) = 0\}, \tag{3.16}$$

of Z vectors, whose projections on T_xM is zero, to find a basis for $\ker\left(V_{(x,p)}\right)$ we find the $\hat{Z}$ vectors such that $\pi_*(x,p)(\tilde{Z}) = X^\mu_{(x,p)} \frac{\partial}{\partial x^\mu}\Big|_{(x,p)} = 0$, so $\tilde{Z} = P_{\mu(x,p)} \frac{\partial}{\partial p_\mu}$ at each point (x,p) the vertical subspace $V_{(x,p)}$ is generated by the n basis vectors $\{\frac{\partial}{\partial p_\mu}\}$.

Next, we introduce a second subspace, the horizontal subspace $H_{(x,p)}$ of $T_{(x,p)}(T^*M)$ which is transverse to $V_{(x,p)}$. For this, we first introduce the **Connection map** K, induced by the Levi-civita connection ∇ on $\mathcal{M}$, defined as the linear map

$$K_{(x,p)} : T_{(x,p)}(T^*\mathcal{M}) \rightarrow T^*_x\mathcal{M} \tag{3.17}$$

$$Z \mapsto K_{(x,p)}(Z), \tag{3.18}$$

as follows: Let a $\gamma(\lambda) = (x(\lambda), P(\lambda))$ be a smooth curve on $T^*\mathcal{M}$ through (x,p) with the tangent vector $Z \in T_{(x,p)}(T^*\mathcal{M})$ at (x,p), such that $\gamma(0) = (x(0), P(0)) = (x,p)$ with tangent vector $\dot{\gamma}(0) = Z$. This curve $\gamma(\lambda) \in T^*\mathcal{M}$ defines another curve $x(\lambda) \in \mathcal{M}$ and a covector field $P(\lambda) \in T^*_x\mathcal{M}$ along it. We derive covariantly along the tangent vector $\dot{x}(0) = \dot{x}^i(0)\frac{\partial}{\partial x^i}$ the covector field $P(\lambda) = P_k(\lambda)dx^k\Big|_{x(\lambda)}$, the connection map is defined as

$$K_{(x,p)}(Z) := \nabla_{\dot{x}(0)} P(\lambda)\big|_x . \tag{3.19}$$

Calculated explicitly in terms of adapted local coordinates, one obtains

$$\begin{aligned} K_{(x,p)}(Z) &= \left[\dot{x}^\mu(\lambda)\left(\frac{\partial P_\alpha(\lambda)}{\partial x^\mu}\right)dx^\alpha + \dot{x}^\mu(\lambda)P_\alpha(\lambda)\left(\nabla_{\frac{\partial}{\partial x^\mu}}dx^\alpha\right)\right]\Big|_{\lambda=0} \\ &= \left(\dot{x}^\mu(\lambda)\left(\frac{\partial P_\alpha(\lambda)}{\partial x^\mu}\right)dx^\alpha - \dot{x}^\mu(\lambda)P_\alpha(\lambda)\Gamma^\alpha_{\mu\nu}dx^\nu\right)\Big|_{\lambda=0} \\ &= \left(\dot{P}_\nu(0) - \dot{x}^\mu(0)P_\alpha(0)\Gamma^\alpha_{\mu\nu}(x)\right)dx^\nu, \end{aligned} \tag{3.20}$$

such that

$$K_{(x,p)}(Z) = \{\dot{P}_\beta(0) - \Gamma^\mu_{\alpha\beta}(x)\dot{x}^\alpha(0)P_\mu(0)\}dx^\beta, \tag{3.21}$$

where $\gamma(0) = (x(0), P(0))$ and $P(0) = p$ is, by definition, equal to the covector p. In addition, since $\dot{\gamma}(0) = \left(\dot{x}(0), \dot{P}(0)\right) = Z$ where Z is given in (3.3), then we identify $X^\alpha = \dot{x}^\alpha(0)$ and $Y_\alpha = \dot{p}_\alpha(0)$, such that we arrive at the explicit expression

$$K_{(x,p)}(Z) := \{Y_\beta - \Gamma^\alpha_{\mu\beta}(x)X^\mu p_\alpha\}dx^\beta\big|_x. \tag{3.22}$$

The key properties of the connection map are:

- (i): $K_{(x,p)} : T_{(x,p)}(T^*\mathcal{M}) \to T^*_x\mathcal{M}$ is a linear map.
- (ii): We define the **Horizontal subspace** according to: $H_{(x,p)} := \ker(K_{(x,p)})$ which is a $n-$dimensional subspace of $T_{(x,p)}(T^*M)$.
- (iii): $H_{(x,p)} \cap V_{(x,p)} = \{0\}$.

The proof of (i) is trivial if we note that $K_{(x,p)}(Z_1 + \mu Z_2) = K_{(x,p)}(Z_1) + \mu K_{(x,p)}(Z_2)$ for all $\mu \in \mathbb{R}$, $Z_1, Z_2 \in T_{(x,p)}(T^*\mathcal{M})$. For the proof of (ii) we want to find a basis for $\ker\left(K_{(x,p)}\right)$. These vectors $\hat{Z}$ are such that $K_{(x,p)}(\hat{Z}) = 0$, $\hat{Z} = \hat{Z}^\mu e_\mu$ where

$$e_\mu|_{(x,p)} := \frac{\partial}{\partial x^\mu} + \Gamma^\alpha_{\mu\beta}(x)p_\alpha\frac{\partial}{\partial p_\beta}, \tag{3.23}$$

$\{e_\mu\}$ is a basis for $\ker\left(K_{(x,p)}\right)$, from which it follows that it n dimensional. For (iii), the basis $\{e_\mu\}$ of the horizontal subspace (3.23) and the vector basis of the vertical subspace, $\{\frac{\partial}{\partial p_\mu}\}$ are easily shown to be linearly independent.

At each point $(x,p) \in T^*\mathcal{M}$, the tangent space $T_{(x,p)}(T^*\mathcal{M})$ to the cotangent bundle, is split naturally in two parts $T_{(x,p)}(T^*\mathcal{M}) = H_{(x,p)} \oplus V_{(x,p)}$, so that each tangent vector $Z \in T_{(x,p)}(T^*\mathcal{M})$ can be decomposed in a unique way as $Z = Z^H + Z^V$ with $Z^H \in H_{(x,p)}$ and $Z^V \in V_{(x,p)}$. In terms of the vector basis $\{e_\mu|_{(x,p)}, \frac{\partial}{\partial p_\mu}\Big|_{(x,p)}\}$, the horizontal and vertical components can be described as

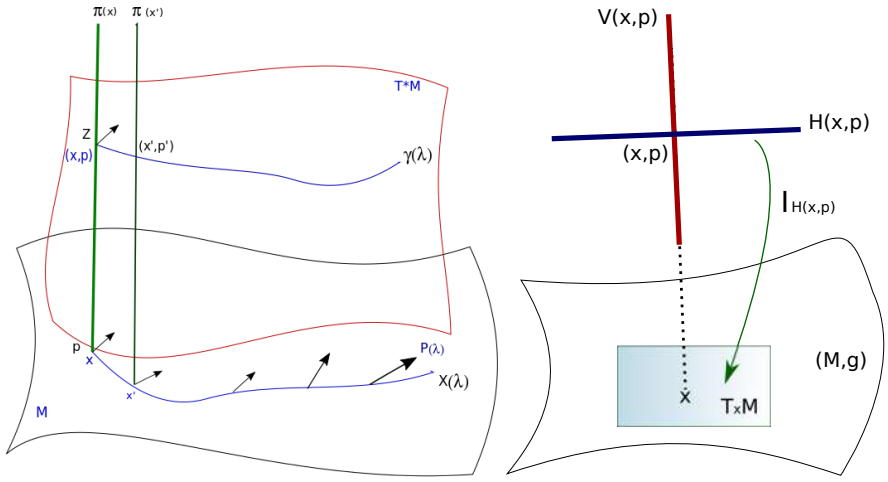

Figure 3.1: Left panel: Vector field $P(\lambda)$ along the curve $x(\lambda)$. The connection map consists in comparing p with $P(\lambda)$ at $x \in \mathcal{M}$ through the covariant derivative. Right panel: Decomposition of $T^*\mathcal{M}$ in the vertical $(V_{(x,p)})$ and horizontal subspaces $(H_{(x,p)})$, and the map I_H from $H_{(x,p)}$ to $T_x\mathcal{M}$.

$Z^H = Z^\mu_H \, e_\mu|_{(x,p)}$ and $Z^V = Z^V_\mu \, \frac{\partial}{\partial p_\mu}\Big|_{(x,p)}$ respectively, with $Z^\mu_H = dx^\mu_{(x,p)}(Z)$ and $Z^V_\mu = \theta_{\mu(x,p)}(Z)$, where

$$\theta_{\mu(x,p)} := dp_{\mu(x,p)} - \Gamma^\beta_{\alpha\mu} p_\beta dx^\alpha_{(x,p)}, \tag{3.24}$$

such that $\{dx^\mu_{(x,p)}, \theta_{\mu(x,p)}\}$ in the basis on $T^*_{(x,p)}(T^*\mathcal{M})$ which is dual to $\{\, e_\mu|_{(x,p)} \,,\, \frac{\partial}{\partial p_\mu}\Big|_{(x,p)}\}$.

Finally, we define the **Sasaki metric** $\hat{g}_{(x,p)}$ on $T^*\mathcal{M}$. This metric $\hat{g}$ is induced by the metric g on $\mathcal{M}$ and the associated Levi-Civita connection ∇ and can be defined easily by means of the maps π_* and $K_{(x,p)}$. We take the vectors $W, Z \in T_{(x,p)}(T^*\mathcal{M})$, and write

$$\begin{aligned} \hat{g}_{(x,p)}(W,Z) &= \hat{g}_{(x,p)}(W_H + W_V, Z_H + Z_V) \\ &= \hat{g}_{(x,p)}(W_H, Z_H) + \hat{g}_{(x,p)}(W_V, Z_V) + \hat{g}_{(x,p)}(W_H, Z_V) + \hat{g}_{(x,p)}(W_V, Z_H)\,. \end{aligned}$$

We impose that the decomposition of these vectors in horizontal and vertical components, be **orthogonal** (do not have crossed terms), with respect to $\hat{g}$. Then, the above reduces to

$$\hat{g}_{(x,p)}(W,Z) = \hat{g}_{(x,p)}(W_H + W_V, Z_H + Z_V) = \hat{g}_{(x,p)}(W_H, Z_H) + \hat{g}_{(x,p)}(W_V, Z_V)\,.$$

Using the linear maps $\pi_{*(x,p)} : T_{(x,p)}(T^*\mathcal{M}) \to T_x\mathcal{M}$ and $K_{(x,p)} : T_{(x,p)}(T^*\mathcal{M}) \to$

$T^*_x\mathcal{M}$ and the metric g on $\mathcal{M}$, we define the Sasaki metric by

$$\hat{g}_{(x,p)}\left(W,Z\right) := g_x\left(\pi_{*(x,p)}(Z_H), \pi_{*(x,p)}(W_H)\right) + g_x^{-1}\left(K_{(x,p)}(Z_V), K_{(x,p)}(W_V)\right). \tag{3.25}$$

Explicitly in terms of adapted local coordinates,

$$\hat{g}_{(x,p)}\left(W,Z\right) = g_x\left(Z_H^\mu \frac{\partial}{\partial x^\mu}\bigg|_x, W_H^\alpha \frac{\partial}{\partial x^\alpha}\bigg|_x\right) + g_x^{-1}\left(Z_\mu^V dx^\mu\big|_x, W_\alpha^V dx^\alpha\big|_x\right) = Z_H^\mu W_H^\alpha g_{\mu\alpha} + W_\alpha^V Z_\alpha^V g^{\mu\alpha}. \tag{3.26}$$

Hence, with respect to the basis of $2n$ covectors $\{dx^\alpha(x,p), \theta_{\alpha(x,p)}\}$ given by equation (3.24), one can write

$$\hat{g}_{(x,p)} = g_{\mu\nu}(x) dx^\mu_{(x,p)} \otimes dx^\nu_{(x,p)} + g^{\mu\nu}(x)\theta_{\mu(x,p)} \otimes \theta_{\nu(x,p)}, \tag{3.27}$$

or in matrix notation

$$\hat{g} = \begin{bmatrix} g_{\mu\nu} & 0 \\ 0 & g^{\mu\nu} \end{bmatrix}_{2n\times 2n}.$$

It follows that $\hat{g}$ has signature $(2, 2n-2)$ [2], and the determinant of the Sasaki metric in this basis is $|\hat{g}| = 1$ so that it is a non-degenerate metric.

Some extra definitions, related to the split in horizontal and vertical subspaces, are useful

$$\begin{aligned} I^H_{(x,p)} := \pi_{*(x,p)}\Big|_{H_{(x,p)}}, \quad I^H_{(x,p)} : H_{(x,p)} &\to T_x\mathcal{M} \\ Z^H &\mapsto \pi_{*(x,p)}\left(Z^H\right) \end{aligned} \tag{3.28}$$

$$\begin{aligned} I^V_{(x,p)} := K_{(x,p)}\Big|_{V_{(x,p)}}, \quad I^V_{(x,p)} : V_{(x,p)} &\to T^*_x\mathcal{M}, \\ Z^V &\mapsto K_{(x,p)}\left(Z^V\right), \end{aligned} \tag{3.29}$$

These maps are invertible, because $\ker H_{(x,p)} = \{0\}$ and $\ker V_{(x,p)} = \{0\}$. We define

$$\left(I^H_{(x,p)}\right)^{-1} : T_x\mathcal{M} \to H_{(x,p)} : \quad Horizontal \quad lift, \tag{3.30}$$

$$\left(I^V_{(x,p)}\right)^{-1} : T^*_x\mathcal{M} \to V_{(x,p)} : \quad Vertical \quad lift. \tag{3.31}$$

With this, the Sasaki metric can also be written as

$$\hat{g}(W,Z) = g\left(I^H(Z^H), I^H(W^H)\right) + g^{-1}(I^V(Z^V), I^V(W^V)). \tag{3.32}$$

[2] In particular in dimension $n = 4$, the signature is $(-1,-1,1,1,1,1,1,1)$.

We can relate $H_{(x,p)}$ and $V_{(x,p)}$ in the following way

$$\begin{aligned} Q_{(x,p)} &: H_{(x,p)} \to V_{(x,p)} \\ & Z^H \mapsto Q(Z^H) := \left(I^V_{(x,p)}\right)^{-1} \circ g\left(I^H_{(x,p)}(Z^H)\right) \qquad (3.33) \\ Q^{-1}_{(x,p)} &: V_{(x,p)} \to H_{(x,p)} \\ & Z^V \mapsto Q^{-1}(Z^V) := \left(I^H_{(x,p)}\right)^{-1} \circ g^{-1}\left(I^V_{(x,p)}(Z^V)\right) \qquad (3.34) \\ J_{(x,p)} &: T_{(x,p)}(T^*M) \to T_{(x,p)}(T^*M) \\ J_{(x,p)}(Z) &= J_{(x,p)}(Z^H + Z^V) := Q_{(x,p)}(Z^H) - Q^{-1}_{(x,p)}(Z^V), \qquad (3.35) \end{aligned}$$

and verified that

$$J(Z^\mu_H e_\mu + Z^V_\mu \frac{\partial}{\partial p_\mu}) = Z^\mu_H g_{\mu\nu} \frac{\partial}{\partial p_\nu}\Big|_{(x,p)} - Z^V_\mu g^{\alpha\mu} e_\alpha\big|_{(x,p)}, \qquad (3.36)$$

where the structure J is named a almost complex structure ($J^2 = -1$), thats satisfied the following properties: (1) $\hat{g}$ is invariant respect to the J, and satisfied $\hat{g}_{(x,p)}(J(Z), J(W)) = \hat{g}_{(x,p)}(Z, W)$ where $Z, W \in T_{(x,p)}(T^*\mathcal{M})$ that can be prove using equation 3.36, and the orthogonality of Sasaki metric

$$\begin{aligned} \hat{g}_{(x,p)}(J(Z), J(W)) &= \hat{g}\left(Z^\mu_H g_{\mu\nu} \frac{\partial}{\partial p_\nu} - Z^V_\mu g^{\alpha\mu} e_\alpha, W^\lambda_H g_{\lambda\beta} \frac{\partial}{\partial p_\beta} - W^V_\lambda g^{\beta\lambda} e_\beta\right) \\ \hat{g}_{(x,p)}(J(Z), J(W)) &= Z^\mu_H g_{\mu\nu} W^\lambda_H g_{\lambda\beta} \hat{g}_{(x,p)}\left(\frac{\partial}{\partial p_\nu}, \frac{\partial}{\partial p_\beta}\right) + Z^V_\mu g^{\alpha\mu} W^V_\lambda g^{\beta\lambda} \hat{g}_{(x,p)}\left(e_\alpha, e_\beta\right) \\ &= Z^\mu_H g_{\mu\nu} W^\nu_H + Z^V_\mu g^{\alpha\mu} W^V_\alpha = \hat{g}_{(x,p)}(Z, W). \qquad (3.37) \end{aligned}$$

Next, the second property (2) is about defined the symplectic form with the almost complex form J, $\Omega_s(Z, W) = \hat{g}(Z, J(W))$, to prove this, we see how the symplectic form acts on the basis

$$\begin{aligned} \Omega_s\left(e_\mu, e_\nu\right) &= \hat{g}\left(e_\mu, \frac{\partial}{\partial p^\nu}\right) = 0, \qquad (3.38) \\ \Omega_s\left(\frac{\partial}{\partial p^\mu}, \frac{\partial}{\partial p^\nu}\right) &= \hat{g}\left(\frac{\partial}{\partial p^\mu}, -e_\nu\right) = 0, \qquad (3.39) \\ \Omega_s\left(e_\mu, \frac{\partial}{\partial p^\nu}\right) &= -\hat{g}\left(e_\mu, g^{\nu\lambda} e_\lambda\right) = -g^{\nu\lambda} g_{\mu\lambda} = -\delta^\nu_\mu, \qquad (3.40) \end{aligned}$$

and using the property (1), we check that $\Omega_s(Z, W) = \hat{g}(Z, J(W)) = \hat{g}(J(Z), -W) = -\hat{g}(W, J(Z))$, that reflects the antisymmetric nature of Ω_s.

Through these maps, we can also define Liouville's vector field as follows:

$$L_{(x,p)} := I^{-H}_{(x,p)}(\hat{p}), \quad \hat{p} = g^{-1}(p), \quad p \in T^*_x\mathcal{M}, \quad \hat{p} \in T_x\mathcal{M}, \qquad (3.41)$$

that is, $L_{(x,p)}$ is the horizontal lift of p. In terms of adapted local coordinates, $Z^H = Z^\mu e_\mu$, $I^H(Z^H) = Z^\mu \frac{\partial}{\partial x^\mu}$ and

$$L_{(x,p)} = \hat{p}^\mu e_\mu|_{(x,p)} = g^{\mu\nu} p_\nu \left(\frac{\partial}{\partial x^\mu} + \Gamma^\alpha_{\mu\beta} p_\alpha \frac{\partial}{\partial p_\beta} \right).$$

Using the fact that $\Gamma^\alpha_{\mu\beta} p_\alpha p^\mu = -\frac{1}{2} g^{\alpha\tau}_{,\beta} p_\alpha p_\tau$ and $\frac{\partial g^{\alpha\beta}}{\partial x^\sigma} = -g^{\alpha\mu} g^{\beta\nu} \frac{\partial g_{\mu\nu}}{\partial x^\sigma}$, we may retrieve the previous expression for the Liouville vector field

$$L_{(x,p)} := g^{\mu\nu} p_\nu \frac{\partial}{\partial x^\mu} - \frac{1}{2} p_\alpha p_\beta \frac{\partial g^{\alpha\beta}}{\partial x^\sigma} \frac{\partial}{\partial p_\sigma}, \tag{3.42}$$

Hence we see that both definitions found in (3.15) and (3.42) agree with each other, that is the Liouville vector field can be regarded as either the horizontal lift of $\hat{p}$, or as the Hamiltonian vector field belonging to the one-particle Hamiltonian. In this work the latter will turn out to be more useful.

The symplectic form can be written in the simple form as a wedge product of the co-vector basis on $T^*\mathcal{M}$, such that

$$\Omega_{s(x,p)} = \theta_{(x,p)\mu} \wedge dx^\mu.$$

Using the definition (3.24), $\Omega_{s(x,p)} = dp_\mu \wedge dx^\mu - \Gamma^\beta_{\alpha\mu} p_\beta dx^\alpha \wedge dx^\mu$, but due to the symmetries and anti-symmetries of $\Gamma^\beta_{\alpha\mu}$ and $dx^\alpha \wedge dx^\mu$ one recover the expression (3.7)

$$\Omega_{s(x,p)} = dp_\mu \wedge dx^\mu = d\Theta. \tag{3.43}$$

3.3 Volume form

The Sasaki metric induces a natural volume form $\eta_{T^*\mathcal{M}}$ on the cotangent bundle $T^*\mathcal{M}$, which is defined as follows:

$$\begin{aligned}
\eta_{T^*\mathcal{M}} &= -|\hat{g}| dx^0 \wedge dx^1 \wedge dx^2 \wedge dx^3 \wedge \theta_0 \wedge \theta_1 \wedge \theta_2 \wedge \theta_3 \\
&= -1 dx^0 \wedge dx^1 \wedge dx^2 \wedge dx^3 \wedge \left(dp_0 - \Gamma^\beta_{\alpha 0} p_\beta dx^\alpha \right) \wedge ... \wedge \left(dp_3 - \Gamma^\beta_{\alpha 3} p_\beta dx^\alpha \right) \\
&= -1 dx^0 \wedge dx^1 \wedge dx^2 \wedge dx^3 \wedge dp_0 \wedge dp_1 \wedge dp_2 \wedge dp_3,
\end{aligned} \tag{3.44}$$

where we have used the fact that the determinant $|\hat{g}| = 1$, and the basis product is written explicitly from the definition (3.24).

Now we want relate the symplectic form with the product of $n-$fold product of the symplectic forms:

$$\begin{aligned}
\Omega_s \wedge \Omega_s \wedge ... \wedge \Omega_s &= dp_{\alpha_0} \wedge dx^{\alpha_0} \wedge dp_{\alpha_1} \wedge dx^{\alpha_1} .... \wedge dp_{\alpha_{(n-1)}} \wedge dx^{\alpha_{(n-1)}} \\
\Omega_s \wedge \Omega_s \wedge ... \wedge \Omega_s &= (-1)^1 \times (-1)^2 \times ... (-1)^n dx^{\alpha_0} \wedge dx^{\alpha_1} ... dx^{\alpha_{n-1}} \wedge dp_{\alpha_0} \wedge dp_{\alpha_1} ... \wedge dp_{\alpha_{n-1}} \\
\Omega_s \wedge \Omega_s \wedge ... \wedge \Omega_s &= (-1)^k dx^{\alpha_0} \wedge dx^{\alpha_1} ... dx^{\alpha_{n-1}} \wedge dp_{\alpha_0} \wedge dp_{\alpha_1} ... \wedge dp_{\alpha_{n-1}} \\
\Omega_s \wedge \Omega_s \wedge ... \wedge \Omega_s &= (-1)^k \varepsilon_{\alpha_0 \alpha_1 \alpha_2 ... \alpha_{n-1}} \varepsilon^{\alpha_0 \alpha_1 \alpha_2 ... \alpha_{n-1}} dx^0 \wedge dx^1 ... dx^{n-1} \wedge dp_0 \wedge dp_1 ... \wedge dp_{n-1}
\end{aligned}$$

Where $k = n(n+1)/2$ is the sum of the first n terms of an arithmetic progression of numbers between $1...n$, and the general version of the contraction $\varepsilon_{\alpha_0\alpha_1\alpha_2...\alpha_d}\varepsilon^{\beta_0\beta_1\beta_2...\beta_d} = n!\delta^{\beta_0}_{[\alpha_0}\delta^{\beta_1}_{\alpha_1}...\delta^{\beta_d}_{\alpha_d]} = n!$. Therefore,

$$\Omega_s \wedge \Omega_s \wedge ... \wedge \Omega_s = (-1)^k n! dx^0 \wedge dx^1 ... dx^{n-1} \wedge dp_0 \wedge dp_1 ... \wedge dp_{n-1}, \quad (3.45)$$

and we see that the volume form $\eta_{T^*\mathcal{M}}$ can also be written equivalently as

$$\eta_{T^*\mathcal{M}} = (-1)^{k-1} \frac{\Omega_s \wedge \Omega_s \wedge ... \wedge \Omega_s}{n!} \quad (n - fold), \quad (3.46)$$

From this we can see the **Lioville's theorem**, that is formulate $\mathcal{L}_L \eta_{T^*\mathcal{M}} = 0$, i.e. $(divL)\,\eta = 0$.
The poof is derived from the Cartan formula

$$\mathcal{L}_L \eta_{T^*\mathcal{M}} = (i_L d + d i_L)\,\eta = i_L d\,(d\Theta \wedge d\Theta \wedge d\Theta \wedge d\Theta) + d i_L \eta = d i_L \eta,$$

but $d i_L \Omega = d(-dH) = -d^2 H = 0$, hence we demonstrate that $\mathcal{L}_L \eta_{T^*\mathcal{M}} = 0$, on the other hand, we recognize that $d\,(i_L \eta) = (divL)\,\eta_{T^*\mathcal{M}}$.

3.4 Observables on the cotangent bundle

To calculate the physical observables associated with a collisionless relativistic kinetic gas, we define a general observable, through a "test" function $\varphi(x,p)$ over the phase space, that can be thought of a device which measures the properties of the system (e.g. energy, mean velocity etc.) in a small region of phase space, and N_φ is the corresponding value measured by this device, where f describes the state of the gas [3].

$$N_\varphi[f] := \int_{\Gamma_m} f(x,p)\varphi(x,p)\eta_{T^*\mathcal{M}}. \quad (3.47)$$

This observable $N_\varphi[f]$ measures a particular property of the gas whose state is described by the one-particle distribution function $f(x,p)$ that is solution of the Liouville equation and the special cases in which we choose the test function in the form $\varphi(x,p) = p(X)\frac{\delta(x-x_0)}{\sqrt{-\det(g_{\mu\nu})}}$, where X is a vector field on $\mathcal{M}$, the observable reduces to

$$N_\varphi[f] = \int_{\pi^{-1}(x_0)} f(x_0,p)p(X)dvol_{x_0}(p) := J_{x_0}(X), \quad (3.48)$$

[3]The test function can be defined either over Γ or over the mass-shell Γ_m, in the last one should be restrict the volume form over the mass shell, see by example the section 4. C in **??**.

and we obtain the particle current density (3.48) along X. Similarly, if we choose the test function $\tilde{\varphi}(x,p) = p(X)p(Y)\frac{\delta(x-x_0)}{\sqrt{-\det(g_{\mu\nu})}}$ for X, Y vector fields on $\mathcal{M}$

$$N_{\tilde{\varphi}}[f] = \int\limits_{\pi^{-1}(x_0)} f(x_0,p)p(X)p(Y)dvol_{x_0}(p) := T_{x_0}(X,Y), \quad (X,Y) \in T_xM, \tag{3.49}$$

and we obtain the $X-Y$ components of the Stress-Energy-Momentum tensor (3.49). In (3.49) and (3.48) here $\pi^{-1}(x_0)$ refers to the fiber over the point x_0 which, corresponds to the inverse image of x.
The volume element in these integrals is

$$dvol_x(p) := \sqrt{-det(g^{\mu\nu}(x))}d^4p,$$

induced by the inverse metric ${g_x}^{-1}$. In adapted local coordinates,

$$J_\mu(x) = \int\limits_{\pi^{-1}(x)} p_\mu f(x,p)dvol_x(p), \tag{3.50}$$

$$T_{\mu\nu}(x) = \int\limits_{\pi^{-1}(x)} p_\mu p_\nu f(x,p)dvol_x(p). \tag{3.51}$$

These quantities have zero divergence, i.e. $DivJ_x = \int\limits_{\pi^{-1}(x)} L[f]dvol_x(p) = 0$, provided the Liouville equation $L[f] = 0$ is satisfied. The proof consists choosing Gaussian coordinates x^μ so that $g_{\mu\nu}(x) = \eta_{\mu\nu}$, and $\partial_\sigma g_{\mu\nu}(x) = 0$ at a fixed point $x \in \mathcal{M}$, with coordinates x^μ. Expanding

$$\begin{aligned} DivJ_x &= \eta^{\mu\nu}\frac{\partial}{\partial x^\nu}\, J_\mu|_x = \eta^{\mu\nu}\frac{\partial}{\partial x^\nu}\int_{\pi^{-1}(x)} f(x,p)p_\mu dvol_x(p), \qquad (3.52)\\ &= \eta^{\mu\nu}\int \frac{\partial f(x,p)}{\partial x^\nu}p_\mu\sqrt{-det(g^{\mu\nu}(x))}d^4p\Big|_x, \\ &= \int \eta^{\mu\nu}p_\mu\frac{\partial f(x,p)}{\partial x^\nu}\sqrt{-det(g^{\mu\nu}(x))}d^4p\Big|_x, \qquad (3.53)\\ &= \int\limits_{\pi^{-1}(x)} g^{\mu\nu}p_\mu\frac{\partial f(x,p)}{\partial x^\nu}dvol_x(p), = \int\limits_{\pi^{-1}(x)} L[f(x,p)]dvol_x(p) = 0, \end{aligned}$$

where we have used the fact that $L[f]|_x = p^\nu\frac{\partial f}{\partial x^\nu}\Big|_x - \frac{1}{2}\cancelto{0}{\frac{\partial g^{\alpha\beta}}{\partial x^\mu}}p_\alpha p_\beta\frac{\partial f}{\partial p_\mu}\Big|_x = 0$ if $L[f] = 0$.
The proof for the energy-momentum tensor is analogous. Their application in physical problems as in accretion-related models will be discussed in Paper I and II.

Chapter 4

The Einstein-Liouville System

To solve the problem of accretion of collisionless particles in the relativistic context, one in principle needs to solve the Einstein-Liouville system of equations [1]

$$G_{\mu\nu} = R_{\mu\nu}[g] - \frac{1}{2}R[g]g_{\mu\nu} = 8\pi T_{\mu\nu}[f], \qquad L[f] = 0, \tag{4.1}$$

with $T_{\mu\nu}[f]$ the stress-energy tensor defined in equation (3.51), and the Liouville operator $L[f]$ (3.15).
There exists several methods for solving this problem: (i) look for special solutions assuming symmetries, (ii) solve the full system with numerical calculations, (iii) using a perturbative approach, as well as, a combination of these strategies. Here we focus on a perturbative description, which we present now in more detail. Physically, we assume that the gas is sufficiently diluted, such that the kinetic matter causes a small perturbation on the spacetime, represented through a perturbation $\epsilon \propto \rho_{max}$, with ρ_{max} the maximum density, in the full-phase space.

With this idea in mind, the one-particle distribution function $f(t, x, p)$ and the metric are expanded as follows:

$$f(t, x, p) = f_0 + \epsilon f_1 + \epsilon^2 f_2 + ... \tag{4.2}$$

$$g_{\mu\nu} = g_{0\mu\nu} + \epsilon g_{1\mu\nu} + \epsilon^2 g_{2\mu\nu} + ... \tag{4.3}$$

with $f_0 = 0$ since there is no matter when $\epsilon = 0$. Additionally, the Liouville operator is ,we linearize the Liouville operator and the Einstein tensor:

$$\begin{aligned} L_g[f] &= 0 \\ L_{g_0+\epsilon g_1+...}[f] &= L_{(0)}[f] + \epsilon L_{(1)}[f] + \epsilon^2 L_{(2)}[f] + ... \\ L_g[\epsilon f_1 + \epsilon^2 f_2 + ..] &= L_{(0)}[\epsilon f_1 + \epsilon^2 f_2 + ...] + \epsilon L_{(1)}[\epsilon f_1 + \epsilon^2 f_2 + ...] + \mathcal{O}(\epsilon^3), \\ L_g[f] &= \epsilon L_{(0)}[f_1] + +\mathcal{O}(\epsilon^2). \end{aligned}$$

[1] We use geometrized units in which $G = 1$, $c = 1$.

The Einstein equations expanded in ϵ have the structure

$$\begin{aligned} G_{\mu\nu} &= T_{\mu\nu}|_g\,[f] \\ G_{\mu\nu}|_{g_0+\epsilon g_1+...} &= T_{\mu\nu}|_{g_0+\epsilon g_1+..}\,[\epsilon f_1+...] \\ G^{(0)}_{\mu\nu}+\epsilon G^{(1)}_{\mu\nu}+\mathcal{O}(\epsilon^2) &= T^{(0)}_{\mu\nu}[\epsilon f_1+...]+\epsilon T^{(1)}_{\mu\nu}[\epsilon f_1+...]+\mathcal{O}(\epsilon^2), \\ G^{(0)}_{\mu\nu}+\epsilon G^{(1)}_{\mu\nu}+\mathcal{O}(\epsilon^2) &= \epsilon T^{(0)}_{\mu\nu}[f_1]++\mathcal{O}(\epsilon^2). \end{aligned} \tag{4.4}$$

so the system of coupled equations, to zeroth and first order in ϵ, is given by

$$0) \qquad G^{(0)}_{\mu\nu}=0, \tag{4.5}$$

$$1) \qquad L_{(0)}[f_1]=0, \quad G^{(1)}_{\mu\nu}=T^{(0)}_{\mu\nu}[f_1], \tag{4.6}$$

where the equation (4.5) represents the Einstein field equations for the background metric g_0.

We will solve partially the system (4.6), which means that we are not interested at the moment on the metric perturbations g_1. With this we will solve $L^{(0)}[f_1]=0$ and compute the observables $T^{(0)}_{\mu\nu}[f_1]$. This will allows to calculate the dynamics of the particles and the associated energy momentum tensor and current density $T_{\mu\nu}, J_\mu$ (3.50) and (3.51).
With these observables we can analyze the phenomenology, in the particular case of this thesis the phenomenology is the behavior of the relativistic kinetic gas particles for accretion processes and for dynamics disk configurations.
It is obviously much simpler to solve (4.6) than the coupled Einstein-Liouville problem. Nonetheless, the equation $L[f_1]=0$ is still complicated due to the fact that the background metric might be curved, see the equation (3.15). Therefore, the strategy that will be used is, assuming that g_0 (the vacumm solution of einstein equations) has an integrable geodesic flow, such that can be applied tools from the Hamiltonian dynamics to express the Liouville equation in terms of action-angle variables.

Chapter 5

Integrable Hamiltonian systems and action-angle variables

To solve the Liouville equation, in most general form possible, we use the action-angle variables, described in classics textbooks as [37, 38] and the notes [39]. We start with a brief summary of the main ideas involved for solving an integrable Hamiltonian system in terms of action-angle variables.

We want to solve a system with n degrees of freedom, that is described by a trajectory in $2n$ dimensional phase space $\mathcal{N}$ (a symplectic manifold). The dynamics of this system is determined by Hamilton's equations (3.11, 3.12). This can be solved analytically reducing the system to one-dimensional problems if we known the n first integrals. This idea is behind the definition of an integrable system.

Definition of Integrable System: An integrable system is a $2n$ dimensional phase space manifold $\mathcal{N}$ with n independent functions $F_i, \quad 1, \ldots, n$ (which means that over $\mathcal{N}$, we have n well-defined 1-forms dF_i which should be linearly independent at each point of $\mathcal{N}$), such that these functions Poisson commute with each other $\{F_i, F_j\} = 0, \quad j, k = 1, \ldots, n$ and where $F_1 = H$ is equal to the Hamiltonian.

Arnold-Liouville Theorem: Let $\mathcal{N}, F_1, ...F_n$ be an integrable system with a Hamiltonian $H = F_1$ and consider the level sets defined by the functions F_i:

$$\mathcal{N}_c = \{(x, p) \in \mathcal{N}; F_k(x, p) = c_k\}, \quad c_k = const, \quad k = 1, \ldots, n.$$

Suppose, $\mathcal{N}_c \neq \varnothing$ is not empty. Then, the following statements are satisfied:

1) $\mathcal{N}_c$ is a smooth submanifold of N, invariant under the phase flow with Hamiltonian function $H = F_1$, and also under the phase flow of $F_2, F_3 ... F_n$.

2) The restriction of the Poincaré one-form $\Theta|_{\mathcal{N}_c}$ on $\mathcal{N}_c$ is closed.

3) If $\mathcal{N}_c$ is compact and connected, then it is diffeomorphic to the n-torus $T^n := S^1 \times S^1 ... \times S^1$, and one can introduce the action-angle coordinates (J, Q) which are canonical variables with $0 \leq Q_k \leq 2\pi$. The angles coordinates over $\mathcal{N}_c$, and where the actions coordinates $J_k = J_k(F_1, ..., F_n)$ are functions of the first integrals.

4) The canonical equations of motion (3.11,3.12), become $\dot{J}_k = 0$, $\dot{Q}_k = \omega_k(J_1, \ldots, J_n)$, where $\omega_k = \frac{\partial H}{\partial J_k}$, with $k = 1, \ldots, n$. This integrable system can be solved trough a elementary operations, such as, one-dimensional integrals, algebraic operations, etc provided $F_1, ...F_n$ functions that are known explicitly.

For details and proof of the Theorem, see [37, 38, 39]. In order to illustrate how to apply the theorem in a concrete and simple example, we consider the two dimensional setting that represents a system of kinetic gas particles (Newtonian) confined to $\mathbb{R}^2$ and under the influence of an external, rotationally-invariant potential $\Phi : U \to \mathbb{R}$, with $U := \mathbb{R}^2 \setminus (0, 0)$. The Hamiltonian in spherical coordinates is [1]

$$H(x,p) := \frac{1}{2}\left(p_r^2 + \frac{p_\varphi^2}{r^2}\right) + \Phi(r) = \frac{{p_r}^2}{2} + \frac{\ell^2}{2r^2} + \Phi(r) = \frac{1}{2}p_r^2 + \Phi_{eff}(r). \quad (5.1)$$

In the following we assume that the potential function $\Phi : (0, \infty) \to \mathbb{R}$ is C^∞ smooth, strictly monotonously increasing, such that the function $r \to r^3\Phi'(r)$ in increasing from $0 \to \infty$ as r increases from $0 \to \infty$. The last condition implies for each $\ell \neq 0$ the existence of a unique global minimum of the effective potential, $\Phi_{eff}(r) = \frac{\ell^2}{2r^2} + \Phi(r)$, determined by the equation $r_0^3\Phi'(r_0) = \ell^2$. This minimum corresponds to a circular trajectory with minimum energy $E_0(\ell) = \Phi_{eff}(r_0)$.

For the following, the phase space is restricted to the invariant subset corresponding to the bound, non-circular trajectories[2]

$$\Gamma_{bound} := \{(x,p) \in U \times \mathbb{R}^2 : \ell = p_\varphi \neq 0, E_0(\ell) < H(x,p) < \Phi_\infty\}, \quad (5.2)$$

where Φ_∞ is the asymptotic value of the potential. Here, ℓ is a conserved quantity associated to $\dot{p}_\varphi = -\frac{\partial H}{\partial \varphi} = 0 \to p_\varphi = \ell = cte$ is the angular momentum. Since this classical Hamiltonian does not depend explicitly on time, the second conserved quantity is trivially the energy $H(x, p) = E$.
In summary, the following quantities are conserved along the trajectories

$$E = H(x,p), \quad \ell = p_\varphi, \quad (5.3)$$

Consequently, we introduce the smooth functions on the phase space $F_0, F_1 : \Gamma_{bound} \to \mathbb{R}$, defined by

$$F_0(x,p) := H(x,p), \quad F_1(x,p) = p_\varphi, \quad (5.4)$$

[1] Here, $\Phi_{eff}(r) = \frac{\ell^2}{2r^2} + \Phi(r)$ denotes the effective potential.
[2] Here Γ_{bound} represents the manifold $\mathcal{N}$ in the Arnold-Liouville theorem.

that obviously Poisson commute with each other $\{F_0, F_1\} = 0$. Now we define the invariant subspace [3]

$$\Gamma_{E,\ell} \quad := \quad \{(x,p) \in \Gamma_{bound} : F_0(x,p) = E, F_1(x,p) = \ell\}. \tag{5.5}$$

Γ_{bound} has 4 dimensions, while the conditions defining $\Gamma_{E,\ell}$ yields two restrictions; $(x,p) \in \Gamma_{E,\ell}$ have 2 dimensions only if dF_0, dF_1 are linear independent. To continue the construction of the action-angle variable. We should check that these functions are linear independent over four-dimensional submanifold Γ_{bound}. For this we compute

$$dH = p_r dp_r + \frac{p_\varphi}{r^2} dp_\varphi - \frac{p_\varphi^2}{r^3} dr + \Phi'(r) dr, \qquad dp_\varphi = d\ell,$$

and we see that dH and dp_φ are linear independent if and only if

$$p_r dp_r + \left(-\frac{\ell^2}{r^3} + \Phi'(r) \right) dr \neq 0.$$

This is satisfied, unless $p_r = 0$ and $\frac{\ell^2}{r^3} = \Phi'(r)$, which corresponds to the case of circular trajectories [4]. Note that, this is the reason we have restricted ourselves to non-circular orbits in the definition of Γ_{bound} in (5.2).

Over this submanifold we can define appropriately symplectic coordinates $Q^r, Q^\varphi, J_r, J_\varphi$, adapted to $\Gamma_{E,\ell}$. Further $\Gamma_{E,\ell}$ is topologically equal to $T^2 : S^1 \times S^1$, as can be seen by projection on the (r, p_r)-plane and the (φ, p_φ)-cilinder.

In practice, we find the action-angle variables, as follows: We define the variable J through integration over the Poincaré one-form $\Theta = p_\alpha dx^\alpha$

$$J_r \quad := \quad \frac{1}{2\pi} \oint \left(p_r dr + \cancelto{0}{p_\varphi d\varphi} \right) \Big|_{\varphi = cte} = \frac{1}{2\pi} \oint p_r dr = \frac{A(E,\ell)}{2\pi}, \tag{5.6}$$

$$J_\varphi \quad := \quad \frac{1}{2\pi} \oint \left(\cancelto{0}{p_r dr} + p_\varphi d\varphi \right) \Big|_{r = cte} = \frac{1}{2\pi} \int_0^{2\pi} p_\varphi d\varphi = \ell, \tag{5.7}$$

where the radial momentum is defined by $p_r = \pm\sqrt{2(E - \Phi_{eff}(r))}$, the area function as $A(E,\ell) := \oint p_r dr$ [5]. In Fig 5.1, we can see some example for an one-dimensional effective potential ($\ell = 0$), and the respective projection on the (r, p_r) plane, as well as the values of the turning point that depends on the energy curve.

[3] This definition corresponds to the invariant subset $\mathcal{N}_c$ defined previously.

[4] In this limit, $\Gamma_{E,\ell}$ degenerates to a 1 dimension sub manifold of Γ_{bound}.

[5] The Area function is defined by $A(E,\ell) = 2 \int_{r_1}^{r_2} |p_r| dr$ and represents the area enclosed by the energy curve in the plane (r, p_r) for different values of (E,ℓ) and with turning points $r_1(E,\ell) < r_2(E,\ell)$.

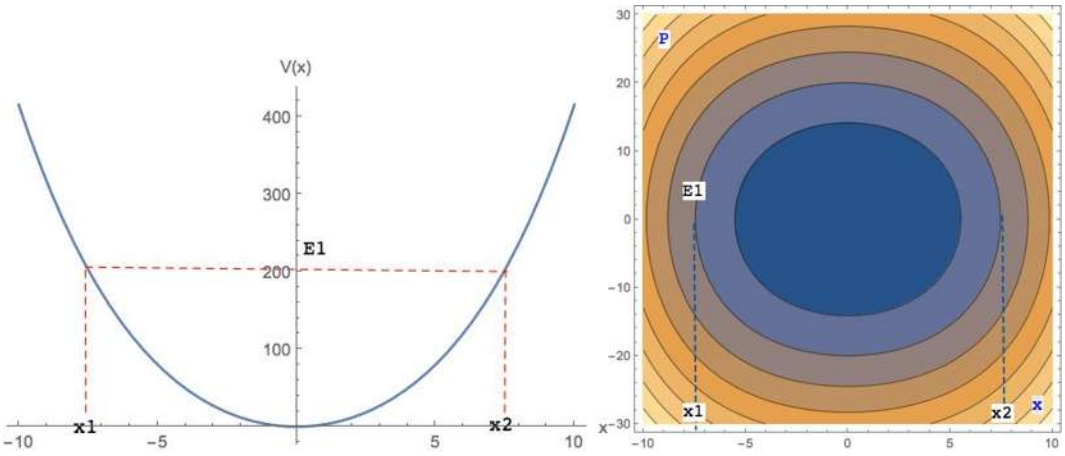

Figure 5.1: A graph of the potential $\Phi(x) = k\frac{x^2}{2} + s\frac{x^4}{4}$, with parameter values $k = 5.76, s = 0.051$ and the respective energy curves. Also illustrated are the values of the turning points x_1, x_2 for the particular energy value $E_1 = 200$.

Now we define the corresponding frequencies, representing

$$\omega_r := \frac{\partial H}{\partial J_r}, \tag{5.8}$$

$$\omega_\varphi := \frac{\partial H}{\partial J_\varphi}, \tag{5.9}$$

these frequencies correspond to the projections of the trajectories in the (r, p_r) and (φ, p_φ) subspaces.

and the generating function $S(Q, J) := \int d\Theta = \int_{x_0}^{x} p_\alpha dx^\alpha$ where x_0 is some chosen point on the torus [6] the angle is calculated through $Q_i = \frac{\partial S}{\partial J_i}$.

$$S(r, \varphi; J_r, J_\varphi) = \ell\varphi + \int_{\gamma(r,p_r)} p_r dr$$

here, $\gamma_{(r,p_r)}$ denotes the curve connecting some point named x_0 to (r, p_r) clockwise along the energy curve. From the generatrix, we find $(Q_r, Q_\varphi) = \left(\frac{\partial S}{\partial J_r}, \frac{\partial S}{\partial J_\varphi}\right)$. In order to perform these calculations we use the chain rule. The variable transformation $(E, \ell) \mapsto \left(J_r = \frac{A(E,\ell)}{2\pi}, J_\varphi = \ell\right)$ with the Jacobean matrix

[6] This definition does not depend on the deformation of the path linking $x_0 \to x$, but note that it does depends on the winding number of this path, giving additional factors of $2\pi J_r$ or $2\pi J_\varphi$.

$$\begin{bmatrix} \frac{\partial J_r}{\partial E} & \frac{\partial J_r}{\partial \ell} \\ \frac{\partial J_\varphi}{\partial E} & \frac{\partial J_\varphi}{\partial \ell} \end{bmatrix} = M = \begin{bmatrix} \frac{1}{2\pi}\oint \frac{dr}{p_r} & \frac{1}{2\pi}\oint \frac{\ell dr}{-r^2 p_r} \\ 0 & 1 \end{bmatrix},$$

the inverse matrix is required for computing the $Q's$ variables,

$$M^{-1} = \begin{bmatrix} \frac{2\pi}{\oint \frac{dr}{p_r}} & \frac{\oint \frac{\ell dr}{r^2 p_r}}{\oint \frac{dr}{p_r}}. \\ 0 & 1 \end{bmatrix},$$

With this the angle-variable can be expressed as

$$Q_r = \frac{2\pi}{\oint \frac{dr}{p_r}} \left(\int_\gamma \frac{dr}{p_r} \right), \tag{5.10}$$

$$Q_\varphi = \left(\int_\gamma \frac{dr}{p_r} \right) \frac{\oint \frac{\ell dr}{r^2 p_r}}{\oint \frac{dr}{p_r}} - \int_\gamma \frac{\ell dr}{r^2 p_r} + \varphi. \tag{5.11}$$

Computing the frequencies in equations (5.8, 5.9), from the inverse matrix M^{-1}, we obtain:

$$\omega_r = \frac{2\pi}{\oint \frac{dr}{p_r}}, \quad \omega_\varphi = \frac{\oint \frac{\ell dr}{r^2 p_r}}{\oint \frac{dr}{p_r}}, \tag{5.12}$$

with corresponding periods

$$T_r(E,\ell) = \frac{2\pi}{\omega_r} = \oint \frac{dr}{p_r} = 2 \int_{r_1(E,\ell)}^{r_2(E,\ell)} \frac{dr}{\sqrt{2(E - \Phi_{eff}(r))}} = \frac{\partial A(E,\ell)}{\partial E}, \tag{5.13}$$

$$T_\varphi(E,\ell) = \frac{2\pi}{\omega_\varphi} = \frac{2\pi}{\oint \frac{\ell dr}{r^2 p_r}} \oint \frac{dr}{p_r} = \frac{2\pi T_r}{\Delta\psi}, \quad \Delta\psi = -\frac{\partial A(E,\ell)}{\partial \ell}. \tag{5.14}$$

Note that the trajectories over the tori are closed if and only if the phase function $\Delta\psi(E,\ell)$ is a multiple rational of 2π.

Solution of Liouville equation: In terms of the action-angle variables (5.16) introduced previously, the Newtonian version of Liouville equation (5.15) reads

$$\frac{\partial f}{\partial t} + \{f, H\} = 0, \tag{5.15}$$

$$\frac{\partial f}{\partial t} + \omega_r \frac{\partial f}{\partial Q_r} + \omega_\varphi \frac{\partial f}{\partial Q_\varphi} = 0. \tag{5.16}$$

The most general solution of equation (5.16) is of the form

$$f(t,x,p) = F(Q_r - \omega_r(J_r, J_\varphi)t, Q_\varphi - \omega_\varphi(J_r, J_\varphi)t, J_r, J_\varphi), \tag{5.17}$$

with F a smooth function of the variables which is $2-\pi$ periodic in its first two entries.

The assumptions in the Arnold-Liouville theorem include the hypothesis for the subset $\mathcal{N}_c$ to be compact. In the relativistic cases this assumption is not satisfied. Here, the motion on the phase space is not bound in time direction, which implies that the invariant subset $\mathcal{N}_c$ are not compact. For the relativistic case, this supposition can be relaxed. In subsection II B of the reference [40], they discuss how generalized the action angle variables for non-compact level surfaces, through a generalization of the Liouville-Arnold theorem.

Chapter 6

Results in the research context

In this section I briefly review some results and ideas related to the material exposed in the appended papers (Papers I and Paper II).

In all our results, as mentioned previously, the self-gravity of the gas has been neglected, such that one solves the Liouville equation on a fixed but curved background geometry.

6.1 Accretion on Schwarzschild black hole background

The results developed in this section are interested because they describe new aspects of the relativistic kinetic gas' behavior, exhibiting differences between the case of a isotropic perfect fluid and the case of a relativistic kinetic gas.

The behavior of a relativistic kinetic gas around a Schwarzschild geometry, are studied in detail in the appended Paper I, and in the conference proceeding [41] the last one focused in the analysis of the results and their physical interpretation, that in this section will be partially presented through the analysis of relevant physical observables including the particle current density and the stress energy-momentum tensor.

To compute the observables, first we solve the Liouville equation using tools of integrable Hamiltonian system, and trivialize the Liouville vector field, founding the most general distribution function, that describes the accretion of a collisionless gas into a Schwarzschild black hole. It is important to note that in a collisionless case, the observables have three contributions: first, there is the contribution from the absorbed particles ($T^{\mu}{}_{\nu}{}^{abs}$), secondly the contributions

from the scattered part ($T^{\mu}{}_{\nu}{}^{scatt}$) and finally the contributions from the bound trajectories ($T^{\mu}{}_{\nu}{}^{bound}$). In accretion of particles that fall into a black hole, we are interested in two contributions $T^{\mu}{}_{\nu}{}^{tot} = T^{\mu}{}_{\nu}{}^{abs} + T^{\mu}{}_{\nu}{}^{scatt}$, that joined together constitute the accreted set of particles $T^{\mu}{}_{\nu}{}^{acc}$

In summary the total contribution to the stress-energy tensor is

$$T^{\mu}{}_{\nu} = T^{\mu}{}_{\nu}{}^{abs} + T^{\mu}{}_{\nu}{}^{scatt} + \cancel{T^{\mu}{}_{\nu}{}^{bound}} = T^{\mu}{}_{\nu}{}^{acc}, \tag{6.1}$$

analogously for the current density.
The set accreted trajectories Γ_{acc} consists of incoming trajectories (absorbed) and scattered (reflected) at the centrifugal barrier of the potential generated by the black hole.

To do explicit, applications we assume to the gas configuration is spherically symmetric and steady-state. In this case the distribution only depend on the conserved quantities $F(m, E, \ell)$ (mass, total energy and total angular momentum), here, for fixed values of the total energy, the total angular momentum plays the role of discriminate between infalling particles and the reflected particles.

The results in Paper I show that the particles that fall into the black hole contributes to the accretion rate, but not to the particle density at infinity n_∞, while the reflected particles do not contribute to the accretion rate, but contribute to the n_∞. Furthermore, we compute explicitly the accretion and compression rates, for an example assuming that asymptotically the particles are in thermodynamic equilibrium and are described through the distribution[1]

$$f(x,p) = \alpha\delta(\sqrt{-p^\mu p_\mu} - m)e^{-z\epsilon}, \tag{6.2}$$

where $z = \frac{mc^2}{k_B T}$. In the low temperature limit $z \to \infty$, we find that our result for the accretion rate coincides with the results based on Newtonian calculation in [16],

$$\dot{\mathcal{N}} \approx 4r_h^2 c\sqrt{2\pi z} n_\infty, \tag{6.3}$$

with c speed of light.Moreover, the result differs from the one in the isotropic perfect fluid case ($\dot{\mathcal{N}} \approx z^{3/2}$) by a factor of the order z. Additionally, we computed the energy density and the radial (p_{rad}) and tangential pressures (p_{tan}) at the horizon for low temperatures, finding that $p_{tan} \approx 10 \times p_{rad}$. This provides a partial explanation for the fact that the accretion rate is much smaller than in the Bondi-Michel case of a polytropic perfect fluid (that has $p_{tan} = p_{rad}$).

Here, we assume that the gas configuration is stady-state and spherically symmetric. We analyze the behavior and properties of the observables in detail. In particular, we analyze numerically the behavior of the observables for arbitrary temperatures and different values of the radial coordinate. Through

[1] Here, $\epsilon = E/(mc^2)$ denotes the energy in dimensionless quantities.

this, we observe the physical properties of a relativistic collisionless kinetic gas and its difference with the isotropic perfect fluid case. Finally, we present an argument about why the relativistic kinetic gas particles do not behave as an isotropic perfect fluid in the black hole vicinity, although at infinite it behaves like a perfect fluid.

In the following we summarize the principal results of this analysis. First we compute the particle accretion rate [2], and the energy accretion rate [3], that are explicitly given by

$$\dot{\mathcal{N}} = \frac{zc\pi r_h^2 n_\infty(z)}{4K_2(z)} \int_1^\infty \lambda_c(\epsilon)^2 e^{-z\epsilon} d\epsilon, \tag{6.4}$$

$$\dot{\mathcal{E}} = \frac{zmc^3\pi r_h^2 n_\infty(z)}{4K_2(z)} \int_1^\infty \epsilon\lambda_c(\epsilon)^2 e^{-z\epsilon} d\epsilon, \tag{6.5}$$

and one can analyze their dependency on the inverse temperature z and the dimensionless radial coordinate ξ. Here, n_∞ is the particle density at infinity, $K_2(z)$ is a Bessel function of the second kind, as defined in [42] and $\lambda_c(\epsilon)$ is the (dimensionless) critical value of the total angular momentum as a function of energy, below which the particles are absorbed (See Appendix A in [43]).
In figure 6.1 we plot the dimensionless quantities $\dot{\mathcal{N}}/({r_H}^2 cn_\infty)$ and $\dot{\mathcal{E}}/({r_H}^2 mc^3 n_\infty)$ as a function of the parameter z.

As seen in Figure 6.1, for high temperatures (small values of z), the particle accretion rate compared with the asymptotic value $\dot{\mathcal{N}}/({r_H}^2 cn_\infty)$ converges to a constant. In contrast, the energy accretion rate compared with the asymptotic rest energy of particles $\dot{\mathcal{E}}/({r_H}^2 mc^3 n_\infty)$, diverges like $\frac{1}{z}$. On the other hand, for low temperatures (hight values of z), both accretion rates grow like $\sqrt{z}$.

The explanation for this behavior, is that for small temperatures (the particles in the reservoir have low internal energy), most of the particles are absorbed by the black hole, contributing to a larger accretion rate (compared to $r_h^2 cn_\infty$). In contrast, at hight temperatures, only a small fraction of the infalling particles will be absorbed by the black hole, because most gas particles have large enough angular momenta $\lambda > \lambda_c(\epsilon)$ this yields a small value for $\dot{\mathcal{N}}$, but a large value of $\dot{\mathcal{E}}$ since these particles have high kinetic energy.

We compute the critical impact parameter b in the limit when the dimensionless radial coordinate $r \to \infty$ that is defining as $b = r\alpha_c$, with α_c the critical impact angle that can be computed from the relation $\cos\alpha = \frac{|p_3|}{|p|}$ [4] in the limit

[2] Number of particles that cross the horizon per unit time.
[3] Total energy crossing the horizon per unit time.
[4] Here, $p_3 = \sqrt{E^2 - m - \frac{\ell(E)^2}{r^2}}$ and $|p| = \sqrt{E^2 - m^2}$.

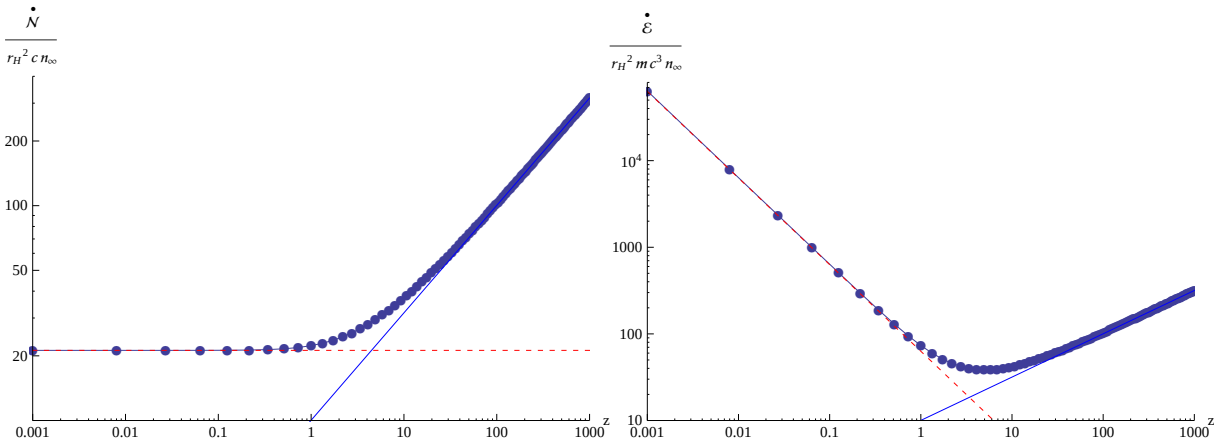

Figure 6.1: Particle and energy accretion rates as a function of the inverse temperature z. The solid blue lines describe the asymptotic behavior in the low temperature limit $z \to \infty$. The red dashed lines describe the behavior in the high temperature limit $z \to 0$.

of $r \to \infty$, $\cos\alpha \approx 1 - \frac{\alpha_c^2}{2} \approx 1 - \frac{\ell_c^2(E)}{2r^2(E^2-m^2)}$ with this the we find

$$b_c(\epsilon) = \frac{\ell_c(E)}{\sqrt{E^2-m^2}} = \frac{\lambda_c(\epsilon)}{2\sqrt{\epsilon^2-1}},$$

observe that for small temperatures $z \to \infty$, $b_c(\epsilon)$ increase, showing that in this case most particles are absorbed. For hight temperatures $z \to 0$ only a small quantity of particles (have $\epsilon > 1$) are absorbed, and the $b_c(\epsilon) \approx 13.5 r_h$ converges to a constant value. Nevertheless, the internal energy of each particle that is absorbed, carries much more energy, giving rise to a large accretion rate.

Comparison with the isotropic perfect fluid case.
We also compute the radial and tangential pressures p_{rad}, p_{tan} that are defined by $T^\mu{}_\nu e_r^\nu = p_{rad} e_r^\mu$, $T^\mu{}_\nu e_\vartheta^\nu = p_{rad} e_\vartheta^\mu$ [5]. We analyze the behavior of these pressures as a function of the dimensionless radial coordinate ξ for finite values of the inverse temperature z.

In figure 6.2 we illustrate two examples of comparison between the pressures divided by the rest mass energy nmc^2. We see here, that for large values of ξ, $\frac{p_{rad}}{nmc^2}$ and $\frac{p_{tan}}{nmc^2}$ are approximately equal to each other as expected. Nevertheless, as one approaches the horizon, $\frac{p_{tan}}{nmc^2}$ increases continuously while $\frac{p_{rad}}{nmc^2}$ decreases, implying that near the horizon, the distribution is anisotropic, which differs from the case of isotropic perfect fluid. The question is, why those models behaves differently from each other near the horizon, although they obey the

[5] Here, e_r is the unit outgoing radial eigenvector and $e_\vartheta = \frac{1}{r}\partial_\vartheta$.

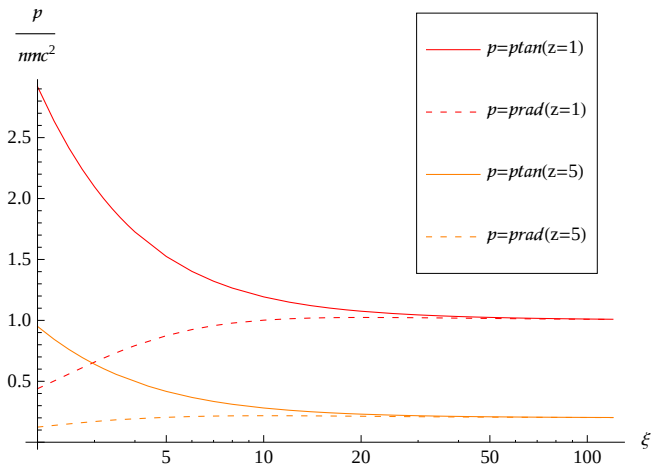

Figure 6.2: A comparison between the radial and tangential pressure profiles for two different values of z. The solid lines refer to the tangential pressure, the dashed lines to the radial one. While the ratio p_{tan}/p_{rad} converges to one as $\xi \to \infty$, it increases as one approaches the horizon, reaching a value of about 5 for $z = 1$ and about 8 for $z = 5$.

same boundary conditions at infinity. One might think naively that in some limit the kinetic model should have reproduced the hydrodynamic flow [6].

One of the key points is that in our model, we neglected collisions. Although, we use that our distribution function in equation (6.2) corresponds to an equilibrium distribution function at infinity, in fact it is not an equilibrium distribution function at finite radius. We remember that in our model [43] the support of the distribution function is restricted to a region on the phase space Γ_{accr}, that corresponds to particle trajectories of physical interest, where we have eliminated the contributions of the bound trajectories. It is clear that contributions from bound trajectories would not affect the observables in the vicinity of the horizon. Most important is the fact that, the restriction to Γ_{accr} also eliminates the possibility of those particles occupying trajectories that emanate from the white hole (see Fig. 6.3) and these contributions, could affect the observables near the horizon. Then, the subspace Γ_{accr} in some sense is truncated, because the particles do not collide and some trajectories will never be occupied. So, the distribution is not an equilibrium distribution function at finite radius.

To understand the limit to hydrodynamic equations, we should take into account collisions. In this case a binary collision may cause an unoccupied

[6]The hydrodynamic equations can be obtained as an appropriate limit of a kinetic gas if we include collisions. For the Newtonian case, see [1, 44], for the relativistic case, see [6, 45]

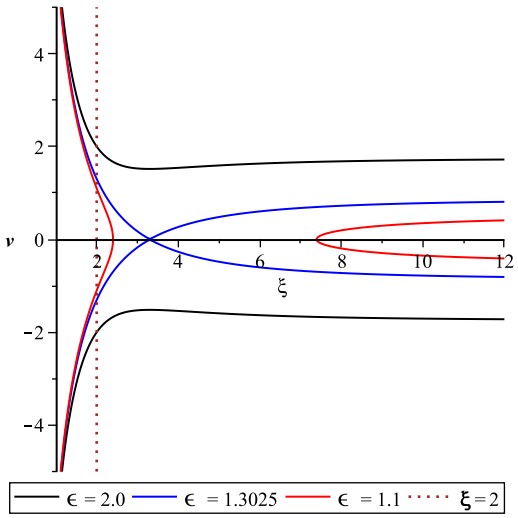

Figure 6.3: (adapted from Fig. 2 in [43]) Projection of the phase diagram onto to $(\xi, v = \dot{r}/mc)$-plane illustrating the particle trajectories for different energy levels ε and total dimensionless angular momentum $\lambda = 6$. The black curve in the region $v < 0$ corresponds to an incoming particle from infinity which is absorbed by the black hole, while the black curve in the region $v > 0$ describes an outgoing particle that is emitted from the white hole and escapes to infinity. The red curve in the region $\xi > 6$ describes a particle that is incoming from infinity but has large enough angular momentum $\lambda > \lambda_c(\varepsilon)$ to be reflected at the potential barrier, and the red curve in the region $\xi < 3$ describes a particle that is emitted by the white hole, is reflected at the potential barrier and absorbed by the black hole. The blue curve describes the separatrix and corresponds to the energy level ε such that $\lambda_c(\varepsilon) = \lambda$.

trajectory to become occupied after the collision takes place. In this case, it does not make sense to restrict the phase space to Γ_{accr}, and the bound trajectories and those emanating from the white hole have to be taken into account. We hope to analyze the effects of collisions in future work.

6.2 Mixing phenomenon

As mentioned previously in Sec. 2, the mixing phenomenon plays an important role as a mechanism where the distribution function that describes a kinetic gas relaxes in time to a stationary configuration.

As a pedagogical introduction, we will introduce the mixing theorem in a "toy model", where the mathematical proof is based on work by Mohout-Villani [28]. First we start introducing our "toy model", which consists in a collisionless, simple (each particle have the same positive mass m that we rescale to one), kinetic gas in one-space dimension which is subject to an external potential $V : I \to \mathbb{R}$, on an interval $I = (a, b)\,, -\infty \leq a < b \leq \infty$. We assume that V is C^∞ smooth, has a unique, non-degenerate stationary point at $x = x_0$ and that $V(x) \to \infty$ when $x \to a$ or $x \to b$, such that $x = x_0$ is a stable equilibrium point with minimum energy $E_0 = V(x_0)$ and such that all the orbits with energy $E > E_0$ are bound and periodic trajectories, with period

$$T(E) := 2 \int_{x_1(E)}^{x_2(E)} \frac{dx}{\sqrt{2(E - V(x))}}, \tag{6.6}$$

with $x_1(E) < x_2(E)$ the turning points of the orbit.
The system is described by a one-particle distribution function in one spatial dimension and time dependence $f(t, x, p)$. This distribution describes the state of the kinetic gas at time t. It is a nonnegative function $f(t, \cdot, \cdot) : \Gamma \to \mathbb{R}$, where the phase space is denoted by $\Gamma := I \times \mathbb{R}$. The dynamics of the distribution satisfies the Liouville or Vlasov equation,

$$\frac{\partial f}{\partial t} + \{H, f\} = \frac{\partial f}{\partial t} + p\frac{\partial f}{\partial x} - \frac{\partial V}{\partial x}\frac{\partial f}{\partial p} = 0. \tag{6.7}$$

In the Newtonian case considered in this "toy" example, the Hamiltonian is given by $H(x, p) = p^2/2 + V(x)$. Given an initial distribution at time $t = 0$, f_0 (in the space $L^1(\Gamma)$ of Lebesgue integrable functions on Γ), Eq. (6.7) possesses a unique solution $f(t, \cdot, \cdot)$ for all $t \in \mathbb{R}$ such that $f(0, \cdot, \cdot) = f_0$.

Now, we introduce a test function $\varphi \in C_0^\infty(\Gamma)$ on phase space.

We consider the time-dependent observable which is obtained by integrating the product of the distribution function with φ [7]

$$N_\varphi(t) := \int_\Gamma f(t, x, p)\varphi(x, p)dxdp. \tag{6.8}$$

A physical interpretation of the test function is that φ can be thought of a device which measures the properties of the system (e.g. energy, mean velocity etc.)

[7] Note that here time is absolute. In the relativistic case, the proof and formulation of the theorem is presented in Paper II [22]

in a small region of phase space, and N_φ is the corresponding value measured by this device, where f describes the state of the gas[8].

The question is, what is the asymptotic behavior of N_φ for large times. Naively, we think that N_φ should oscillate in time, because this represents an average over a distribution of particles that oscillates within the potential. However, the limit of the observable $\lim_{t\to\infty} N_\varphi(t)$ exists and can be calculated from the initial data f_0, as we explain now.

As explained previously, the solution of the Liouville equation (6.7) can be represented explicitly in terms of action-angle variables (Q, J) on phase space Γ [37, 38]. The action variable J (the area enclosed by $C(E)$ in phase space divided by 2π) labels the energy surfaces $C(E)$ [9] and is defined by

$$J(E) := \frac{1}{2\pi} \oint_{C(E)} p dx = \frac{1}{\pi} \int_{x_1(E)}^{x_2(E)} \sqrt{2(E - V(x))} dx. \tag{6.9}$$

As such, $J : (E_0, \infty) \to (0, \infty)$ is a smooth function which is invertible, as $\frac{dJ}{dE}(E) = \frac{T(E)}{2\pi} > 0$. The corresponding angle variable is

$$Q(x, p) := \frac{2\pi}{T(E)} \int_{\gamma_x} \frac{dx}{p}, \tag{6.10}$$

where γ_x is a curve which connects the turning points $x_1(E)$ with some given point (x, p) along the curve $C(E = H(x, p))$, oriented clock-wise. Along a full revolution $C(E)$ this variable changes by a factor of 2π; hence it describes an angle along $C(E)$. The pair (Q, J) defines smooth symplectic coordinates on phase space. The phase space in terms of the new variables (Q, J) is denoted by Γ_0 that is the phase space Γ minus the equilibrium point, that is defined as $\Gamma_0 := \Gamma \setminus \{(x_0, 0)\}$ and has topology $S^1 \times (0, \infty)$.

In terms of the new variables (Q, J) the Hamiltonian becomes a function only of the action variable J, and consequently the Liouville equation (6.7) reduces to the simple form

$$\frac{\partial f}{\partial t} + \omega(J) \frac{\partial f}{\partial Q} = 0, \qquad \omega(J) := \frac{dH}{dJ} = \left(\frac{dJ}{dE}\right)^{-1} = \frac{2\pi}{T(E)}, \tag{6.11}$$

and the most general solution is trivially found:

$$f(t, x, p) = F(Q - \omega(J)t, J), \tag{6.12}$$

where $F : S^1 \times (0, \infty) \to \mathbb{R}$ a smooth function of the variables (Q, J), which parametrizes the initial datum as, $f_0(x, p) = F(Q, J)$. Thus, as expected, the

[8] This observable definition, was be explained before in 3.4, where you can see more details about the relativistic prescription of this definition.

[9] $C(E)$ is a closed curve in phase space.

time evolution of the distribution function corresponds to a rotation on each energy surface $C(E)$ with constant angular velocity $\omega(J)$.

In the completely degenerate case the frequency ω is independent of the energy surface $C(E)$, in which case each of these rotations is in phase and there is no mixing in phase space. However, when the frequencies $\omega(J)$ are different on each energy curve, the phase space flow stretches and spreads the distribution function over the phase space, giving rise to the mixing property.

To illustrate the ideas presented in the previous paragraph, we explore the behavior of the distribution Eq. (6.12) by means of two examples. The first example shown in Fig. 6.4 is a screenshots of the time evolution behavior of the one-particle distribution function, which is plotted on the phase space for some initial datum. This example physically represents a set of relativistic kinetic gas particles under the influence of an harmonic oscillator potential $H_0(x,p) = \frac{p^2}{2} + \frac{x^2}{2}$. Here, the frequency $\omega(J) = 1$ is constant. The second one is an example where the potential is a perturbed harmonic oscillator with a quadratic term $H = H_0(x,p) + \epsilon x^4$. Now, the frequency changes according to $\omega(J) = 1 + \frac{3}{8}\epsilon J$, see Fig. 6.5.
The initial datum at $t = 0$ is taken to be

$$f_0\,(x,p) = e^{-\frac{(x-\bar{x}_0)^2}{\sigma}} e^{-\frac{(p-p_0)^2}{\sigma}}, \quad (x,p) \in \mathbb{R}^2 \tag{6.13}$$

From the plots in 6.5 and 6.4 we observe that the distribution function spreads and stretches over the phase space in a perturbed harmonic oscillator case in contrast with the unperturbed case where distribution just rigidly rotates in phase space.

One-dimensional phase space mixing Theorem
Let $\varphi, f_0 \in C_0^\infty(\Gamma)$ and let $f(t,x,p)$ be the unique solution of equation (6.7) with initial datum $f(0,x,p) = f_0(x,p)$ for all $(x,p) \in \Gamma_0$.
Suppose that for all $E > E_0$,

$$\frac{dT}{dE}(E) \neq 0. \tag{6.14}$$

Then,

$$\lim_{t\to\infty} N_\varphi(t) = \int_{\Gamma_0} \langle f_0 \rangle_{C(E)}(x,p)\varphi(x,p)dxdp, \tag{6.15}$$

where $\langle f_0 \rangle_{C(E)}$ denotes the average of f_0 over the energy surface $C(E) = \{(x,p) \in \Gamma_0 : H(x,p) = E\}$. Therefore, the observable converges in time to the one obtained from averaging the initial distribution function f_0 over each orbit.

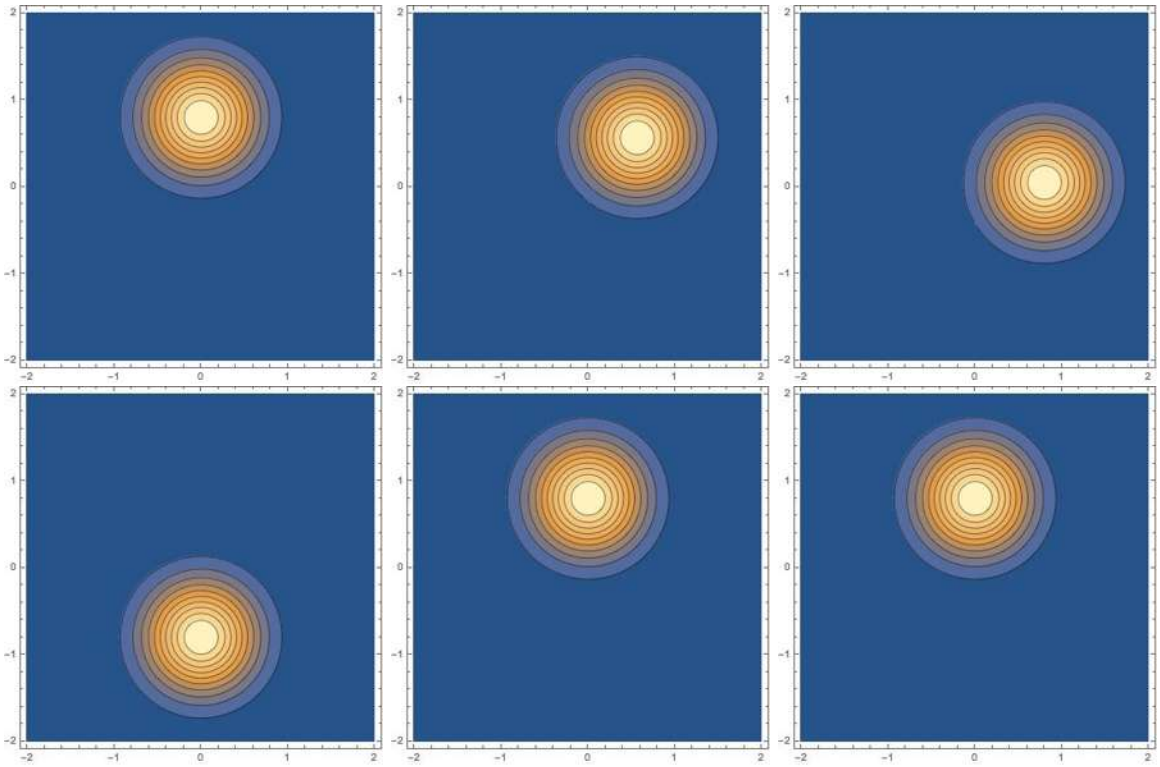

Figure 6.4: Snapshots at times $t = 0$, $\frac{\pi}{4}$, $\frac{\pi}{2}$, π, 20π, 30π of the evolution of the distribution function corresponding to initial datum (6.13) with values of $\sigma = 0.6$, $p_0 = 0.8$ and $x_0 = 0$ in the harmonic oscillator model.

Here, the average distribution, over each energy curve is explicitly defined as

$$\langle f\rangle_{C(E)} = \langle f_0\rangle_{C(E)} = \frac{1}{2\pi}\int_0^{2\pi} F(Q,J)dQ.$$

The proof of the theorem

For a pedagogical explanation, here we exclude the equilibrium point for which $E = E_0$, and restrict ourselves to the subset $(x,p) \in \Gamma_0 := \Gamma \setminus \{(x_0,0)\}$ consisting of points lying away from the equilibrium point. On this set the one-particle distribution function has the form (6.12)

$$f(t,x,p) = F(Q - \omega(J)t, J),$$

with $(Q,J) \in S^1 \times (0,\infty)$ the action-angle coordinates parametrizing the point $(x,p) \in \Gamma_0$, where the one particle-distribution function in these coordinates is $F : S^1 \times (0,\infty) \to \mathbb{R}$ a smooth function which parametrizes the initial datum

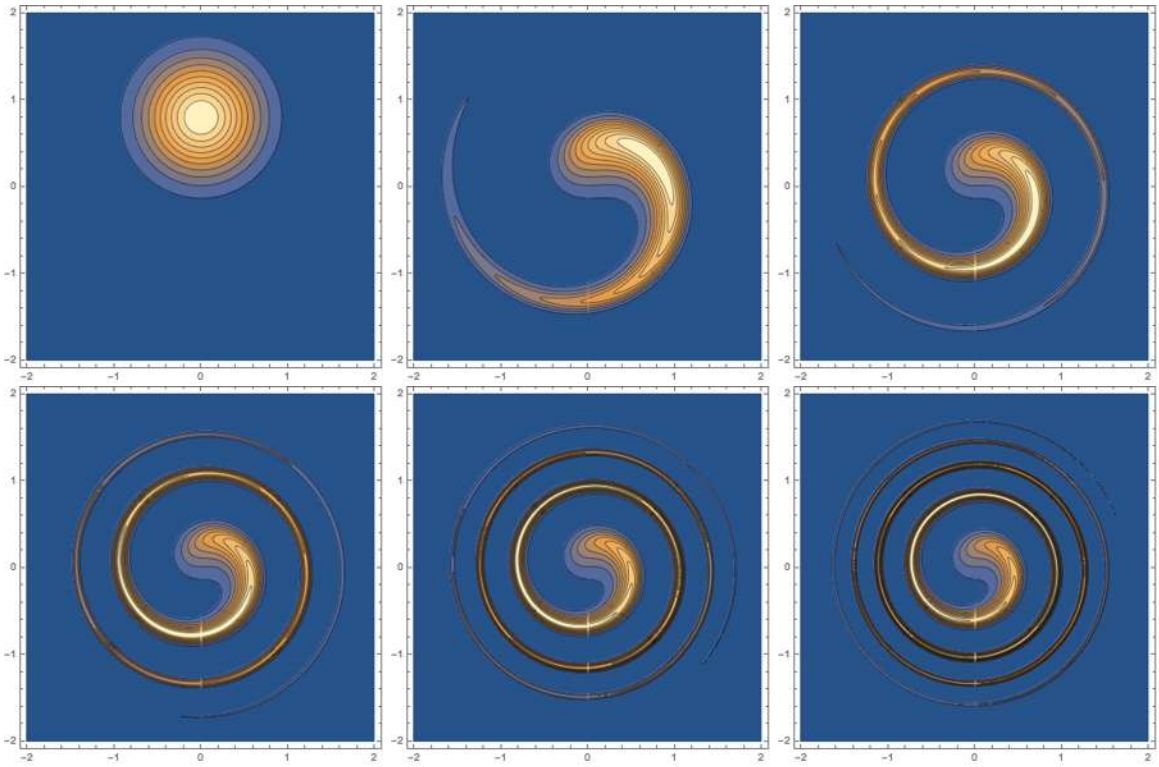

Figure 6.5: Snapshots at times $t = 0$, 10π, 20π, 30π, 40π and 50π, of the evolution of the distribution function corresponding to initial datum (6.13) with values of $\sigma = 0.6$, $p_0 = 0.8$ and $\tilde{x}_0 = 0$ and the value of perturbation $\epsilon = 0.3$ in the perturbed harmonic oscillator model.

given en terms of $f_0(x,p) = F(Q,J)$.

The non-degeneracy condition (6.14) implies that the frequency function $\omega : (0,\infty) \to \mathbb{R}$ defined in equation (6.11) depends monotonically on J, and hence it is possible to invert this relation to express J in terms of ω. Thereby, instead of the function F that describes the solution in (6.12) we consider the new function $G : S^1 \times \mathbb{R} \to \mathbb{R}$ defined by

$$G(Q,\omega) := \begin{cases} F(Q,J)\left|\frac{d\omega}{dJ}(J)\right|^{-1}, & \omega_{min} < \omega < \omega_{max}, \\ 0, & \text{otherwise}, \end{cases} \tag{6.16}$$

where $(\omega_{min}, \omega_{max})$ [10] denotes the image of $\omega : (0,\infty) \to \mathbb{R}$. Note that since the transformation $(x,p) \mapsto (Q,J)$ is symplectic the volume form is preserved.

[10] The precise form of the image $(\omega_{min}, \omega_{max})$ is irrelevant for the proof; generally it must be found by analyzing the explicit value of the potential $V(x)$.

Hence the integration of the one-particle distribution on the phase-space, is equivalent in terms of (6.16) to

$$\int_{\Gamma} f_0(x,p)dxdp = \int_0^{\infty}\int_0^{2\pi} F(Q,J)dQdJ = \int_{-\infty}^{\infty}\int_0^{2\pi} G(Q,\omega)dQd\omega.$$

Note that $G \in L^1(S^1 \times \mathbb{R})$ if and only if $F \in L^1(S^1 \times (0,\infty))$, that is equivalent to $f_0 \in L^1(\Gamma_0)$ which is satisfied according to the hypothesis of the theorem.

Next we define the function $\Psi : S^1 \times \mathbb{R} \to \mathbb{R}$ to be the one corresponding to the test function φ written in terms of the coordinates such that

$$\Psi(Q,\omega) := \begin{cases} \varphi(x,p) & \forall \quad (x,p) \in \Gamma_0, \\ 0, & \forall \quad \omega \notin (\omega_{min}, \omega_{max}). \end{cases} \tag{6.17}$$

One can rewrite the observable N_φ in terms of Eqs. (6.16,6.17) as

$$N_\varphi(t) = \int_{\Gamma} f(t,x,p)\varphi(x,p)dxdp = \int_{-\infty}^{\infty}\int_0^{2\pi} g_t(Q,\omega)\Psi(Q,\omega)dQd\omega, \tag{6.18}$$

where the time dependence lies in the function g_t:

$$g_t(Q,\omega) := G(Q - \omega t, \omega). \tag{6.19}$$

The advantage of parametrizing the distribution and test function in terms of the frequency ω instead of J, is that in this representation (6.19) is formally equivalent to the distribution function for a collisionless kinetic gas on a periodic interval, with Q and ω corresponding to the position and velocity, respectively, of the particle. The problem now can be treated using standard Fourier techniques[11].
We can express the one-particle distribution function extended labeled as (6.19) on the Fourier coefficients in the following steps

[11] See Sec.4 in the article by Mohout and Villani [28]

$$g_t(Q,\omega) = \int_{-\infty}^{\infty}\int_{0}^{2\pi} G(Q-\omega t,\omega)dQd\omega, \tag{6.20}$$

$$\hat{g}_t(k,\eta) = \frac{1}{2\pi}\int_{-\infty}^{+\infty}\int_{0}^{2\pi} G(Q-\omega t,\omega)e^{-ikQ}e^{-i\eta\omega}dQd\omega, \tag{6.21}$$

$$= \frac{1}{2\pi}\int_{-\infty}^{+\infty}\int_{0}^{2\pi} G(Q',\omega)e^{-ik(Q'+\omega t)}e^{-i\eta\omega}dQ'd\omega \tag{6.22}$$

$$= \frac{1}{2\pi}\int_{-\infty}^{+\infty}\int_{0}^{2\pi} G(Q',\omega)e^{-ikQ'}e^{-i\omega(\eta+kt)}dQ'd\omega \tag{6.23}$$

where we have used the variable substitution $Q' = Q - \omega t$. Therefore,

$$\hat{g}_t(k,\eta) = \hat{G}(k,\eta+kt) = \frac{1}{2\pi}\int_{-\infty}^{+\infty}\int_{0}^{2\pi} G(Q,\omega)e^{-ikQ}e^{-i\omega(\eta+kt)}dQd\omega, \tag{6.24}$$

for the one-particle distribution function on the phase space that satisfied the Liouville equation (i.e have a explicit and particular relation between the time and action-angle variables). Expressed in the Fourier space with the non-degeneracy condition, reveals the particular relation $\hat{g}_t(k,\eta) = \hat{G}(k,\eta+kt)$. This means that a rotation in the Q variable in phase-space is transformed in a translation in time in the frequency space. More precisely, as mentioned in [28] *"phase space mixing transfers the energy from each nonzero spatial frequency k, to large velocity frequencies η and this transfer occurs at a speed proportional to k"*.

To see the behavior in the limit, when $t \to \infty$, we use the Riemann-Lebesgue lemma, see for instance [46]. This formally requires that the distribution G will be bound and $f(t,\cdot,\cdot) \in L^1(\Gamma)$ as was mentioned before. Therefore, $\lim_{t\to\infty}\hat{g}(t,k,\eta) = \hat{G}(k,\infty) = 0$, for $k \neq 0$ and only the mode $k = 0$ survives. With this we can write

$$\lim_{t\to\infty}\hat{g}(t,k\eta) = \delta_{k,0}\hat{G}(0,\eta) := \hat{g}_\infty(k,\eta). \tag{6.25}$$

returning to the phase-space, the corresponding function $g_\infty(Q,\omega)$ is obtained

from the inverse Fourier transform

$$g_\infty(Q,\omega) = \frac{1}{2\pi}\int_{-\infty}^{+\infty}\sum_{k=-\infty}^{\infty}\delta_{k,0}\hat{G}(0,\eta)e^{ikQ}e^{i\eta\omega}d\eta, \tag{6.26}$$

$$g_\infty(Q,\omega) = \frac{1}{2\pi}\int_{-\infty}^{+\infty}\hat{G}(0,\eta)e^{i\eta\omega}d\eta,$$

$$g_\infty(Q,\omega) = \frac{1}{(2\pi)^2}\int_{-\infty}^{+\infty}\int_{-\infty}^{+\infty}\int_{0}^{2\pi}G(Q',\omega')e^{-i\eta\omega'}dQ'd\omega'e^{i\eta\omega}d\eta, \tag{6.27}$$

developing the integration over η

$$g_\infty(Q,\omega) = \frac{1}{2\pi}\int_{-\infty}^{+\infty}\int_{0}^{2\pi}G(Q',\omega')\delta(w-w')dQ'd\omega',$$

$$g_\infty(Q,\omega) = \frac{1}{2\pi}\int_{0}^{2\pi}G(Q',\omega)dQ' = \langle G\rangle_{C(E)}(Q,\omega), \tag{6.28}$$

Therefore, we find the limit function $g_\infty(Q,\omega)$ is just the average of the distribution function defined in (6.16).
Next, the observable $N_\varphi(t)$ is obtained using **Parseval identity**. Remember that, for two functions that both are 2π periodic in Q, the product

$$(g(Q),f(Q)) = \int_0^{2\pi}g^*(Q)f(Q)dQ = \sum_{k=-\infty}^{+\infty}\hat{g}_k^*\hat{f}_k, \tag{6.29}$$

and for two functions $G(x)$ and $F(x)$ that not are periodic in x, but L^2- integrable

$$(G,F) = \int_{-\infty}^{\infty}G^*(x)F(x)dx = \int_{-\infty}^{+\infty}\hat{G}^*(k)\hat{f}(k)dk = \left(\hat{G},\hat{F}\right). \tag{6.30}$$

Using this, we can express $N_\varphi(t)$ in the following manner

$$N_\varphi(t) = \int_{-\infty}^{\infty}\int_{0}^{2\pi}g(t,Q,\omega)\Psi(Q,\omega)dQd\omega \tag{6.31}$$

$$= \int_{-\infty}^{+\infty}\sum_{k=-\infty}^{\infty}\hat{g}^*(t,k,\eta)\hat{\Psi}(k,\eta)d\eta. \tag{6.32}$$

In order to calculate the limit $t \to \infty$ for the observable, we use Lebesgue's dominated convergence theorem. For this, we should bound the integrand:

$$|\hat{g}(t,k,\eta)\hat{\Psi}(k,\eta)| \quad \leq \quad H\,(k,\eta) \quad such \quad that \int_{-\infty}^{\infty} \sum_{k} H(k,\eta)d\eta < \infty.$$

Indeed

$$\begin{aligned} |\hat{g}(t,k,\eta)| \cdot |\hat{\Psi}(k,\eta)| \quad &\leq \quad H\,(k,\eta)\,, \quad H\,(k,\eta) = \frac{\|G\|_{L^1}}{2\pi}|\hat{\Psi}(k,\eta)|, \\ since \qquad &|\hat{G}(k,\eta+kt)| \leq \frac{\|G\|_{L^1}}{2\pi} \end{aligned} \tag{6.33}$$

and $\hat{\Psi}$ is a Schwartz function, so we can apply Lebesgue's dominated convergence theorem [47].
Using again the Parseval identity and the relation (6.28), we obtain

$$\begin{aligned} \lim_{t\to\infty} N_\phi(t) \quad &= \quad \int_{-\infty}^{+\infty} \sum_{k=-\infty}^{\infty} \hat{g}^*_\infty(k,\eta)\hat{\Psi}(k,\eta)d\eta = \int_{-\infty}^{+\infty}\int_{0}^{2\pi} g_\infty(k,\eta)\Psi(Q,\omega)dQd\omega, \\ &= \quad \int_{-\infty}^{+\infty}\int_{0}^{2\pi}\left(\frac{1}{2\pi}\int_{0}^{2\pi} G(Q',\omega)dQ'\right)\Psi(Q,\omega)dQd\omega. \end{aligned} \tag{6.34}$$

Returning to the variable J with the condition (6.14), and reexpresing the distribution function G in terms of F,

$$\lim_{t\to\infty} N_\varphi(t) \quad = \quad \int_{-\infty}^{+\infty}\int_{0}^{2\pi}\left(\frac{1}{2\pi}\int_{0}^{2\pi} F(Q',J)dQ'\frac{dJ}{d\omega}\right)\Psi(Q,\omega(J))dQd\omega \tag{6.35}$$

$$= \quad \int_{0}^{+\infty}\int_{0}^{2\pi} \langle F(J)\rangle\,\Psi(Q,\omega(J))dQdJ, \tag{6.36}$$

where we have used the fact that $\langle F(J)\rangle = \frac{1}{2\pi}\int_0^{2\pi} F(Q',J)dQ'$ is the average of the one-particle distribution function over the Q variable (i.e each energy curve) on the phase space.
Finally, in terms of the variables (x,p), we have that

$$\lim_{t\to\infty} N_\varphi(t) = \int_\Gamma \langle f_0\rangle_{C(E)}\,\varphi(x,p)dxdp.$$

This concludes the proof of the theorem for the case that the equilibrium point is non contained in the support of φ. The generalization of the proof for the case in the support of φ will be give in [48].

To illustrate the conclusion of the theorem with the examples of the harmonic oscillator and the perturbed harmonic oscillator mentioned above, we plot in Fig. 6.6 the asymptotic behavior of an observable ρ_m at a fixed point x_0, defined as the particle density and given by the equation, $\rho_m(t, x_0) = \int_{-\infty}^{\infty} f(t, x_0, p)pdp$, the evolution of the particle density in time calculated from the solution for the distribution function (6.12), and from initial datum of the form (6.13). Here, for the perturbed case (frequency is not constant) the convergence of the observable in time is observed, in contrast with the oscillation of the observable in the unperturbed case.

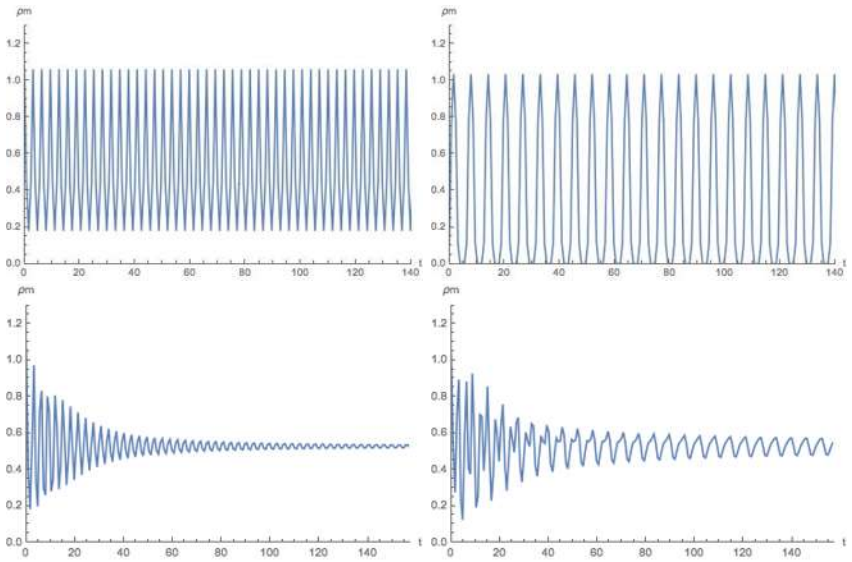

Figure 6.6: Snapshots of mass density for the harmonic oscillator (top panels) for different points $x_0 = 0$, $x_0 = 0.9$, and for the perturbed harmonic oscillator (bottom panels) for different points $x_0 = 0$, $x_0 = 0.1$. The evolution of the mass density is numerically obtained, and correspond to initial datum of the form (6.13) with values of $\sigma = 0.6$, $p_0 = 0.8$ and $\tilde{x}_0 = 0$ and the value of perturbation $\epsilon = 0.3$ in the perturbed harmonic oscillator case.

In Paper II we use this "toy model idea" to formulate and prove an analogue theorem of the mixing over the equatorial plane of a Kerr black hole. To prove this, first we study the bound trajectories for the geodesic flux that are represented analytically in terms of action-angle variables (which in turn are express

in terms of elliptics integrals). In the Kerr case, the complications come from the fact that time is not absolute and how to define the observables in these cases. The details of the proof are given in Paper II appended in the next section.

For applications of the mixing property in a dark matter halo, see the paper [20]. Here, the collisionless kinetic gas particles corresponds to a physical inhomogeneities (spherical perturbation) of the halo. The authors, directly integrate numerically the Vlasov equation in spherical symmetry and with fixed total angular momentum for different models of galactic halo (Isothermal, Isothermal-turncated, NFW, Burkert), they find that the distribution reaches a stationary state which is named "virialization" of the system for the authors, but this corresponds to a consequence of the theorem. More details about the application of the theorem to find the final state of the system and the respective comparison with this dark matter application, will be show in [48].

Appended Papers

Part II

Appended Paper I:

Accretion of a relativistic, collisionless kinetic gas into a Schwarzschild black hole.

IOP Publishing Classical and Quantum Gravity

Class. Quantum Grav. **34** (2017) 095007 (48pp) https://doi.org/10.1088/1361-6382/aa65fa

Accretion of a relativistic, collisionless kinetic gas into a Schwarzschild black hole

Paola Rioseco and Olivier Sarbach

Instituto de Física y Matemáticas, Universidad Michoacana de San Nicolás de Hidalgo, Edificio C-3, Ciudad Universitaria, 58040 Morelia, Michoacán, Mexico

E-mail: prioseco@ifm.umich.mx and sarbach@ifm.umich.mx

Received 14 November 2016, revised 24 February 2017
Accepted for publication 10 March 2017
Published 4 April 2017

Abstract

We provide a systematic study for the accretion of a collisionless, relativistic kinetic gas into a nonrotating black hole. To this end, we first solve the relativistic Liouville equation on a Schwarzschild background spacetime. The most general solution for the distribution function is given in terms of appropriate symplectic coordinates on the cotangent bundle, and the associated observables, including the particle current density and stress energy-momentum tensor, are determined. Next, we explore the case where the flow is steady-state and spherically symmetric. Assuming that in the asymptotic region the gas is described by an equilibrium distribution function, we determine the relevant parameters of the accretion flow as a function of the particle density and the temperature of the gas at infinity. In particular, we find that in the low temperature limit the tangential pressure at the horizon is about an order of magnitude larger than the radial one, showing explicitly that a collisionless gas, despite exerting kinetic pressure, behaves very differently than an isotropic perfect fluid, and providing a partial explanation for the known fact that the accretion rate is much lower than in the hydrodynamic case of Bondi–Michel accretion. Finally, we establish the asymptotic stability of the steady-state spherical flows by proving pointwise convergence results which show that a large class of (possibly nonstationary and nonspherical) initial conditions for the distribution function lead to solutions of the Liouville equation which relax in time to a steady-state, spherically symmetric configuration.

Keywords: relativistic kinetic theory, black hole accretion, integrable Hamiltonian systems

(Some figures may appear in colour only in the online journal)

1. Introduction

The relativistic kinetic theory of gases started over 100 years ago with papers by Jüttner [1, 2] who generalized the well-known Maxwell–Boltzmann distribution function to the special relativistic case. Over the years, the theory was further developed and cast into the context of general relativity, see for example [3–6]. By now, the formal structure of the theory is well understood, and manifestly covariant formulations based on the tangent bundle associated with the spacetime manifold have been given which exploit their natural metric and symplectic structures, see for instance [7–12] and references therein.

Recently, there has been a growing interest in applications of the theory, both from a mathematical and an astrophysical point of view. From the point of view of mathematical relativity, there has been a lot of activity in studying the qualitative properties of the solutions of the Einstein–Liouville system[1] of equations, describing a self-gravitating collisionless gas, see [13] for a recent review on this topic. These studies include the analysis of the well posedness of the Cauchy problem and the existence of global in time solutions and their asymptotic properties with applications to the nonlinear stability of Minkowski spacetime [14–17] and the future stability of the Universe [18–20]. Other works analyze the complete gravitational collapse of a collisionless kinetic gas (see for instance [21–23] and [24] and references therein for numerical work on critical collapse), which constitutes a more general model than the simple dust collapse one which, as is well-known, leads to the formation of naked shell-focusing singularities [25–27]. Further mathematical results establish the existence of static, spherically symmetric solutions [28–30] (see [31] for related numerical work) or axisymmetric solutions which are either static or stationary (see [32, 33] for recent work and [34] for a related numerical study). A further interesting, more difficult problem is the stability analysis of these solutions. For a numerical investigation in spherical symmetry, see [35]. For work on the relativistic Boltzmann equation including the collision term, see for instance [36–38].

Regarding applications towards astrophysics, the relativistic kinetic theory of gases is playing an increasingly important role in view of recent and near-future observations of supermassive black holes in the center of galaxies, like the ones in the Milky Way and M87, at scales smaller than their gravitational radius [39]. These observations often require specific models for describing the matter and plasma surrounding such black holes, and clearly a fully consistent description should be based on a general relativistic formulation. Other astrophysical applications of the relativistic kinetic theory include the description of a distribution of stars around a supermassive black hole (see [40, 41] for standard references based on the Newtonian approximation and [42] for a relativistic treatment based on N-body simulations) and the modeling of dark matter (see, for instance [43]). The relativistic Boltzmann equation also plays an important role in the modeling of the early Universe [44]; see also [45, 46] for related recent analytic work.

Although none of these astrophysical applications will be directly addressed in the present work (only a simpler astrophysical example will be discussed in section 5), they serve as a motivation for a thorough mathematical investigation for the propagation of a relativistic kinetic gas on a curved spacetime geometry. In this work, we initiate such a systematic study for the case in which the spacetime is generated by an isolated black hole. More specifically, we work under the assumption that the gas is sufficiently diluted for its self-gravity to be neglected. Assuming that no other matter sources are present and that the accretion rate is

[1] In this article, we denote by the 'Liouville equation' the collisionless Boltzmann equation, which is also known as the 'Vlasov equation' in the literature.

small enough such that the black hole can be considered to be stationary, the no-hair theorems [47] imply that the spacetime geometry belongs to the two-parameter family of Kerr solutions, which are characterized by their mass and angular momentum. For simplicity, we further assume that the rotation of the black hole can be neglected, in which case the background spacetime reduces to the Schwarzschild geometry. Finally, we work on the hypothesis that collisions between the gas particles can be neglected. Therefore, the gas in our model is described by a one-particle distribution function satisfying the relativistic Liouville equation on a Schwarzschild background. A study towards more realistic models relaxing some of these assumptions will be provided in future work.

The main results presented in this article are the following: (i) we derive the most general collisionless distribution function on a Schwarzschild background. This derivation is based on the theory of integrable Hamiltonian systems and parallels the earlier presentation in [12] for the Kerr background. However, in contrast to the result derived in [12], here we also compute the spacetime observables (namely, the current density and the stress energy-momentum tensor). Furthermore, in this work the distribution function and the observables are expressed in terms of horizon-penetrating coordinates which facilitates their interpretation on the horizon. We emphasize that although the spacetime metric is static and spherically symmetric, our solutions for the distribution function and the corresponding observables do not necessarily posses any symmetries (in particular they could be time-dependent and nonspherical). (ii) As a specific example of astrophysical interest, we specialize our result to the case where the distribution function is static and spherically symmetric and we provide explicit expressions for the observables assuming that in the asymptotic region the distribution function is described by an equilibrium distribution function. Next, we apply these results to the spherical accretion problem and compute the accretion and compression rates of the gas. Finally, in the low-temperature limit, we compare our results to previous calculations based on the Newtonian approximation [48, 49] and find agreement. By computing the radial and tangential pressures at the horizon, we also shed light on the reason for which the accretion rate is much lower than in the corresponding Bondi–Michel accretion models [50–52] in the hydrodynamic case. (iii) Finally, we study the nonlinear stability of the static, spherically symmetric solutions described in (ii). To this end, we consider initial data for the distribution function on a hypersurface in phase space of constant time t which is not necessarily spherically symmetric, but converges (in an appropriate sense) to a function $f_\infty(E)$ depending only on the energy E of the gas particles in the asymptotic region $r \to \infty$. Further assuming that this initial distribution function is uniformly bounded by an equilibrium distribution function and only populates unbounded trajectories, we analyze the behavior of the observables along the world lines of future-directed timelike observers reaching timelike infinity. Assuming that these observers have a constant asymptotic, purely radial velocity, we prove that the components of the particle current density and stress energy-momentum tensor with respect to a Fermi-propagated frame converge pointwise to those computed from $f_\infty(E)$, thus establishing the stability of the static, spherically symmetric solution belonging to $f_\infty(E)$. In particular, the observables decay pointwise to zero if $f_\infty = 0$, meaning that in this case the gas disperses completely.

The remainder of this article is organized as follows. In section 2 we provide a brief review of the geometrical structures that are relevant for the formulation of relativistic kinetic theory in this work. Contrary to many previous works in the literature which are based on the tangent bundle TM, in this article we find it more convenient to formulate the theory on the cotangent bundle T^*M associated with the spacetime manifold (M, g) since it is more naturally adapted to the Hamiltonian formalism on which this work is based. Our review includes a discussion of the symplectic form and the Liouville vector field on T^*M and the properties of the complete

lift $\hat{\xi}$ of a Killing vector field ξ on (M,g). These notions from classical Hamiltonian mechanics are key for the construction of the new symplectic coordinates (Q^μ, P_μ), $\mu = 0, 1, 2, 3$, which are required for the explicit representation formula of the distribution function.

Next, in section 3, we analyze in detail the structure of the invariant submanifolds of T^*M which are determined by the constants of motion. An important part of our analysis is the restriction of the phase space to unbounded trajectories emanating from the asymptotic region which are relevant for the accretion process. Exploiting the fact that the geodesic motion in the Schwarzschild spacetime constitutes an integrable Hamiltonian system, we derive the most general solution of the Liouville equation on a Schwarzschild background in horizon-penetrating coordinates. In general, this solution depends on the seven phase space variables (Q^1, Q^2, Q^3, P_μ); hence, it does not need to be stationary nor spherically symmetric. However, a time-independent and spherical distribution function is obtained after requiring the distribution function to be invariant with respect to the complete lifts of the Killing vector fields of the Schwarzschild spacetime. In this case, the distribution function depends only on the mass, energy and total angular momentum of the particle.

Next, in section 4 we specify the observables on the spacetime manifold M which, at each $x \in M$, are obtained from a fibre integral of the distribution function over the canonical momentum $p \in T^*_x M$. Besides giving results which are applicable to the general solution of the Liouville equation, we also specialize these expressions to the case where the distribution function depends only on the energy E of the gas particles, in which case the fibre integrals simplify considerably. Furthermore, we compare the structure of the observables to those belonging to an isotropic, perfect fluid.

In section 5 we apply our results to the accretion problem. First, we focus on the spherical, steady-state case in which all the gas particles have the same rest mass. Further, we assume that the gas is in thermodynamic equilibrium at temperature T at infinity, implying that the distribution function is proportional to $\mathrm{e}^{-\frac{E}{k_B T}}$, with k_B Boltzmann's constant. We compute the particle and energy fluxes j_n and j_ε, respectively, and also the particle density n_∞, energy density ε_∞ and pressure p_∞ at infinity which, as a consequence of our assumptions, obey the ideal gas equation. Next, we calculate the radial and tangential kinetic pressure of the gas, p_{rad} and p_{tan}, and the particle and energy densities n_H and ε_H on the horizon. In particular, we note that in the low temperature limit the tangential pressure is almost ten times larger than the radial one, implying that the gas does not behave as an isotropic perfect fluid at the horizon, although it does so in the asymptotic region. The fact that the tangential pressure becomes more important as the horizon is approached fits well with the known fact that the accretion rate for a collisionless gas is much lower than in the hydrodynamic case.

Second, in section 5 we present a study for the stability of the steady-state, spherical accretion flow. In order to achieve this, it is necessary to relax the symmetry assumptions on the distribution function, and our only essential hypothesis is that the distribution function is bounded by an equilibrium distribution function and that it converges to some functions $f_{\pm\infty}(E)$ of the energy E when $r \to \infty$ along the initial time slice $t = 0$ in phase space, where the $\pm$ sign refers to the sign of the radial velocity of the particles at infinity. Using Lebesgue's dominated convergence theorem, we compute the asymptotic behavior of the components of the observables with respect to a Fermi-propagated frame along the world lines of timelike observers. For static observers, we prove that the observables converge pointwise to the corresponding static and spherical observables associated with the asymptotic function $f_{-\infty}(E)$. For outgoing timelike observers with asymptotically constant, purely radial velocity, we show that the observables also converge to those describing a stationary and spherically symmetric gas; however, in this case the result depends on both $f_{-\infty}(E)$ and $f_{+\infty}(E)$. For the physically most

relevant case $f_{-\infty} = f_{+\infty}$ in which the asymptotic distribution function does not discriminate between in- and outgoing particle, our result implies the asymptotic stability of the steady-state, spherical accretion flow.

Finally, conclusions and an outlook on future work are given in section 6. Technical details, calculations and proofs of certain auxiliary results are given in appendices.

With the exception of some results given in section 5.1 regarding the steady-state, spherical accretion configurations, throughout this work we use geometrized units where the gravitational constant and speed of light are set equal to one. (M,g) denotes a smooth, four-dimensional Lorentzian manifold where we adopt the signature convention $(-,+,+,+)$ for the metric. We denote by $\mathcal{X}(M)$ the class of smooth vector fields on the differentiable manifold M. For $X \in \mathcal{X}(M)$ the symbols i_X and $\pounds_X$ denote, respectively, the inner product and Lie derivative with respect to X.

2. Relativistic kinetic theory on the cotangent bundle

The purpose of this section is to provide a brief review for the formal structure of relativistic kinetic theory and to fix the notation used in this article. For more detailed reviews we refer the reader to the early work by Ehlers [8] and to the more recent work in [10, 12] and references therein.

2.1. Relativistic phase space

Kinetic theory is based on the assumption that the ensemble-averaged properties of the gas can be described by a one-particle distribution function f. Accordingly, $f : \Gamma \to \mathbb{R}$ is a nonnegative function on the one-particle phase space Γ (the '(q, p)-space' at each fixed time). In the relativistic case, Γ is a subset of the cotangent bundle

$$T^*M := \{(x,p) : x \in M, p \in T^*_xM\} \tag{1}$$

associated with the spacetime manifold M which consists of points of the form (x,p), where $x \in M$ is spacetime event, and $p \in T^*_xM$ is a co-vector at this event, representing the canonical momentum of the gas particle at x. Instead of working on the cotangent bundle, one usually formulates kinetic theory on the tangent bundle TM, where $p \in T_xM$ is a tangent vector at x, representing the physical momentum of the particle. Since the present article is strongly based on the Hamiltonian formulation, the choice of the cotangent bundle is more natural. However, we stress that both formulations are equivalent because of the existence of the spacetime metric g which provides a natural isomorphism between TM and T^*M.

We recall:

Lemma 1. *Let M be a n-dimensional differentiable manifold (orientable or not). Then, T^*M is a $2n$-dimensional differentiable and orientable manifold.*

Proof. The proof is standard (see, for example [12, 53] for the tangent bundle case). Given local coordinates (x^μ) on M one defines corresponding *adapted local coordinates* (x^μ, p_μ) on T^*M by expanding each $p \in T^*_xM$ in the form $p = p_\mu \mathrm{d}x^\mu_x$. Taking an atlas of local coordinate charts on M one obtains a corresponding atlas on T^*M, and it is simple to verify that all the transition maps are differentiable and have unit determinant, implying that the transition maps are volume and orientation-preserving. As we will see shortly, this property stems from the fact that the adapted local coordinates (x^μ, p_μ) are symplectic coordinates. □

For the following, we assume that spacetime (M, g) is time-oriented and that all gas particles have positive mass. In this case, the one-particle phase space is the following submanifold of T^*M:[2]

$$\Gamma := \{(x,p) \in T^*M : p \text{ future-directed timelike}\}.$$

If one further assumes that all the gas particles have the same positive rest mass $m > 0$, one obtains instead the *mass shell*

$$\Gamma_m := \{(x,p) \in T^*M : g_x^{-1}(p,p) = -m^2,\ p \text{ future-directed}\}.$$

For generality, in this article we mostly work on Γ although in some applications towards the end we consider a simple gas, that is, a kinetic gas composed of identical particles of the same positive rest mass in which case we restrict ourselves to Γ_m.

2.2. Symplectic structure and Liouville vector field

The cotangent space T^*M admits a natural symplectic structure which can be described as follows. First, the *Poincaré (or canonical) one-form* on T^*M is introduced, which is defined by

$$\Theta_{(x,p)}(X) := p(\mathrm{d}\pi_{(x,p)}(X)), \qquad X \in \mathcal{X}(T^*M), \tag{2}$$

where here $\pi : T^*M \to M, (x,p) \mapsto x$ is the natural projection map and $\mathrm{d}\pi_{(x,p)} : T_{(x,p)}(T^*M) \to T_xM$ its differential at (x,p). In adapted local coordinates,

$$\Theta_{(x,p)} = p_\mu \mathrm{d}x^\mu_{(x,p)}.$$

Its exterior differential

$$\Omega_s := \mathrm{d}\Theta = \mathrm{d}p_\mu \wedge \mathrm{d}x^\mu$$

is seen to define a symplectic structure on T^*M, that is, a closed, non-degenerated two-form on T^*M. This symplectic structure allows one to assign to any function H on T^*M a unique vector field $X_H \in \mathcal{X}(T^*M)$ called the *associated Hamiltonian vector field* which is defined by

$$\mathrm{d}H = -\mathrm{i}_{X_H}\Omega_s = \Omega_s(\cdot, X_H). \tag{3}$$

In adapted local coordinates (x^μ, p_μ) one has

$$X_H = \frac{\partial H}{\partial p_\mu}\frac{\partial}{\partial x^\mu} - \frac{\partial H}{\partial x^\mu}\frac{\partial}{\partial p_\mu},$$

and the integral curves $\gamma(\lambda)$ of X_H are described by *Hamilton's equations*

$$\frac{\mathrm{d}x^\mu}{\mathrm{d}\lambda}(\lambda) = \frac{\partial H}{\partial p_\mu}(\gamma(\lambda)), \qquad \frac{\mathrm{d}p_\mu}{\mathrm{d}\lambda}(\lambda) = -\frac{\partial H}{\partial x^\mu}(\gamma(\lambda)). \tag{4}$$

The *Poisson bracket* between two smooth functions $F, G : T^*M \to \mathbb{R}$ on the cotangent bundle is defined as

$$\{F,G\} := \Omega_s(X_F, X_G) = -\mathrm{d}F(X_G) = \mathrm{d}G(X_F). \tag{5}$$

[2] We define $p \in T^*_xM$ to be future-directed timelike if the corresponding tangent vector $g_x^{-1}(p,\cdot) \in T_xM$ is future-directed timelike.

In particular when $G = H$ is the Hamiltonian of the system, it follows that $\{F, H\} = 0$ if and only if F is constant along the Hamiltonian flow, which is the case if and only if H is invariant under the canonical flow generated by F. For later use we also note the identity[3]

$$[X_F, X_G] = X_{\{F,G\}}. \tag{6}$$

Of particular interest to this article is the free-particle Hamiltonian

$$H(x,p) := \frac{1}{2} g_x^{-1}(p,p) = \frac{1}{2} g^{\mu\nu}(x) p_\mu p_\nu;$$

the associated Hamiltonian vector field $L := X_H$ is called the *Liouville vector field*, and in adapted local coordinates it reads

$$L = g^{\mu\nu}(x) p_\nu \frac{\partial}{\partial x^\mu} - \frac{1}{2} p_\alpha p_\beta \frac{\partial g^{\alpha\beta}(x)}{\partial x^\mu} \frac{\partial}{\partial p_\mu}.$$

The corresponding integral curves, when projected onto (M, g), describe spacetime geodesics. For a given positive mass $m > 0$, the Liouville vector field L at each point $(x,p) \in \Gamma_m$ of the mass shell Γ_m is nonvanishing and tangent to Γ_m. Therefore, when restricted to the relativistic phase space Γ the Liouville vector field does not have any critical points, and the projections of the integral curves of L describe future-directed timelike geodesics of (M, g).

The *Liouville equation*, which describes the evolution of a collisionless distribution function $f : \Gamma \to \mathbb{R}$ is

$$L[f] = 0. \tag{7}$$

In the next section, we find the most general solution of this equation for the case where (M,g) describes the geometry of a Schwarzschild black hole. This will be achieved by introducing new symplectic coordinates on Γ which trivialize the Liouville vector field L.

2.3. Complete lifts of vector fields

Suppose $\xi \in \mathcal{X}(M)$ is a vector field on spacetime generating a one-parameter group of diffeomorphism $\varphi^\lambda : M \to M$. We may lift φ^λ to a corresponding group $\hat{\varphi}^\lambda : T^*M \to T^*M$ on the cotangent bundle by defining

$$\hat{\varphi}^\lambda(x,p) := (\varphi^\lambda(x), [(\mathrm{d}\varphi_x^\lambda)^*]^{-1}(p)), \qquad (x,p) \in T^*M,$$

where $\mathrm{d}\varphi_x^\lambda : T_xM \to T_{\varphi^\lambda(x)}M$ denotes the differential of the map φ^λ at x and $(\mathrm{d}\varphi_x^\lambda)^*$: $T^*_{\varphi^\lambda(x)}M \to T^*_xM$ its adjoint. It is simple to verify that $\hat{\varphi}^0$ is the identity map on T^*M and that $\hat{\varphi}^\lambda \circ \hat{\varphi}^\mu = \hat{\varphi}^{\lambda+\mu}$ for all $\lambda, \mu \in \mathbb{R}$, and thus $\hat{\varphi}^\lambda$ defines a one-parameter group of diffeomorphism, as claimed. The *complete lift of* ξ is defined as

$$\hat{\xi}_{(x,p)} := \left.\frac{\mathrm{d}}{\mathrm{d}\lambda}\right|_{\lambda=0} \hat{\varphi}^\lambda(x,p), \qquad (x,p) \in T^*M.$$

Of course, the same definition applies to a vector field $\xi \in \mathcal{X}(M)$ which only generates a local one-parameter group of diffeomorhism, and hence the complete lift can be introduced in the same way for any $\xi \in \mathcal{X}(M)$.

[3] See for instance page 217 in [54].

In adapted local coordinates one finds the following explicit expression:

$$\hat{\xi}_{(x,p)} = \xi^\mu(x)\frac{\partial}{\partial x^\mu}\bigg|_{(x,p)} - p_\alpha \frac{\partial \xi^\alpha}{\partial x^\mu}(x)\frac{\partial}{\partial p_\mu}\bigg|_{(x,p)}, \qquad \xi_x = \xi^\mu(x)\frac{\partial}{\partial x^\mu}\bigg|_x. \tag{8}$$

The most important properties of the complete lift are summarized in the following proposition. See proposition 5 and lemmas 9 and 10 in [12] and lemma C.9 in [16] for similar statements on the tangent bundle.

Proposition 1.

(i) The complete lift preserves the Lie-brackets, that is $[\hat{\xi}, \hat{\eta}] = \hat{\zeta}$ with $\zeta = [\xi, \eta]$ for all $\xi, \eta \in \mathcal{X}(M)$.

(ii) If $\xi \in \mathcal{X}(M)$, then $\hat{\xi}$ is the infinitesimal generator of a symplectic flow on T^*M, that is, $\pounds_{\hat{\xi}}\,\Omega_s = 0$. Moreover,

$$\hat{\xi} = X_F, \qquad F := \Theta(\hat{\xi}) = p(\xi),$$

which shows that this flow is generated by the function $F = p(\xi)$.

(iii) Let $\xi \in \mathcal{X}(M)$ and $m > 0$. Then, $\hat{\xi}$ is tangent to the mass shell Γ_m at each point $(x, p) \in \Gamma_m$ if and only if ξ is a Killing vector field of (M, g).

Remarks.

1. Unlike the tangent bundle formulation (see proposition 5 in [12]), in the cotangent bundle formulation the vector field ξ is not required to be a Killing vector field in order for $\hat{\xi}$ to generate a symplectic flow.
2. If $\xi \in \mathcal{X}(M)$ is a Killing vector field of (M, g), the properties (ii) and (iii) of the proposition imply that

$$\{F, H\} = \mathrm{d}H(X_F) = \mathrm{d}H(\hat{\xi}) = \pounds_{\hat{\xi}} H = 0,$$

and thus F is conserved along the Liouville flow. In this case it follows that the Hamiltonian vector fields $X_F = \hat{\xi}$ and $X_H = L$ associated with F and H commute, see equation (6):

$$[\hat{\xi}, L] = 0.$$

Proof of proposition 1. Property (i) can be verified by a straightforward calculation using equation (8). As for (ii) and (iii) we first calculate

$$i_{\hat{\xi}}\,\Omega_s = i_{\hat{\xi}}(\mathrm{d}p_\mu \wedge \mathrm{d}x^\mu) = \mathrm{d}p_\mu(\hat{\xi})\mathrm{d}x^\mu - \mathrm{d}x^\mu(\hat{\xi})\mathrm{d}p_\mu.$$

Using the coordinate expression (8) for $\hat{\xi}$ we obtain

$$i_{\hat{\xi}}\,\Omega_s = -p_\alpha \frac{\partial \xi^\alpha}{\partial x^\mu}\mathrm{d}x^\mu - \xi^\mu \mathrm{d}p_\mu = -d(p_\alpha \xi^\alpha) = -\mathrm{d}F,$$

which shows (ii). In particular, the fact that $\mathrm{d}\Omega_s = 0$ implies

$$\pounds_{\hat{\xi}}\,\Omega_s = (\mathrm{d}i_{\hat{\xi}} + i_{\hat{\xi}}\mathrm{d})\,\Omega_s = -d(\mathrm{d}F) = 0.$$

Finally, we note that since Γ_m is a level surface of the free-particle Hamiltonian H, $\hat{\xi}$ is tangent to Γ_m if and only if $\pounds_{\hat{\xi}} H = \mathrm{d}H(\hat{\xi}) = 0$ at each $(x,p) \in \Gamma_m$. On the other hand, the definition of the Liouville vector field and (ii) imply that

$$\mathrm{d}H(\hat{\xi}) = i_{\hat{\xi}}\,\Omega_s(L) = -p_\alpha \frac{\partial \xi^\alpha}{\partial x^\mu} g^{\mu\beta} p_\beta + \xi^\mu \frac{1}{2} p_\alpha p_\beta \frac{\partial g^{\alpha\beta}}{\partial x^\mu} = \frac{1}{2} p_\alpha p_\beta (\pounds_\xi g^{\alpha\beta}).$$

Hence, if ξ is a Killing vector field of (M, g) then $\mathrm{d}H(\hat{\xi}) = 0$ and $\hat{\xi}$ is tangent to Γ_m. Conversely, if $\mathrm{d}H(\hat{\xi}) = 0$ at each point $(x,p) \in \Gamma_m$ then, for any $x \in M$ it follows that $p_\alpha p_\beta (\pounds_\xi g^{\alpha\beta}) = 0$ for all future-directed timelike covectors $p \in T^*_x M$ normalized such that $g_x^{-1}(p,p) = -m^2$, which implies that $\pounds_\xi g^{\alpha\beta}(x) = 0$, and thus that ξ is a Killing vector field on (M, g). □

As an example which will turn out to be relevant for the next section, consider a spherically symmetric, four-dimensional spacetime (M, g). In terms of standard spherical coordinates, the infinitesimal generators ξ_1, ξ_2, ξ_3 of the action of the rotation group $SO(3)$ on M can be represented in the following way:

$$\xi_1 + \mathrm{i}\xi_2 = \mathrm{e}^{\mathrm{i}\varphi}\left(\mathrm{i}\frac{\partial}{\partial \vartheta} - \cot\vartheta \frac{\partial}{\partial \varphi}\right), \tag{9}$$

$$\xi_3 = \frac{\partial}{\partial \varphi}. \tag{10}$$

They satisfy the commutation relations $[\xi_1, \xi_2] = -\xi_3$ (and cyclic permutations of 123) and are tangent to the invariant two-spheres (the orbits of the rotation group). The associated conserved quantities are

$$\ell_1 + i\ell_2 := p(\xi_1 + \mathrm{i}\xi_2) = \mathrm{e}^{\mathrm{i}\varphi}(\mathrm{i}p_\vartheta - \cot\vartheta p_\varphi), \tag{11}$$

$$\ell_3 := p(\xi_3) = p_\varphi, \tag{12}$$

and consequently, the total angular momentum

$$\ell := \sqrt{\ell_1^2 + \ell_2^2 + \ell_3^2} = \sqrt{p_\vartheta^2 + \frac{p_\varphi^2}{\sin^2\vartheta}},$$

is also conserved along the Liouville flow. The complete lifts of the vector fields ξ_a on T^*M are given by

$$\hat{\xi}_1 + \mathrm{i}\hat{\xi}_2 = \mathrm{e}^{\mathrm{i}\varphi}\left[\mathrm{i}\frac{\partial}{\partial \vartheta} - \cot\vartheta \frac{\partial}{\partial \varphi} - \frac{p_\varphi}{\sin^2\vartheta}\frac{\partial}{\partial p_\vartheta} + (p_\vartheta + \mathrm{i}\cot\vartheta p_\varphi)\frac{\partial}{\partial p_\varphi}\right], \tag{13}$$

$$\hat{\xi}_3 = \frac{\partial}{\partial \varphi}. \tag{14}$$

They satisfy the same commutation relations as the ξ_a's; however, now the three vector fields $\hat{\xi}_1, \hat{\xi}_2, \hat{\xi}_3$ are pointwise linearly independent, which means that the orbits of $SO(3)$ in T^*M are three-dimensional submanifolds (as opposed to the orbits in M which are two-dimensional). Therefore, a function on T^*M which is invariant with respect to $SO(3)$ is subject to three independent constraints, whereas a $SO(3)$-invariant function on M is only subject to two.

Finally, note that since $d(\ell^2) = 2(\ell_1 d\ell_1 + \ell_2 d\ell_2 + \ell_3 d\ell_3)$ the Hamiltonian vector field associated with the square of the total angular momentum is

$$X_{\ell^2} = 2(\ell_1\hat{\xi}_1 + \ell_2\hat{\xi}_2 + \ell_3\hat{\xi}_3).$$

3. General solution of the Liouville equation on a Schwarzschild background

In this section, we discuss the most general solution of the Liouville equation (7) describing the accretion into a Schwarzschild black hole. This is achieved using standard techniques from the classical theory of integrable systems, see for example [54].

3.1. Horizon-penetrating coordinates

In standard coordinates $(\bar{t}, r, \vartheta, \varphi)$ the Schwarzschild metric describing a black hole of mass $M_H > 0$ is given by

$$g = -N(r)\mathrm{d}\bar{t}^2 + \frac{\mathrm{d}r^2}{N(r)} + r^2(\mathrm{d}\vartheta^2 + \sin^2\vartheta\,\mathrm{d}\varphi^2), \qquad N(r) := 1 - \frac{2M_H}{r}.$$

Since in this work we shall be interested in computing the observables associated with the kinetic gas in the exterior region $r > 2M_H$ as well as on the future horizon, for what follows we work in regular coordinates $(t, r, \vartheta, \varphi)$. Here, the new time coordinate t is defined by

$$t = \bar{t} + \int^r \left[\frac{1}{N(r)} - \eta(r)\right]\mathrm{d}r,$$

with a smooth function $\eta : (0, \infty) \to \mathbb{R}$. In terms of the new coordinates, the metric takes the form

$$g = -N\mathrm{d}t^2 + 2(1 - N\eta)\mathrm{d}t\mathrm{d}r + \eta(2 - N\eta)\mathrm{d}r^2 + r^2(\mathrm{d}\vartheta^2 + \sin^2\vartheta\,\mathrm{d}\varphi^2),$$

and there are no coordinate singularities for $r > 0$ except at the poles $\vartheta = 0, \pi$[4]. Here, the function η reflects the freedom in choosing the foliation of the Schwarzschild spacetime which is regular at the future horizon. When $\eta = 0$ the surfaces of constant time t are incoming null surfaces and the corresponding coordinates $(t, r, \vartheta, \varphi)$ are called (ingoing) Eddington-Finkelstein coordinates (see for instance [55]). When $\eta(2 - N\eta) > 0$ the constant time surfaces are spacelike. Some interesting choices which have been considered in the literature are:

- Painlevé–Gullstrand coordinates (see for example [56]): $\eta = [1 + \sqrt{1 - N}]^{-1}$.
- Analytic trumpet slices that were recently proposed in [57]:

$$\eta(r) = \frac{r^2}{r - R_0}\frac{1}{r - R_0 + \sqrt{2(M_H - R_0)r + R_0^2}}, \qquad r > R_0,$$

with R_0 a free parameter satisfying $0 < R_0 \leqslant M_H$. In this case the function η is only defined on the interval (R_0, ∞), but otherwise it satisfies all the required properties mentioned above. Replacing r with the new radial coordinate $\rho = r - R_0$ (denoted by r in [57]) leads to spatially homogenous coordinates.

[4] These coordinate singularities can be removed by replacing (r, ϑ, φ) with Cartesian-like coordinates $(x, y, z) = r(\cos\varphi\sin\vartheta, \sin\varphi\sin\vartheta, \cos\vartheta)$.

For the calculations below, we shall focus on the simple case $\eta = 1$, in which the inverse metric reads

$$g^{-1} = -\left(1 + \frac{2M_H}{r}\right)\frac{\partial}{\partial t} \otimes \frac{\partial}{\partial t} + \frac{4M_H}{r}\frac{\partial}{\partial t} \otimes_s \frac{\partial}{\partial r} + \left(1 - \frac{2M_H}{r}\right)\frac{\partial}{\partial r} \otimes \frac{\partial}{\partial r} + \frac{1}{r^2}\left(\frac{\partial}{\partial \vartheta} \otimes \frac{\partial}{\partial \vartheta} + \frac{1}{\sin^2\vartheta}\frac{\partial}{\partial \varphi} \otimes \frac{\partial}{\partial \varphi}\right), \tag{15}$$

where $\otimes_s$ denotes the symmetrized tensor product.

From now on, we consider the region M of the (extended) Schwarzschild manifold which is covered by the horizon-penetrating coordinates (t,r) with $t \in \mathbb{R}$ and $r > 0$.

3.2. Hamiltonian flow, conserved quantities and invariant submanifolds

The free-particle Hamiltonian computed from the inverse metric (15) is

$$H(x,p) = \frac{1}{2}\left[-\left(1 + \frac{2M_H}{r}\right)p_t^2 + \frac{4M_H}{r}p_t p_r + \left(1 - \frac{2M_H}{r}\right)p_r^2 + \frac{1}{r^2}\left(p_\vartheta^2 + \frac{p_\varphi^2}{\sin^2\vartheta}\right)\right]. \tag{16}$$

Since the underlying spacetime is stationary and spherically symmetric, the following quantities are conserved along the particle trajectories:

$$m = \sqrt{-2H} \quad \text{(rest mass)}, \tag{17}$$

$$E = -p_t \quad \text{(energy)}, \tag{18}$$

$$\ell_z = p_\varphi \quad \text{(azimuthal angular momentum)}, \tag{19}$$

$$\ell = \sqrt{p_\vartheta^2 + \frac{p_\varphi^2}{\sin^2\vartheta}} \quad \text{(total angular momentum)}. \tag{20}$$

Accordingly, we introduce the smooth functions $F_0, F_1, F_2, F_3 : T^*M \to \mathbb{R}$ on the cotangent bundle defined by[5]

$$F_0(x,p) := -H(x,p), \qquad F_1(x,p) := -p_t, \qquad F_2(x,p) := p_\varphi, \qquad F_3(x,p) := p_\vartheta^2 + \frac{p_\varphi^2}{\sin^2\vartheta}. \tag{21}$$

It is not difficult to verify that these quantities Poisson-commute with each other:

$$\{F_\alpha, F_\beta\} = 0, \qquad \alpha, \beta = 0, 1, 2, 3.$$

For the following, we consider for each given value of (m, E, ℓ_z, ℓ) the (possibly empty) subset

$$\Gamma_{m,E,\ell_z,\ell} := \left\{(x,p) \in \Gamma : F_0(x,p) = \frac{1}{2}m^2, F_1(x,p) = E, F_2(x,p) = \ell_z, F_3(x,p) = \ell^2\right\}$$

[5] With respect to Cartesian-like coordinates, one can rewrite $p_\varphi = xp_y - yp_x$ and $\ell^2 = |(x,y,z) \wedge (p_x,p_y,p_z)|^2$ with $\wedge$ denoting the vector product, which shows that these quantities are indeed smooth functions on T^*M.

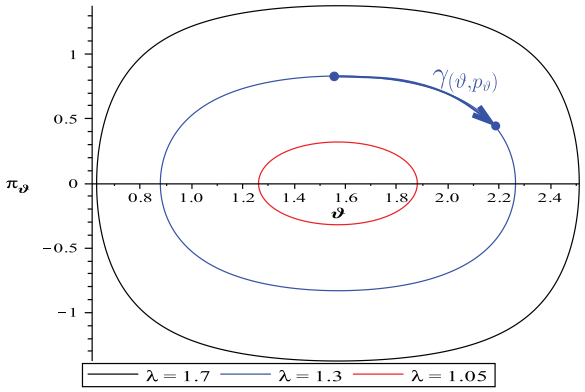

Figure 1. Phase diagram illustrating the projection of the invariant sets onto the (ϑ, p_ϑ)-plane. Here, we use the dimensionless variables $\pi_\vartheta = p_\vartheta/(M_H m)$ and $\lambda = \ell/(M_H m)$ and rescaled the variables such that $\ell_z = M_H m$. When $\lambda \to 1$ the curves shrink to a point, corresponding to motion confined to the equatorial plane $\vartheta = \pi/2$.

of the one-particle phase space Γ. By construction, these sets are invariant under the Hamiltonian flow. The main result of this section is the following:

Proposition 2. *Suppose that $E > m > 0$ and that $|\ell_z| < \ell$. In addition, suppose that the condition $\ell \neq \ell_c(E)$ holds (see below for the definition of $\ell_c(E)$). Then, $\Gamma_{m,E,\ell_z,\ell}$ is a smooth, four-dimensional submanifold of Γ which is invariant with respect to the Hamiltonian flows associated with F_0, F_1, F_2 and F_3. It consists of three connected components, each of which has the topology $\mathbb{R}^2 \times S^1 \times S^1$.*

Furthermore, the restriction of the Poincaré one-form Θ defined in equation (2) on $\Gamma_{m,E,\ell_z,\ell}$ is closed.

In order to prove the proposition, we separate the adapted local coordinates (x^μ, p_μ) into the conjugate pairs (t, p_t), (φ, p_φ), (ϑ, p_ϑ), (r, p_r) and notice that $\Gamma_{m,E,l_z,\ell}$ consists of those points of Γ for which these pairs fulfill the following restrictions:

$$(t, p_t) : p_t = -E, \tag{22}$$

$$(\varphi, p_\varphi) : p_\varphi = \ell_z, \tag{23}$$

$$(\vartheta, p_\vartheta) : p_\vartheta^2 + \frac{\ell_z^2}{\sin^2\vartheta} = \ell^2, \tag{24}$$

$$(r, p_r) : \left(1 - \frac{2M_H}{r}\right)p_r^2 - \frac{4M_H}{r}Ep_r - \left(1 + \frac{2M_H}{r}\right)E^2 + m^2 + \frac{\ell^2}{r^2} = 0. \tag{25}$$

From these conditions it is clear that the time coordinate t and the azimuthal angle φ are free, whereas for $0 < |\ell_z| < \ell$ the pair (ϑ, p_ϑ) is confined to a closed curve in the (ϑ, p_ϑ)-plane which winds around the equilibrium point $(\vartheta, p_\vartheta) = (\pi/2, 0)$, see figure 1[6].

[6] The exceptional cases $\ell_z = 0$ and $\ell_z = \pm\ell$ correspond, respectively, to motion confined in a plane which contains de z axis and to motion in the equatorial plane, see lemma 2 below for more information on these cases. Since they give rise to zero measure sets in the phase space, we will not consider these particular cases further.

Next, let us analyze the set in the (r, p_r)-plane described by equation (25) in more detail. Multiplying both sides of equation (25) by $N(r) = 1 - 2M_H/r$ and assuming that $N(r) \neq 0$ we can rewrite this equation as

$$\left[\left(1 - \frac{2M_H}{r}\right)p_r - \frac{2M_H}{r}E\right]^2 + V_{m,\ell}(r) = E^2, \tag{26}$$

with the effective potential

$$V_{m,\ell}(r) = \left(1 - \frac{2M_H}{r}\right)\left(m^2 + \frac{\ell^2}{r^2}\right). \tag{27}$$

By Hamilton's equations the particle's radial velocity is

$$\dot{r} := \frac{\mathrm{d}r}{\mathrm{d}\lambda} = \frac{\partial H}{\partial p_r} = \left(1 - \frac{2M_H}{r}\right)p_r + \frac{2M_H}{r}p_t = \left(1 - \frac{2M_H}{r}\right)p_r - \frac{2M_H}{r}E,$$

so as long as $N(r) \neq 0$ the set defined by equation (25) is equivalent to $\dot{r}^2 + V_{m,\ell}(r) = E^2$, and the sign of the expression inside the square parenthesis in equation (26) determines whether the particle is incoming or outgoing. In the (r, p_r)-plane, equation (25) can be written as

$$p_r = p_{r\pm}(r) := \frac{\frac{2M_H}{r}E \pm \sqrt{E^2 - V_{m,\ell}(r)}}{N(r)}, \tag{28}$$

where the $\pm$ sign corresponds to the one of $\dot{r}$.

The properties of the set in the (r, p_r) plane described by equation (25) thus depend on the shape of the effective potential and the value of E. Since we are only interested in particle trajectories that emanate from the asymptotic region $r \to \infty$, and since the linear momentum p of the particle is restricted to be future-directed, we assume $E > m > 0$ in what follows. For a given $E > m$, denote by $\ell_c(E)$ the value of ℓ for which $V_{m,\ell}$ has a centrifugal barrier whose maximum is equal to E^2, see appendix A for details and explicit expressions. We distinguish between the following two cases:

(I) *Absorbed particles* $0 < \ell < \ell_c(E)$. In this case, the trajectories describe incoming particles from infinity which are absorbed by the black hole (negative values of $\dot{r}$) or particles which emanate from the white hole and escape to infinity (positive values of $\dot{r}$). There are also other trajectories which take place entirely inside the black hole (see figure 2) and will not be considered further. For the purpose of the present article, we focus on the first kind of trajectories which consist of open lines in the (r, p_r)-plane.

(II) *Scattered particles* $\ell > \ell_c(E)$. This corresponds to trajectories which are incoming from infinity, but in contrast to the previous case they carry enough angular momentum to be reflected at the potential barrier and so they escape again to infinity. There are also two further open lines corresponding to particles that are emitted from the white hole and reabsorbed by the black hole, or particle trajectories taking place entirely inside the black hole (see figure 2) that will not be considered further for our purposes.

To conclude the proof of proposition 2, we show in the next lemma that the differentials $\mathrm{d}F_0$, $\mathrm{d}F_1$, $\mathrm{d}F_2$, and $\mathrm{d}F_3$ are linearly independent at each point of $\Gamma_{m,E,\ell_z,\ell}$, implying that $\Gamma_{m,E,\ell_z,\ell}$ is a four-dimensional submanifold of Γ with linearly independent tangent vector fields X_{F_0}, X_{F_1}, X_{F_2}, and X_{F_3}. Since $\Omega_s(X_{F_\alpha}, X_{F_\beta}) = \{F_\alpha, F_\beta\} = 0$ it then follows that the restriction of $\Omega_s = \mathrm{d}\Theta$ to $\Gamma_{m,E,\ell_z,\ell}$ vanishes.

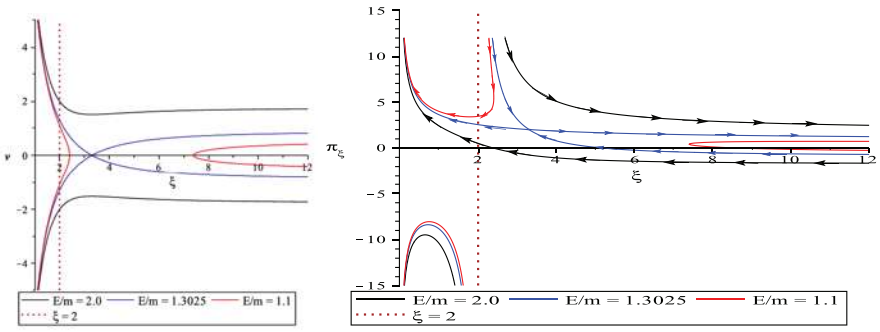

Figure 2. Phase diagrams illustrating the projection of the invariant sets onto the (r, p_r)-plane. Left panel: $v = \dot{r}/m$ versus $\xi = r/M_H$ for different energy levels E and $\ell = 6M_H m$. The black curve in the region $v < 0$ corresponds to an incoming particle from infinity which is absorbed by the black hole (case (I)), while the black curve in the region $v > 0$ describes an outgoing particle that is emitted from the white hole and escapes to infinity. The red curve in the region $\xi > 6$ describes a particle that is incoming from infinity but has large enough angular momentum $\ell > \ell_c(E)$ to be reflected at the potential barrier (case (II)), and the red curve in the region $\xi < 3$ describes a particle that is emitted by the white whole, is reflected at the potential barrier and absorbed by the black hole. The blue curve describes the separatrix and corresponds to the energy level E such that $\ell_c(E) = \ell$. Right panel: The same situation showing $\pi_\xi = p_r/m$ versus $\xi = r/M_H$. Since $\pi_\xi = (1 - 2\xi^{-1})^{-1}(v + 2E/(m\xi))$, the curves in the previous diagrams in the region $v > 0$ split into two separate parts, one of them lying entirely in the region $\xi < 2$ and $\pi_\xi < 0$ inside the black hole region.

Lemma 2. *Let E, $m > 0$. The differentials $\mathrm{d}F_0$, $\mathrm{d}F_1$, $\mathrm{d}F_2$ and $\mathrm{d}F_3$ are linearly independent from each other unless one of the following two cases occur:*

(a) Motion confined to the equatorial plane: $|\ell_z| = \ell$,
(b) Circular trajectories:

$$V_{m,\ell}(r) = E^2, \qquad \frac{\mathrm{d}}{\mathrm{d}r} V_{m,\ell}(r) = 0.$$

Proof. We first note that $\mathrm{d}F_1 = -\mathrm{d}p_t \neq 0$, $\mathrm{d}F_2 = \mathrm{d}p_\varphi \neq 0$. Next, we compute[7]

$$\mathrm{d}F_3 = 2\left(p_\vartheta \mathrm{d}p_\vartheta - \frac{\ell_z^2}{\sin^2\vartheta} \cot\vartheta \mathrm{d}\vartheta + \ell_z \frac{\mathrm{d}F_2}{\sin^2\vartheta} \right),$$

from which we see that $\mathrm{d}F_2$ and $\mathrm{d}F_3$ are linearly independent from each other unless $p_\vartheta = 0$ and $\vartheta = \pi/2$, which corresponds to case (a). Finally, computing

$$\mathrm{d}F_0 = \left[\left(1 + \frac{2M_H}{r}\right)E + \frac{2M_H}{r} p_r \right] \mathrm{d}F_1 - \left[\left(1 - \frac{2M_H}{r}\right)p_r - \frac{2M_H}{r} E \right] \mathrm{d}p_r - \frac{1}{2r^2} \mathrm{d}F_3 - \left[\frac{M_H}{r}(E + p_r)^2 - \frac{\ell^2}{r^2} \right] \frac{\mathrm{d}r}{r}$$

[7] Note that $\sin\vartheta \neq 0$ as long as $\ell_z \neq 0$. When $\ell_z = 0$ we can use Cartesian coordinates at the poles to show that $\mathrm{d}F_3$ is linearly independent of $\mathrm{d}F_2$.

we see that $\mathrm{d}F_0$ is linearly independent from $\mathrm{d}F_1$, $\mathrm{d}F_2$ and $\mathrm{d}F_3$ unless

$$\left(1-\frac{2M_H}{r}\right)p_r-\frac{2M_H}{r}E=0, \qquad \frac{M_H}{r}(E+p_r)^2-\frac{\ell^2}{r^2}=0.$$

A short calculation reveals that these conditions are equivalent to (b). □

Remarks.

1. In the following, we restrict ourselves to the subset Γ_{accr} of the relativistic one-particle phase space Γ which consists of the union of those invariant submanifolds $\Gamma_{m,E,\ell_z,\ell}$ corresponding to the cases (I) and (II) discussed above. This is the relevant submanifold describing the accretion of a collisionless kinetic gas into a Schwarzschild black hole.
2. Note that the subset Γ_{accr} *does not include the bounded trajectories*, which are contained in those invariant submanifolds $\Gamma_{m,E,\ell_z,\ell}$ for which $\sqrt{8/9}<E/m<1$ and $\ell_c(E)<\ell<\ell_{ub}(E)$, see appendix A. In this case, $\Gamma_{m,E,\ell_z,\ell}$ have topology $\mathbb{R}\times S^1\times S^1\times S^1$. This case will be considered in separate work [58].
3. The subset Γ_{accr} does not include those particle trajectories that emanate from the white hole either, since they are not relevant for the accretion of a collisionless gas.

In the next section, we shall construct new symplectic coordinates (Q^μ,P_μ) on Γ_{accr} which are adapted to the invariant submanifolds $\Gamma_{m,E,\ell_z,\ell}$ and which trivialize the Liouville vector field L.

3.3. New symplectic coordinates adapted to the invariant submanifolds

Following [54] we construct new symplectic local coordinates (Q^μ,P_μ) on Γ_{accr} from the generating function

$$S(x;m,E,\ell_z,\ell):=\int_{\gamma_x}\Theta, \tag{29}$$

where Θ is the Poincaré one-form defined in equation (2) and the line integral is performed over a curve γ_x which is confined to the invariant submanifold $\Gamma_{m,E,\ell_z,\ell}$, see figure 3. This curve γ_x connects a fixed reference point $(x_0,p_0)\in\Gamma_{m,E,\ell_z,\ell}$ to a point in the intersection between $\Gamma_{m,E,\ell_z,\ell}$ and the fibre $\pi^{-1}(x)$ over $x\in M$. We choose the reference point (x_0,p_0) as the one parametrized by $(t,p_t)=(0,\ -E)$, $(\varphi,p_\varphi)=(0,\ell_z)$, $(\vartheta,p_\vartheta)=(\pi/2,\sqrt{\ell^2-\ell_z^2})$ and $(r,p_r)=(r_0,p_{r-}(r_0))$, where the function $p_{r-}(r)$ is defined in equation (28) and $r_0=2M_H$ in case (I) and r_0 corresponds to the turning point in case (II).

Since the restriction of Θ to $\Gamma_{m,E,\ell_z,\ell}$ is closed, the value of $S(x;m,E,\ell_z,\ell)$ is independent of deformations of the curve γ_x within $\Gamma_{m,E,\ell_z,\ell}$ which leave its endpoints fixed. On the other hand, the value of $S(x;m,E,\ell_z,\ell)$ does depend on how many times and in which direction the curve γ_x winds around the two cycles S^1 of $\Gamma_{m,E,\ell_z,\ell}$. To analyze this dependency in more detail and in order to obtain a more explicit expression for the generating function we recall that in adapted local coordinates the Poincaré one-form reads $\Theta=p_\mu\mathrm{d}x^\mu$. Consequently,

$$S(x;m,E,\ell_z,\ell)=-Et+\ell_z\varphi+\int_{r_0}^{r}p_r\mathrm{d}r+\int_{\pi/2}^{\vartheta}p_\vartheta\mathrm{d}\vartheta.$$

Here, it is important to notice that the last two integrals should be interpreted as line integrals. The first integral is a line integral along the projection $\gamma_{(r,p_r)}$ of the curve γ_x onto the

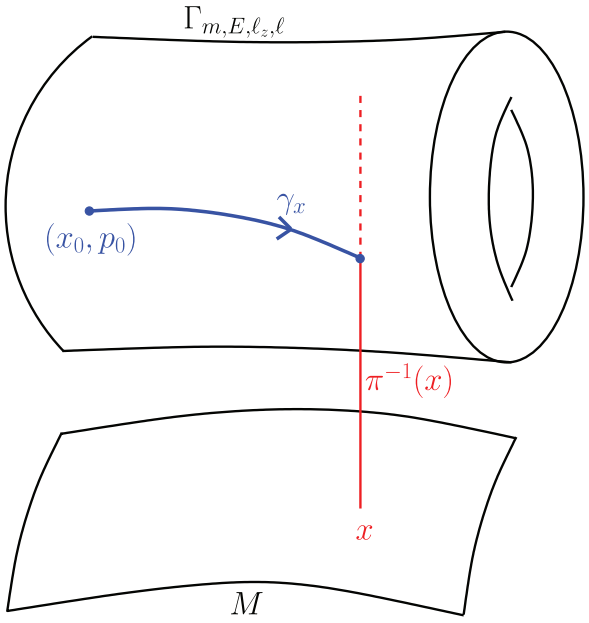

Figure 3. Illustration showing the invariant submanifold $\Gamma_{m,E,\ell_z\ell}$ and the curve γ_x connecting the reference point (x_0, p_0) to a point in the intersection between $\Gamma_{m,E,\ell_z,\ell}$ and the fibre $\pi^{-1}(x)$ over $x \in M$.

(r, p_r)-plane, while the second integral is a line integral (oriented clockwise) along the projection $\gamma_{(\vartheta,p_\vartheta)}$ of γ_x onto the (ϑ, p_ϑ)-plane, see figure 1.

It is clear that S changes by the additive constant $2\pi\ell_z$ under a full revolution $\varphi \to \varphi + 2\pi$ about the z-axis. Likewise, under a full clockwise revolution along the curve $\gamma_{(\vartheta,p_\vartheta)}$, S increases by[8]

$$\Delta S = 4\int_{\pi/2}^{\vartheta_{\max}(\ell_z,\ell)} \sqrt{\ell^2 - \frac{\ell_z^2}{\sin^2\vartheta}}\,\mathrm{d}\vartheta = 2\pi(\ell - |\ell_z|),$$

where $\vartheta_{\max}(\ell_z, \ell) > \pi/2$ is the angle corresponding to the turning point, such that $\sin\vartheta_{\max}(\ell_z, \ell) = \ell_z/\ell$. It follows from these observations that the quantities ℓ_z and $\ell - |\ell_z|$ are action variables [54].

The function S defined in equation (29) generates new symplectic coordinates (Q^μ, P_μ) as follows: the coordinates P_μ are defined by the conserved quantities:

$$P_0 := \sqrt{2F_0} = \sqrt{-2H}, \tag{30}$$

$$P_1 := F_1 = -p_t, \tag{31}$$

$$P_2 := F_2 = p_\varphi, \tag{32}$$

[8] The same integral appears in the discussion of the Kepler problem, see for instance section 10.8 in [59].

$$P_3 := \sqrt{F_3} = \sqrt{p_\vartheta^2 + \frac{p_\varphi^2}{\sin^2\vartheta}}, \tag{33}$$

such that each invariant set $\Gamma_{m,E,\ell_z,\ell}$ is parametrized simply by $P_0 = m$, $P_1 = E$, $P_2 = \ell_z$ and $P_3 = \ell$. The corresponding Q variables are defined by $Q^\mu = \partial S/\partial P_\mu$, that is

$$Q^0 := \frac{\partial S}{\partial m} = -m\int_{\gamma_{(r,p_r)}} \frac{\mathrm{d}r}{Np_r - \frac{2M_H}{r}E}, \tag{34}$$

$$Q^1 := \frac{\partial S}{\partial E} = -t + \int_{\gamma_{(r,p_r)}} \frac{\frac{2M_H}{r}p_r + \left(1+\frac{2M_H}{r}\right)E}{Np_r - \frac{2M_H}{r}E}\mathrm{d}r, \tag{35}$$

$$Q^2 := \frac{\partial S}{\partial \ell_z} = \varphi - \ell_z\int_{\gamma_{(\vartheta,p_\vartheta)}} \frac{\mathrm{d}\vartheta}{p_\vartheta \sin^2\vartheta}, \tag{36}$$

$$Q^3 := \frac{\partial S}{\partial \ell} = -\ell\int_{\gamma_{(r,p_r)}} \frac{\mathrm{d}r}{r^2\left(Np_r - \frac{2M_H}{r}E\right)} + \ell\int_{\gamma_{(\vartheta,p_\vartheta)}} \frac{\mathrm{d}\vartheta}{p_\vartheta}. \tag{37}$$

In deriving these equations, we have used the differentials of the relations (24) and (25). As before, the integrals should be interpreted as line integrals in the $(r,\, p_r)$-plane and (ϑ, p_ϑ)-plane, respectively, where the curves connect the reference point to the given points (r, p_r) and (ϑ, p_ϑ) along the projections of the invariant submanifold $\Gamma_{m,E,\ell_z,\ell}$ onto these planes. Given $(x,p) \in \Gamma_{\mathrm{accr}}$, the invariant submanifold is determined by the parameters $m{:}= P_0(x,\, p)$, $E{:}= P_1(x,\, p)$, $\ell_z := P_2(x,\, p)$ and $\ell := P_3(x,\, p)$. Note that by virtue of equations (24) and (26) we have

$$Np_r - \frac{2M_H}{r}E = \pm\sqrt{E^2 - V_{m,\ell}(r)}, \qquad p_\vartheta = \pm\sqrt{\ell^2 - \frac{\ell_z^2}{\sin^2\vartheta}},$$

where the correct choice for the sign depends on which part of the curve one is integrating over.

By construction, the function S satisfies

$$\frac{\partial S}{\partial x^\mu}(x; m, E, \ell_z, \ell) = p_\mu,$$

with $p = p_\mu \mathrm{d}x^\mu$ such that $P_0(x,\, p) = m$, $P_1(x,\, p) = E$, $P_2(x,\, p) = \ell_z$ and $P_3(x,\, p) = \ell$. Since

$$\Omega_s = \mathrm{d}p_\mu \wedge \mathrm{d}x^\mu = \frac{\partial^2 S}{\partial P_\nu \partial x^\mu}\mathrm{d}P_\nu \wedge \mathrm{d}x^\mu = \frac{\partial Q^\nu}{\partial x^\mu}\mathrm{d}P_\nu \wedge \mathrm{d}x^\mu = \mathrm{d}P_\nu \wedge \mathrm{d}Q^\nu,$$

the coordinates (Q^μ, P_μ) are new symplectic coordinates on Γ_{accr}. Note that the new momenta P_μ parametrize the invariant four-dimensional submanifolds $\Gamma_{m,E,\ell_z,\ell}$ while the Q^μ's define local coordinates on $\Gamma_{m,E,\ell_z,\ell}$, with Q^2 and Q^3 changing by integer multiples of 2π under revolutions about the azimuthal angle φ or about the curve $\gamma_{(\vartheta,p_\vartheta)}$. Therefore, Q^2 and Q^3 can be regarded as angle variables parametrizing the two cycles S^1 in $\Gamma_{m,E,\ell_z,\ell} \simeq \mathbb{R}^2 \times S^1 \times S^1$.

3.4. Most general collisionless distribution function describing accretion

Since in the new symplectic local coordinates (Q^μ, P_μ) the one-particle Hamiltonian is $H = -P_0^2/2$, the associated Hamiltonian vector field acquires the simple form

$$X_H = \frac{\partial H}{\partial P_\mu}\frac{\partial}{\partial Q^\mu} - \frac{\partial H}{\partial Q^\mu}\frac{\partial}{\partial P_\mu} = -P_0\frac{\partial}{\partial Q^0}.$$

Therefore, the Liouville equation (7) in these coordinates reads,

$$\frac{\partial f}{\partial Q^0} = 0,$$

and the most general solution of the Liouville equation can be expressed in closed form,

$$f(x,p) = \mathcal{F}(Q^1, Q^2, Q^3, P_0, P_1, P_2, P_3), \tag{38}$$

where $\mathcal{F}$ is an arbitrary function of its argument which is 2π-periodic in Q^2 and Q^3.

Note that so far, no symmetry assumptions have been made on the distribution function; our construction only relies on the symmetries of the underlying spacetime manifold (M, g) and the fact that the geodesic motion on this manifold is described by an integrable Hamiltonian system. If required, the invariance of f with respect to the symmetry group of (M, g) (or subgroups thereof) can be imposed using the complete lift introduced in section 2.3. The isometry group of the Schwarzschild manifold (M, g) is generated by the Killing vector fields $k := \frac{\partial}{\partial t}$ and the vector fields ξ_a, $a = 1, 2, 3$, defined in equations (9) and (10). The complete lifts of these generators are given by

$$\hat{k} = \frac{\partial}{\partial t}$$

and the vector fields $\hat{\xi}_a$, $a = 1, 2, 3$, defined in equations (13) and (14). In terms of the new symplectic coordinates (Q^μ, P_μ) one finds

$$\hat{k} = -\frac{\partial}{\partial Q^1}, \qquad \hat{\xi}_1 + \mathrm{i}\hat{\xi}_2 = \mathrm{e}^{\mathrm{i}\varphi}(\hat{\eta}_1 + \mathrm{i}\hat{\eta}_2), \qquad \hat{\xi}_3 = \frac{\partial}{\partial Q^2},$$

where

$$\hat{\eta}_1 = p_\vartheta\left[\frac{\partial}{\partial P_2} + \ell\int_{\gamma(\vartheta,p_\vartheta)}\frac{\mathrm{d}\vartheta}{p_\vartheta^3\sin^2\vartheta}\left(\ell_z\frac{\partial}{\partial Q^3} - \ell\frac{\partial}{\partial Q^2}\right)\right] - \cot\vartheta\frac{\partial}{\partial Q^2},$$

$$\hat{\eta}_2 = \ell_z\cot\vartheta\left[\frac{\partial}{\partial P_2} + \ell\int_{\gamma(\vartheta,p_\vartheta)}\frac{\mathrm{d}\vartheta}{p_\vartheta^3\sin^2\vartheta}\left(\ell_z\frac{\partial}{\partial Q^3} - \ell\frac{\partial}{\partial Q^2}\right)\right] - \frac{\ell_z}{p_\vartheta\sin^2\vartheta}\frac{\partial}{\partial Q^2} + \frac{\ell}{p_\vartheta}\frac{\partial}{\partial Q^3}.$$

Note also that the Hamiltonian vector field X_ℓ associated with the total angular momentum $\ell = P_3$ is

$$X_\ell = \frac{\partial}{\partial Q^3}.$$

From these observations it follows immediately that the distribution function is spherically symmetric (that is, invariant with respect to the flows generated by the lifted generators $\hat{\xi}_a$, $a = 1, 2, 3$) if and only if $\mathcal{F}$ is independent of Q^2, Q^3, and P_2.

We summarize the main results of this section in the following theorem.

Theorem 1. *On the invariant submanifold $\Gamma_{\rm accr} \subset \Gamma$ of phase space, the most general collisionless distribution function is given by equation (38), where the function $\mathcal{F}$ is 2π-periodic in the angle variables Q^2 and Q^3, and the action-angle-like variables (Q^μ, P_μ) are defined in equations (30)–(37).*

Further, the distribution function is stationary if and only if $\mathcal{F}$ is independent of Q^1, axisymmetric if and only if $\mathcal{F}$ is independent of Q^2, and spherically symmetric if and only if $\mathcal{F}$ is independent of Q^2, Q^3 and P_2.

Remarks.

1. It follows from the theorem that a stationary and spherically symmetric collisionless distribution function on $\Gamma_{\rm accr}$ only depends on the conserved quantities m, E and ℓ. This result is closely related to Jeans' theorem in the Newtonian case, which states that a stationary, spherically symmetric solution of the Poisson-Liouville system is described by a distribution function depending only on E and ℓ (see [60] for a precise formulation). However, it has been shown that the generalization of Jeans' theorem to the general relativistic case is false in general [29, 61]. The reason that in our setting a stationary and spherically symmetric distribution function must nevertheless be a function of only (m, E, ℓ) is due to the fact that we work on a fixed Schwarzschild background (neglecting the self-gravity of the gas) and to our restriction to the subset $\Gamma_{\rm accr}$ of phase space.
2. Unlike the spherically symmetric case, it is in general not true that a stationary, collisionless distribution function depends only on the conserved quantities arising from the spacetime symmetries. For instance, a stationary axisymmetric distribution function may depend on Q^3 apart from the quantities m, E, ℓ and ℓ_z.

4. Particle current density and stress energy-momentum tensor

In this section, we analyze the relevant observables of a relativistic, collisionless kinetic gas on the Schwarzschild spacetime (M, g). These observables are the particle current density and the stress energy-momentum tensor, and they are defined invariantly as follows:

$$J_x(X) := \int_{\pi^{-1}(x)} p(X) f(x,p) \mathrm{dvol}_x(p), \quad T_x(X,Y) := \int_{\pi^{-1}(x)} p(X) p(Y) f(x,p) \mathrm{dvol}_x(p), \quad X, Y \in T_xM, \tag{39}$$

where here $\pi^{-1}(x) = \{(x,p) : p \in T_x^*M\} \simeq T_x^*M$ is the fibre over x and

$$\mathrm{dvol}_x(p) := \sqrt{-\det(g^{\mu\nu}(x))}\, \mathrm{d}^4p$$

is the invariant volume element on $\pi^{-1}(x)$ induced by the inverse metric g_x^{-1}. Using local adapted coordinates (x^μ, p_μ) one can rewrite these quantities as

$$J_\mu(x) = \int_{\pi^{-1}(x)} p_\mu f(x,p) \mathrm{dvol}_x(p), \qquad T_{\mu\nu}(x) = \int_{\pi^{-1}(x)} p_\mu p_\nu f(x,p) \mathrm{dvol}_x(p). \tag{40}$$

It can be shown that by virtue of the Liouville equation (7) these quantities are divergence-free. In the next section, we express these quantities more explicitly in terms of dimensionless quantities. The resulting expressions will be used in the next section in order to discuss physical applications regarding the accretion problem.

4.1. Explicit expressions for the observables

In order to simplify the computation of the fibre integrals, it is convenient to re-express the new symplectic variables (Q^μ, P_μ) in terms of dimensionless quantities. For this purpose, we write

$$t = M_H\tau, \quad r = M_H\xi, \quad p_r = m\pi_\xi, \quad p_\vartheta = M_H m\pi_\vartheta,$$

and

$$E = m\varepsilon, \quad \ell = M_H m\lambda, \quad \ell_z = M_H m\lambda_z,$$

with the new quantities τ, ξ, π_ξ, π_ϑ, ε, λ, λ_z being dimensionless. The relevant Q variables are

$$Q^1 = M_H m\left[G_{\varepsilon,\lambda}(\xi,\pi_\xi) - \tau\right], \tag{41}$$

$$Q^2 = \varphi - \lambda_z \int_{\gamma_{(\vartheta,\pi_\vartheta)}} \frac{\mathrm{d}\vartheta}{\pi_\vartheta \sin^2\vartheta}, \tag{42}$$

$$Q^3 = -\lambda \int_{\gamma_{(\xi,\pi_\xi)}} \frac{\mathrm{d}\xi}{\xi^2\left[\left(1-\frac{2}{\xi}\right)\pi_\xi - \frac{2}{\xi}\varepsilon\right]} + \lambda \int_{\gamma_{(\vartheta,\pi_\vartheta)}} \frac{\mathrm{d}\vartheta}{\pi_\vartheta}. \tag{43}$$

Here, we have introduced the function

$$G_{\varepsilon,\lambda}(\xi,\pi_\xi) := \int_{\gamma_{(\xi,\pi_\xi)}} \frac{\frac{2}{\xi}\pi_\xi + \left(1+\frac{2}{\xi}\right)\varepsilon}{\left(1-\frac{2}{\xi}\right)\pi_\xi - \frac{2}{\xi}\varepsilon}\mathrm{d}\xi, \tag{44}$$

where the curve $\gamma_{(\xi,\pi_\xi)}$ connects a reference point to the given point (ξ,π_ξ) along the set determined by

$$\left(1-\frac{2}{\xi}\right)\pi_\xi^2 - \frac{4}{\xi}\varepsilon\pi_\xi - \left(1+\frac{2}{\xi}\right)\varepsilon^2 + 1 + \frac{\lambda^2}{\xi^2} = 0, \tag{45}$$

or, equivalently,

$$\pi_\xi = \pi_{\xi\pm}(\xi) := \frac{\frac{2}{\xi}\varepsilon \pm \sqrt{\varepsilon^2 - U_\lambda(\xi)}}{1-\frac{2}{\xi}} = \frac{1+\frac{\lambda^2}{\xi^2} - \left(1+\frac{2}{\xi}\right)\varepsilon^2}{\frac{2}{\xi}\varepsilon \mp \sqrt{\varepsilon^2 - U_\lambda(\xi)}}, \tag{46}$$

where the dimensionless effective potential is given by

$$U_\lambda(\xi) := \left(1-\frac{2}{\xi}\right)\left(1+\frac{\lambda^2}{\xi^2}\right). \tag{47}$$

As explained in the previous section, in case (I) we choose the reference point to lie on the horizon, $(2, \pi_{\xi-}(2))$, while in case (II) we choose the reference point to be the turning point $(\xi_0, \pi_{\xi+}(\xi_0) = \pi_{\xi-}(\xi_0))$, where $U_\lambda(\xi_0) = \varepsilon^2$. The curve $\gamma_{(\vartheta,\pi_\vartheta)}$ appearing in the definitions of Q^2 and Q^3 connects the reference point $(\vartheta = \pi/2, \pi_\vartheta = \sqrt{\lambda^2 - \lambda_z^2})$ to the given point $(\vartheta, \pi_\vartheta)$ clockwise along the set given by

$$\pi_\vartheta^2 + \frac{\lambda_z^2}{\sin^2\vartheta} = \lambda^2. \tag{48}$$

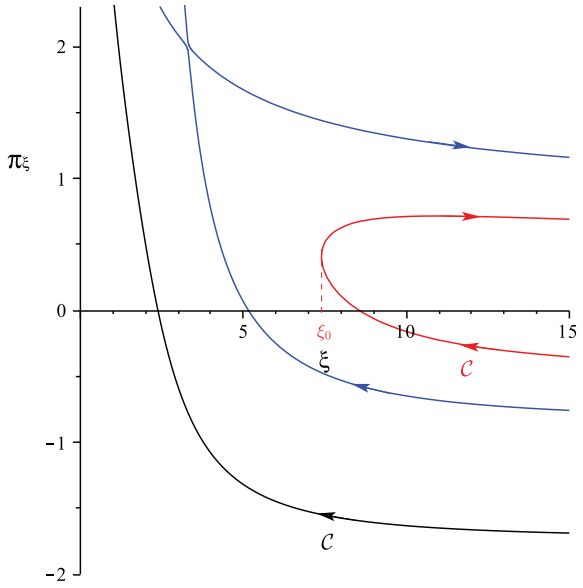

Figure 4. The curve $\mathcal{C}$ for the three different cases. Black curve: case (I). Red curve: case (II). Blue curve: the separatrix corresponding to the limit between the two cases.

As already mentioned previously, Q^2 and Q^3 increase by 2π along a full revolution along this curve, so these quantities are angle variables. For the applications in the next section the following result on the behavior of the function $G_{\varepsilon,\lambda}$ which determines the range of the variable Q^1 is important.

Lemma 3. *Let $\varepsilon > 1$ and $\lambda \geqslant 0$, $\lambda \neq \lambda_c(\varepsilon)$ be fixed, and denote by $\mathcal{C}$ the curve in the (ξ, π_ξ)-plane determined by equation (45). Then, the function $G_{\varepsilon,\lambda} : \mathcal{C} \to \mathbb{R}$ defined in equation (44) is smooth and takes the following values:*

(a) If $0 \leqslant \lambda < \lambda_c(\varepsilon)$, corresponding to case (I) of absorbed particles, $G_{\varepsilon,\lambda}$ increases monotonously from $-\infty$ to 0 as one moves along the curve $\mathcal{C}$ from $\xi = \infty$ to $\xi = 2$.
(b) If $\lambda > \lambda_c(\varepsilon)$, corresponding to case (II) of the scattered particles, $G_{\varepsilon,\lambda}$ increases monotonously from $-\infty$ to $+\infty$ as one moves clockwise along the curve $\mathcal{C}$, see figure 4.

Proof. We rewrite equation (44) as

$$G_{\varepsilon,\lambda}(\xi, \pi_\xi) = \int_{\gamma_{(\xi,\pi_\xi)}} \iota_{\mathcal{C}}^* \omega,$$

with the one-form ω on the (ξ, π_ξ)-plane given by

$$\omega_{(\xi,\pi_\xi)} = \frac{\frac{2}{\xi}\pi_\xi + \left(1 + \frac{2}{\xi}\right)\varepsilon}{\left(1 - \frac{2}{\xi}\right)\pi_\xi - \frac{2}{\xi}\varepsilon} \mathrm{d}\xi,$$

and where $\iota_{\mathcal{C}} : \mathcal{C} \subset \mathbb{R}^2 \to \mathbb{R}^2$ denotes the inclusion map. The one-form ω is well-defined and smooth except at points where the denominator $v := (1 - 2/\xi)\pi_\xi - 2\varepsilon/\xi$ vanishes.

In case (I), π_ξ is given by the expression in equation (46) corresponding to the minus sign ($\pi_{\xi-}$) along $\mathcal{C}$, and thus,

$$G_{\varepsilon,\lambda}(\xi, \pi_\xi) = \int_2^\xi f_-(x)\mathrm{d}x, \qquad f_-(\xi) = -\frac{1}{\sqrt{\varepsilon^2 - U_\lambda(\xi)}} \frac{\varepsilon^2\left(1 + \frac{2}{\xi}\right) + \frac{4}{\xi^2}\left(1 + \frac{\lambda^2}{\xi^2}\right)}{\varepsilon + \frac{2}{\xi}\sqrt{\varepsilon^2 - U_\lambda(\xi)}}.$$

Here, the function $f_- : [2, \infty) \to \mathbb{R}$ is well-defined, smooth and negative. Further, since $f_-(\xi) \to -\varepsilon/\sqrt{\varepsilon^2 - 1}$ as $\xi \to +\infty$, statement (a) follows.

In case (II), the denominator vanishes at the turning point $\xi = \xi_0$ of $\mathcal{C}$. Away from the turning point,

$$\iota_{\mathcal{C}}^* \omega = \begin{cases} f_-(\xi)\mathrm{d}\xi, & v < 0, \\ f_+(\xi)\mathrm{d}\xi, & v > 0, \end{cases} \qquad f_\pm(\xi) = \frac{\frac{2}{\xi}\sqrt{\varepsilon^2 - U_\lambda(\xi)} \pm \varepsilon}{\left(1 - \frac{2}{\xi}\right)\sqrt{\varepsilon^2 - U_\lambda(\xi)}},$$

which is regular for $\xi \neq \xi_0$. To analyze the behavior in the vicinity of the turning point, we use the new coordinates (ξ, v), in terms of which the curve $\mathcal{C}$ is parametrized by $v^2 + U_\lambda(\xi) = \varepsilon^2$, so that $2v\mathrm{d}v = -U_\lambda'(\xi)\mathrm{d}\xi$ along $\mathcal{C}$. Hence,

$$\iota_{\mathcal{C}}^* \omega = \frac{1}{1 - \frac{2}{\xi}}\left(\frac{2v}{\xi} + \varepsilon\right)\frac{\mathrm{d}\xi}{v} = \frac{-2}{1 - \frac{2}{\xi}}\left(\frac{2v}{\xi} + \varepsilon\right)\frac{\mathrm{d}v}{U_\lambda'(\xi)},$$

which is manifestly regular near the turning point, since $U_\lambda'(\xi_0) \neq 0$. Because $f_-(\xi) < 0 < f_+(\xi)$ for all $\xi > \xi_0$ and $f_\pm(\xi) \to \pm\varepsilon/\sqrt{\varepsilon^2 - 1}$ as $\xi \to +\infty$, statement (b) follows. □

Remarks.

1. Since $Q^1 = M_H m[G_{\varepsilon,\lambda}(\xi, \pi_\xi) - \tau]$ is constant along the particle trajectories, the function $G_{\varepsilon,\lambda}$ describes the evolution of the dimensionless time coordinate τ along the trajectories. Observe that in the limit case $\lambda = \lambda_c(\varepsilon)$ (corresponding to the blue curve in figure 4) the saddle point $(\xi_0, \pi_{\xi-}(\xi_0))$ is approached in infinite time, since in this case $U_\lambda'(\xi_0) = 0$.
2. As a consequence of lemma 3 the variable Q^1 is always negative for $\tau \geqslant 0$ in case (I). In contrast to this, in case (II), the two terms $G_{\varepsilon,\lambda}(\xi, \pi_\xi)$ and $-\tau$ compete against each such that Q^1 can be positive or negative. This competition will be important later, when analyzing the asymptotic behavior of the flow as $\tau \to \infty$.

After these remarks concerning the properties of Q^1 we return to the computation of the observables. In order to compute them, we find it convenient to introduce an angle χ such that

$$\begin{aligned} \pi_\vartheta &= \lambda \cos\chi, \\ \frac{\lambda_z}{\sin\vartheta} &= \lambda \sin\chi. \end{aligned}$$

In terms of the dimensionless quantities, the volume element is

$$\mathrm{dvol}_x(p) = \frac{m^3 \mathrm{d}m\mathrm{d}\varepsilon(\lambda\mathrm{d}\lambda)\mathrm{d}\chi}{\xi^2\left|\left(1-\frac{2}{\xi}\right)\pi_\xi - \frac{2}{\xi}\varepsilon\right|} = \frac{m^3 \mathrm{d}m\mathrm{d}\varepsilon(\lambda\mathrm{d}\lambda)\mathrm{d}\chi}{\xi^2\sqrt{\varepsilon^2 - U_\lambda(\xi)}}. \tag{49}$$

We split the fibre integral into two parts, corresponding to cases (I) and (II) introduced in the previous section. In both cases, the fibre integrals defining the observables range over $m \in (0,\infty)$ and $\chi \in (0, 2\pi)$. The ranges for ε and λ are as follows:

(I) In this case $\varepsilon \in (1,\infty)$ and $\lambda \in (0, \lambda_c(\varepsilon))$, where $\lambda_c(\varepsilon)$ is the critical angular momentum below which the particles fall into the black hole. Here, one has to choose the solution $\pi_{\xi-}(\xi)$ in equation (46) which, from the second expression in that equation, is seen to be regular on the horizon $\xi = 2$.

(II) In this case the ranges for ε and λ are more complicated since they are restricted by several conditions, some of which depend on the position ξ of the fibre. First, we need $\lambda > \lambda_c(\varepsilon)$ in order for the particle to be reflected at the centrifugal barrier. Next, since we are only considering particles that are incoming from infinity and reflected (as opposed to those that are coming from the white hole region and scattered at the potential before falling into the black hole), we need to ensure that ξ is larger than the location of the maximum of the effective potential, $\xi_{\max}(\lambda)$. Finally, ξ needs to lie in the allowed region where $U_\lambda(\xi) \leqslant \varepsilon^2$.
The precise bounds on ε and λ which fulfill these conditions are given in the next lemma. Note that in this case both solutions $\pi_{\xi+}(\xi)$ and $\pi_{\xi-}(\xi)$ in equation (46) have to be taken into account and summed over when computing the fibre integral.

Lemma 4. *Let $\xi > 2$ and $\varepsilon > 1$, and define*

$$\varepsilon_{\min}(\xi) := \begin{cases} \infty, & \xi \leqslant 3, \\ \sqrt{\left(1-\frac{2}{\xi}\right)\left(1+\frac{1}{\xi-3}\right)}, & 3 < \xi < 4, \\ 1, & \xi \geqslant 4. \end{cases} \qquad \lambda_{\max}(\varepsilon,\xi) := \xi\sqrt{\frac{\varepsilon^2}{1-\frac{2}{\xi}} - 1}\,. \tag{50}$$

Then, the ranges corresponding to case (II) are:

$$\varepsilon > \varepsilon_{\min}(\xi), \qquad \lambda_c(\varepsilon) < \lambda < \lambda_{\max}(\varepsilon,\xi).$$

Proof. First, we note that $U_{\lambda_{\max}}(\xi) = \varepsilon^2$, hence the condition $\lambda < \lambda_{\max}$ is equivalent to $U_\lambda(\xi) < \varepsilon^2$. Therefore, the inequalities $\lambda_c(\varepsilon) < \lambda < \lambda_{\max}(\varepsilon,\xi)$ are necessary for case (II).

In order to justify the first condition $\varepsilon > \varepsilon_{\min}(\xi)$ we first note that since $\xi_{\max}(\lambda)$ decreases monotonically from 6 to 3 as λ^2 increases from 12 to ∞ (see appendix A), the condition $\xi > \xi_{\max}(\lambda)$ is never satisfied for $\xi \leqslant 3$. Hence, in this case the integration region is empty. When $3 < \xi \leqslant 6$ the condition $\xi > \xi_{\max}$ is equivalent to $\lambda > \xi/\sqrt{\xi-3}$, which in turn implies

$$\varepsilon^2 \geqslant U_\lambda(\xi) > \left(1-\frac{2}{\xi}\right)\left(1+\frac{1}{\xi-3}\right).$$

For $3 < \xi \leqslant 4$ the right-hand side is equal to $\varepsilon_{\min}(\xi)^2$, for $4 < \xi \leqslant 6$ the right-hand side is smaller than 1. But since $\varepsilon > 1$ it follows that $\varepsilon > \varepsilon_{\min}(\xi)$.

Conversely, if $\varepsilon > \varepsilon_{\min}(\xi)$ and $\lambda > \lambda_c(\varepsilon)$, then the monotonicity of λ_c and a short calculation reveal that

$$\lambda^2 > \lambda_c(\varepsilon)^2 > \lambda_c(\varepsilon_{\min}(\xi))^2 = \begin{cases} \dfrac{\xi^2}{\xi - 3}, & 3 < \xi \leqslant 4, \\ 16, & 4 < \xi < 6, \end{cases}$$

which implies $\lambda > \xi/\sqrt{\xi - 3}$ in both cases, and hence $\xi > \xi_{\max}(\lambda)$.

Finally, when $\xi \geqslant 6$, the condition $\xi > \xi_{\max}(\xi)$ is automatically satisfied and the only bounds are $\varepsilon > 1$ and $\lambda_c(\varepsilon) < \lambda < \lambda_{\max}(\varepsilon, \xi)$. □

After these remarks we are ready to compute the observables. A fibre integral of the form

$$I(x) := \int_{\pi^{-1}(x)} f(x,p)\mathrm{dvol}_x(p)$$

is written as

$$I(x) = I^{(abs)}(x) + I^{(\mathrm{scat})}(x),$$

with the contribution from the absorbed particles

$$I^{(abs)}(x) = \frac{1}{\xi^2}\int_1^\infty \int_0^{2\pi}\int_0^{\lambda_c(\varepsilon)} \mathcal{F}_3(G_{\varepsilon,\lambda}(\xi,\pi_\xi) - \tau, Q^2, Q^3, \varepsilon, \lambda\sin\chi\sin\vartheta, \lambda)\Big|_{\pi_\xi = \pi_{\xi-}(\xi)} \frac{\lambda \mathrm{d}\lambda\mathrm{d}\chi\mathrm{d}\varepsilon}{\sqrt{\varepsilon^2 - U_\lambda(\xi)}} \tag{51}$$

and the one from the scattered particles

$$\begin{aligned} I^{(\mathrm{scat})}(x) = {} & \frac{1}{\xi^2}\int_{\varepsilon_{\min}(\xi)}^\infty \int_0^{2\pi}\int_{\lambda_c(\varepsilon)}^{\lambda_{\max}(\varepsilon,\xi)} \mathcal{F}_3(G_{\varepsilon,\lambda}(\xi,\pi_\xi) - \tau, Q^2, Q^3, \varepsilon, \lambda\sin\chi\sin\vartheta, \lambda)\Big|_{\pi_\xi = \pi_{\xi+}(\xi)} \frac{\lambda \mathrm{d}\lambda\mathrm{d}\chi\mathrm{d}\varepsilon}{\sqrt{\varepsilon^2 - U_\lambda(\xi)}} \\ & + \frac{1}{\xi^2}\int_{\varepsilon_{\min}(\xi)}^\infty \int_0^{2\pi}\int_{\lambda_c(\varepsilon)}^{\lambda_{\max}(\varepsilon,\xi)} \mathcal{F}_3(G_{\varepsilon,\lambda}(\xi,\pi_\xi) - \tau, Q^2, Q^3, \varepsilon, \lambda\sin\chi\sin\vartheta, \lambda)\Big|_{\pi_\xi = \pi_{\xi-}(\xi)} \frac{\lambda \mathrm{d}\lambda\mathrm{d}\chi\mathrm{d}\varepsilon}{\sqrt{\varepsilon^2 - U_\lambda(\xi)}}, \end{aligned} \tag{52}$$

where in the expressions for Q^2 and Q^3 one should substitute $\lambda_z = \lambda\sin\vartheta\sin\chi$ and $\pi_\vartheta = \lambda\cos\chi$. Here we have introduced the mass momenta of the distribution function, defined by

$$\mathcal{F}_n(G, Q^2, Q^3, \varepsilon, \lambda_z, \lambda) := \int_0^\infty m^n \mathcal{F}(M_H m G, Q^2, Q^3, m, m\varepsilon, M_H m\lambda_z, M_H m\lambda)\mathrm{d}m, \qquad n = 0, 1, 2, 3, \ldots \tag{53}$$

General expressions for the current density and stress energy-momentum tensor can be computed similarly, taking into account that $p_\tau = -m\varepsilon$, $p_r = m\pi_\xi$, $p_\vartheta = M_H m\lambda\cos\chi$, $p_\varphi = M_H m\lambda\sin\chi\sin\vartheta$. Since the momentum p is proportional to m, the current density depends on $\mathcal{F}_4$ and the stress energy-momentum tensor on $\mathcal{F}_5$. The fact that the observables only depend on the mass momenta $\mathcal{F}_n$ of the distribution function is due to the weak equivalence principle.

4.2. Observables in the spherically symmetric case

In the spherically symmetric case, the $\mathcal{F}_n$ are independent of Q^2, Q^3 and λ_z, and we obtain the following expressions for the observables associated with the absorbed particles:

$$J_a^{(abs)}(\tau,\xi) = \frac{2\pi}{\xi^2}\int_1^\infty\int_0^{\lambda_c(\varepsilon)} u_{a-}\mathcal{F}_4(G_{\varepsilon,\lambda}(\xi,\pi_{\xi-}(\xi)) - \tau, \varepsilon, \lambda)\frac{\lambda\mathrm{d}\lambda\mathrm{d}\varepsilon}{\sqrt{\varepsilon^2 - U_\lambda(\xi)}}, \qquad a = \tau, r, \tag{54}$$

$$T^{(abs)}_{ab}(\tau,\xi) = \frac{2\pi}{\xi^2}\int_1^\infty \int_0^{\lambda_c(\varepsilon)} u_{a-}u_{b-}\mathcal{F}_5(G_{\varepsilon,\lambda}(\xi,\pi_{\xi-}(\xi))-\tau,\varepsilon,\lambda)\frac{\lambda \mathrm{d}\lambda \mathrm{d}\varepsilon}{\sqrt{\varepsilon^2-U_\lambda(\xi)}}, \qquad a,b=\tau,r, \tag{55}$$

$$T^{(abs)}_{\vartheta\vartheta}(\tau,\xi) = M_H^2\frac{\pi}{\xi^2}\int_1^\infty \int_0^{\lambda_c(\varepsilon)} \lambda^2\mathcal{F}_5(G_{\varepsilon,\lambda}(\xi,\pi_{\xi-}(\xi))-\tau,\varepsilon,\lambda)\frac{\lambda \mathrm{d}\lambda \mathrm{d}\varepsilon}{\sqrt{\varepsilon^2-U_\lambda(\xi)}}, \tag{56}$$

with $T^{(abs)}_{\varphi\varphi} = \sin^2\vartheta\, T^{(abs)}_{\vartheta\vartheta}$ and the remaining components of $J^{(abs)}_\mu$ and $T^{(abs)}_{\mu\nu}$ being zero. Here we have introduced the shorthand notation $(u_{\tau\pm}, u_{r\pm}) = (-\varepsilon, \pi_{\xi\pm}(\xi))$ and for simplicity we have removed the entries Q^2, Q^3 and λ_z from $\mathcal{F}_n$. The nonvanishing components of the scattering part are

$$J^{(\mathrm{scat})}_a(\tau,\xi) = \frac{2\pi}{\xi^2}\int_{\varepsilon_{\min}(\xi)}^\infty \int_{\lambda_c(\varepsilon)}^{\lambda_{\max}(\varepsilon,\xi)} \sum_\pm [u_{a\pm}\mathcal{F}_4(G_{\varepsilon,\lambda}(\xi,\pi_{\xi\pm}(\xi))-\tau,\varepsilon,\lambda)]\frac{\lambda \mathrm{d}\lambda \mathrm{d}\varepsilon}{\sqrt{\varepsilon^2-U_\lambda(\xi)}}, \tag{57}$$

$$T^{(\mathrm{scat})}_{ab}(\tau,\xi) = \frac{2\pi}{\xi^2}\int_{\varepsilon_{\min}(\xi)}^\infty \int_{\lambda_c(\varepsilon)}^{\lambda_{\max}(\varepsilon,\xi)} \sum_\pm [u_{a\pm}u_{b\pm}\mathcal{F}_5(G_{\varepsilon,\lambda}(\xi,\pi_{\xi\pm}(\xi))-\tau,\varepsilon,\lambda)]\frac{\lambda \mathrm{d}\lambda \mathrm{d}\varepsilon}{\sqrt{\varepsilon^2-U_\lambda(\xi)}}, \tag{58}$$

$$T^{(\mathrm{scat})}_{\vartheta\vartheta}(\tau,\xi) = M_H^2\frac{\pi}{\xi^2}\int_{\varepsilon_{\min}(\xi)}^\infty \int_{\lambda_c(\varepsilon)}^{\lambda_{\max}(\varepsilon,\xi)} \lambda^2\sum_\pm [\mathcal{F}_5(G_{\varepsilon,\lambda}(\xi,\pi_{\xi\pm}(\xi))-\tau,\varepsilon,\lambda)]\frac{\lambda \mathrm{d}\lambda \mathrm{d}\varepsilon}{\sqrt{\varepsilon^2-U_\lambda(\xi)}}, \tag{59}$$

and $T^{(\mathrm{scat})}_{\varphi\varphi} = \sin^2\vartheta\, T^{(\mathrm{scat})}_{\vartheta\vartheta}$, with $\sum_\pm$ indicating the sum over the contributions from the two signs in $\pi_{\xi\pm}$.

4.3. Example of a simple, steady-state, spherically symmetric isotropic gas

As an explicit example, we consider a steady-state, spherically symmetric, collisionless gas consisting of identical particles of rest mass $m > 0$. Furthermore, we assume that in the asymptotic region the gas is isotropic. These assumptions imply that the distribution function must have the form

$$f(x,p) = \delta(P_0(x,p)-m) f_\infty(\varepsilon)\big|_{\varepsilon=P_i(x,p)/m}, \tag{60}$$

with $f_\infty : (1,\infty)\to\mathbb{R}$ a smooth, non-negative function which is bounded and decays sufficiently fast at infinity (see below). The associated mass momenta are

$$\mathcal{F}_n(G,Q^2,Q^3,\varepsilon,\lambda_z,\lambda) = m^n f_\infty(\varepsilon), \qquad n=0,1,2,3,\ldots$$

Since the $\mathcal{F}_n$ only depend on the energy variable ε, the integrals over the total angular momentum λ can be computed explicitly in equations (54)–(59). Using the integral identities in appendix B, we obtain

$$\begin{pmatrix} J^\tau \\ J^r \end{pmatrix}^{(abs)}(\xi) = \frac{2\pi m^4}{\xi^2}\int_1^\infty \frac{\lambda_c(\varepsilon)^2}{\sqrt{\varepsilon^2-U_0(\xi)}+\sqrt{\varepsilon^2-U_c(\xi)}}\begin{pmatrix} v^\tau \\ v^r \end{pmatrix} f_\infty(\varepsilon)\mathrm{d}\varepsilon, \tag{61}$$

$$\begin{pmatrix} T^{\tau}{}_{\tau} & T^{\tau}{}_{r} \\ T^{r}{}_{\tau} & T^{r}{}_{r} \end{pmatrix}^{(abs)}(\xi) = \frac{2\pi m^5}{\xi^2}\int_1^\infty \frac{\lambda_c(\varepsilon)^2}{\sqrt{\varepsilon^2 - U_0(\xi)} + \sqrt{\varepsilon^2 - U_c(\xi)}} \begin{pmatrix} v^{\tau}v_{\tau} & v^{\tau}v_r + \frac{2}{\xi}W \\ v^r v_{\tau} & v^r v_r + \left(1 - \frac{2}{\xi}\right)W \end{pmatrix} f_\infty(\varepsilon)\mathrm{d}\varepsilon, \tag{62}$$

$$(T^{\vartheta}{}_{\vartheta})^{(abs)}(\xi) = \frac{\pi m^5}{3\xi^4}\int_1^\infty \lambda_c(\varepsilon)^4 \frac{2\sqrt{\varepsilon^2 - U_0(\xi)} + \sqrt{\varepsilon^2 - U_c(\xi)}}{\left(\sqrt{\varepsilon^2 - U_0(\xi)} + \sqrt{\varepsilon^2 - U_c(\xi)}\right)^2} f_\infty(\varepsilon)\mathrm{d}\varepsilon, \tag{63}$$

where we have introduced the shorthand notation $U_c(\xi) := U_{\lambda_c(\varepsilon)}(\xi)$, defined the quantity

$$W := -\frac{1}{4}\left(\frac{1}{\varepsilon + \sqrt{\varepsilon^2 - U_0(\xi)}} - \frac{1 + \frac{\lambda_c(\varepsilon)^2}{\xi^2}}{\varepsilon + \sqrt{\varepsilon^2 - U_c(\xi)}}\right)^2 + \frac{1}{3\xi^4}\frac{\lambda_c(\varepsilon)^4}{\left(\sqrt{\varepsilon^2 - U_0(\xi)} + \sqrt{\varepsilon^2 - U_c(\xi)}\right)^2},$$

and the two-vector

$$\begin{pmatrix} v^{\tau} \\ v^r \end{pmatrix} = \begin{pmatrix} \varepsilon + \frac{1}{\xi}\frac{1}{\varepsilon + \sqrt{\varepsilon^2 - U_0(\xi)}} + \frac{1}{\xi}\frac{1 + \frac{\lambda_c(\varepsilon)^2}{\xi^2}}{\varepsilon + \sqrt{\varepsilon^2 - U_c(\xi)}} \\ -\frac{1}{2}\left(\sqrt{\varepsilon^2 - U_0(\xi)} + \sqrt{\varepsilon^2 - U_c(\xi)}\right) \end{pmatrix},$$

with corresponding co-vector

$$\begin{pmatrix} v_{\tau} \\ v_r \end{pmatrix} = \begin{pmatrix} -\varepsilon \\ -\varepsilon + \frac{1}{2}\frac{1}{\varepsilon + \sqrt{\varepsilon^2 - U_0(\xi)}} + \frac{1}{2}\frac{1 + \frac{\lambda_c(\varepsilon)^2}{\xi^2}}{\varepsilon + \sqrt{\varepsilon^2 - U_c(\xi)}} \end{pmatrix}.$$

For the terms corresponding to the scattered particles, we find

$$\begin{pmatrix} J^{\tau} \\ J^r \end{pmatrix}^{(\mathrm{scat})}(\xi) = \frac{4\pi m^4}{\left(1 - \frac{2}{\xi}\right)^2}\int_{\varepsilon_{\min}(\xi)}^\infty \begin{pmatrix} 1 \\ 0 \end{pmatrix} \varepsilon\sqrt{\varepsilon^2 - U_c(\xi)} f_\infty(\varepsilon)\mathrm{d}\varepsilon, \tag{64}$$

$$\begin{pmatrix} T^{\tau}{}_{\tau} & T^{\tau}{}_{r} \\ T^{r}{}_{\tau} & T^{r}{}_{r} \end{pmatrix}^{(\mathrm{scat})}(\xi) = \frac{4\pi m^5}{\left(1 - \frac{2}{\xi}\right)^2}\int_{\varepsilon_{\min}(\xi)}^\infty \begin{pmatrix} -\varepsilon^2 & \frac{2}{3\xi}\frac{4\varepsilon^2 - U_c(\xi)}{1 - \frac{2}{\xi}} \\ 0 & \frac{1}{3}(\varepsilon^2 - U_c(\xi)) \end{pmatrix} \sqrt{\varepsilon^2 - U_c(\xi)} f_\infty(\varepsilon)\mathrm{d}\varepsilon, \tag{65}$$

$$(T^{\vartheta}{}_{\vartheta})^{(\mathrm{scat})}(\xi) = \frac{2\pi m^5}{\left(1 - \frac{2}{\xi}\right)^2}\int_{\varepsilon_{\min}(\xi)}^\infty \left[\left(1 - \frac{2}{\xi}\right)\frac{\lambda_c(\varepsilon)^2}{\xi^2} + \frac{2}{3}(\varepsilon^2 - U_c(\xi))\right]\sqrt{\varepsilon^2 - U_c(\xi)} f_\infty(\varepsilon)\mathrm{d}\varepsilon. \tag{66}$$

Physical applications of these results will be discussed in the next section; for the moment, we just like to emphasize that the expressions $J_\mu^{(abs)}$ and $T_{\mu\nu}^{(abs)}$ are manifestly regular on the horizon $\xi = 2$, while the contributions $J_\mu^{(\mathrm{scat})}$ and $T_{\mu\nu}^{(\mathrm{scat})}$ for the scattered particles vanish inside the photon sphere, that is, for $\xi < 3$ (see the definition of $\varepsilon_{\min}(\xi)$ in equation (50)).

The integrals in equations (61)–(66) are well-defined as long as the function f_∞ decays sufficiently fast as $\varepsilon \to \infty$. For example, this is the case for exponential decay, i.e. if there are constants $\alpha, \beta > 0$ such that

$$0 \leqslant f_\infty(\varepsilon) \leqslant \alpha \mathrm{e}^{-\beta\varepsilon}, \qquad \varepsilon \geqslant 1.$$

4.4. Comparison with the perfect fluid case

We conclude this section with a comparison between the properties of the observables of a collisionless gas with those of an isotropic perfect fluid. In the latter case, the particle current density and the stress energy-momentum tensor are given by

$$J^\mu = nu^\mu, \qquad T^\mu{}_\nu = \rho u^\mu u_\nu + p(u^\mu u_\nu + \delta^\mu{}_\nu), \tag{67}$$

with n, ρ, p and u^μ the particle density, energy density, pressure and four-velocity of the fluid, respectively. The conditions that characterize the observables (67) can be formulated as follows.

(i) $J^\mu = nu^\mu$ is a timelike eigenvector of $T^\mu{}_\nu$, that is $T^\mu{}_\nu u^\nu = -\rho u^\mu$. An important consequence of this property is that the stress energy-momentum tensor can be diagonalized:

$$T^\mu{}_\nu = \rho e_0^\mu e_{0\nu} + p_1 e_1^\mu e_{1\nu} + p_2 e_2^\mu e_{2\nu} + p_3 e_3^\mu e_{3\nu}, \tag{68}$$

with $e_0 = u$ and e_1, e_2, e_3 an orthonormal frame perpendicular to u. In this case, p_1, p_2 and p_3 are called the *principle pressures*. In the spherically symmetric case, e_1 can be chosen in the radial direction, and then $p_1 = p_{\mathrm{rad}}$ describes the radial pressure and $p_2 = p_3 = p_{\mathrm{tan}}$ the tangential one.

(ii) The principal pressures are equal to each other.

In order to compare the properties of the kinetic gas to those of the perfect fluid, let us analyze these conditions for the spherically symmetric accretion case described in the previous section. First, regarding the scattering part given in equations (64)–(66) we observe that the current density is proportional to the Killing vector field $k = \frac{\partial}{\partial t}$. Furthermore, it is seen from equation (65) that k is also an eigenvector of $T^{\mu\,(\mathrm{scat})}_{\ \ \ \nu}$, such that condition (i) is satisfied. To verify the second condition, we introduce the orthonormal frame

$$e_0 = \frac{M_H}{\sqrt{1-\frac{2}{\xi}}}\frac{\partial}{\partial\tau}, \tag{69}$$

$$e_1 = \frac{M_H}{\sqrt{1-\frac{2}{\xi}}}\left[\frac{2}{\xi}\frac{\partial}{\partial\tau} + \left(1-\frac{2}{\xi}\right)\frac{\partial}{\partial\xi}\right], \tag{70}$$

$$e_2 = \frac{M_H}{\xi}\frac{\partial}{\partial\vartheta}, \tag{71}$$

$$e_3 = \frac{M_H}{\xi \sin\vartheta}\frac{\partial}{\partial\varphi}, \tag{72}$$

such that e_0 is parallel to J^{scat}. It is simple to verify that this frame diagonalizes $T^{\mu}{}_{\nu}{}^{(\mathrm{scat})}$, and the associated principle pressures are

$$p^{(\mathrm{scat})}_{\mathrm{rad}} = \frac{4\pi m^5}{\left(1-\frac{2}{\xi}\right)^2}\int_{\varepsilon_{\min}(\xi)}^{\infty}\frac{1}{3}(\varepsilon^2 - U_c(\xi))^{3/2} f_\infty(\varepsilon)\mathrm{d}\varepsilon, \tag{73}$$

$$p^{(\mathrm{scat})}_{\mathrm{tan}} = p^{(\mathrm{scat})}_{\mathrm{rad}} + \frac{2\pi m^5}{1-\frac{2}{\xi}}\int_{\varepsilon_{\min}(\xi)}^{\infty}\frac{\lambda_c(\varepsilon)^2}{\xi^2}(\varepsilon^2 - U_c(\xi))^{1/2} f_\infty(\varepsilon)\mathrm{d}\varepsilon. \tag{74}$$

We see that in general, $p^{(\mathrm{scat})}_{\mathrm{tan}}$ is larger than $p^{(\mathrm{scat})}_{\mathrm{rad}}$, so that the principal pressures are different from each other. In the asymptotic limit $\xi \to \infty$ this difference converges to zero and the gas is fluid-like. For later purposes, we also note that the triad frame $\{e_1, e_2, e_3\}$ is Fermi-transported along the Killing observers, such that it defines a non-rotating frame for these observers.

Regarding the contributions from the absorbed particles described by equations (61)–(63), in general not even the first condition (i) is satisfied, as we will see in an explicit example in the next section. Further, in general $J^{(abs)}$ does not point in the same direction as $J^{(\mathrm{scat})}$. These comments should make clear that the observables belonging to a kinetic gas have a much richer structure than those belonging to a perfect fluid.

5. Applications to the accretion problem

In this section, we apply our results to the accretion of a relativistic, collisionless kinetic gas into a Schwarzschild black hole. We discuss two important results. The first one, discussed in section 5.1, provides the most general steady-state, spherically symmetric accretion solution for a collisionless gas which, at infinity, is given by an equilibrium configuration with some given temperature. From this we compute the relevant physical quantities, like the accretion and compression rates as well as the particle and energy densities and the principle pressures in the asymptotic region and on the horizon.

The second result, discussed in section 5.2, considers dynamical nonlinear perturbations of the spherical, steady-state configurations which arises from rather general (possibly non-spherical) initial data for the distribution function. In particular, we derive an asymptotic stability result implying the stability of the spherically symmetric, steady-state configurations.

5.1. Spherically symmetric, steady-state configurations with given temperature at infinity

Here, we consider the physical scenario in which gas particles are accreted from a reservoir of identical massive and spinless particles at spatial infinity. Like in section 4.3, we assume that the gas is steady-state, spherically symmetric and collisionless. Additionally, we suppose that the reservoir is isotropic and that some physical process in the past drove it to thermodynamic equilibrium. Therefore, we can characterize the state of the gas at infinity by an equilibrium distribution function with given temperature $T > 0$. However, we emphasize that it does not make sense to associate a local temperature to the gas, since we neglect collisions between the gas particles so that at finite radius one does not expect to gas to be in local thermodynamic equilibrium. Hence, T should be regarded as an asymptotic parameter only.

As a consequence of our assumptions, the distribution function has the form

$$f(x,p) = \alpha\delta(P_0(x,p) - m)\mathrm{e}^{-\beta E}\big|_{E=P_{\mathrm{l}}(x,p)}, \tag{75}$$

with $\alpha > 0$ a normalization constant, $m > 0$ the mass of the gas particles and $\beta = (k_{\mathrm{B}}T)^{-1} > 0$ the inverse temperature.[9] The particle current density and stress energy-momentum tensor are given by the expressions in equations (61)–(66) with the function $f_\infty(\varepsilon)$ replaced with $\alpha\mathrm{e}^{-m\beta\varepsilon}$. In the following, we discuss the physical content of these results.

First, we note that using the inverse metric (15) we can easily compute the particle and energy fluxes through a sphere of constant areal radius r,[10]

$$j_n := 4\pi r^2 J^r = -4\pi^2\alpha M_H^2 m^4 \int_1^\infty \lambda_c(\varepsilon)^2\mathrm{e}^{-z\varepsilon}\mathrm{d}\varepsilon, \tag{76}$$

$$j_\varepsilon := -4\pi r^2 T^r{}_\tau = -4\pi^2\alpha M_H^2 m^5 \int_1^\infty \varepsilon\lambda_c(\varepsilon)^2\mathrm{e}^{-z\varepsilon}\mathrm{d}\varepsilon, \tag{77}$$

where we recall that $\lambda_c(\varepsilon)$ is the critical angular momentum calculated in appendix A. Here and in the following, the dimensionless parameter z is defined by

$$z := m\beta = \frac{mc^2}{k_{\mathrm{B}}T},$$

where for convenience we have reintroduced the speed of light c. For typical astrophysical applications this quantity is very large, since the thermal energy is much smaller than the rest energy of the particles. For gas accreted from the interstellar medium, for instance, z is of the order 10^9 [49]. As expected from the conservation laws $\nabla_\mu J^\mu = 0$ and $\nabla_\mu(-T^\mu{}_\nu k^\nu) = 0$ the flux quantities j_n and j_ε are constant. Note that only the absorbed particles contribute to these fluxes; the contributions from the in- and outgoing particles that are scattered at the potential cancel out, such that $(J^r)^{(\mathrm{scat})} = (T^r{}_\tau)^{(\mathrm{scat})} = 0$.

Next, we analyze the observables in the asymptotic region $\xi \to \infty$. In this case, it is only the scattered particles that yield a nonvanishing contribution, and due to our assumptions on the distribution function, the gas in this region behaves as an isotropic, special relativistic perfect fluid [1, 5]. Indeed, taking the limit $\xi \to \infty$ in equations (64)–(66) and noticing that $U_c(\xi) \to 1$ one finds

$$\lim_{r\to\infty} J^\mu = n_\infty u_\infty^\mu, \qquad \lim_{r\to\infty} T^{\mu\nu} = (\varepsilon_\infty + p_\infty)u_\infty^\mu u_\infty^\nu + p_\infty\eta^{\mu\nu},$$

with the four-velocity at infinity given by $u_\infty = k = \frac{\partial}{\partial\tau}$ and $\eta^{\mu\nu}$ denoting the components of the inverse Minkowski metric. The particle density n_∞, energy density ε_∞ and pressure p_∞ at infinity can be expressed in terms of the modified Bessel functions of the second kind:

$$K_l(z) = \int_0^\infty \mathrm{e}^{-z\cosh\psi}\cosh(l\psi)\mathrm{d}\psi = \frac{z^l}{1\cdot 3\cdots(2l-1)}\int_0^\infty \mathrm{e}^{-z\cosh\psi}\sinh^{2l}\psi\,\mathrm{d}\psi, \quad z > 0, \quad l = 1, 2, 3, \ldots$$

[9] As we discuss in [62] the distribution function defined by equation (75) does not describe a local equilibrium state at finite radius, though it does so at infinity.

[10] The coordinate-invariant definition of these quantities is $j_n = 4\pi r^2\mathrm{d}r(\mathbf{J})$ and $j_\varepsilon = -4\pi r^2\mathrm{d}r(\mathbf{T}(k))$, where r is the areal radius, $\mathbf{J} = J^\mu\partial_\mu$ the current density vector and $\mathbf{T}(k) := T^\mu{}_\nu k^\nu\partial_\mu$ the contraction of the stress energy-momentum tensor with the Killing vector field k.

as

$$n_\infty(z) = 4\pi\alpha m^4 \frac{K_2(z)}{z}, \tag{78}$$

$$\varepsilon_\infty(z) = 4\pi\alpha m^5\left[\frac{K_1(z)}{z} + 3\frac{K_2(z)}{z^2}\right], \qquad p_\infty(z) = 4\pi\alpha m^5 \frac{K_2(z)}{z^2}, \tag{79}$$

and the ideal gas equation $p_\infty = k_B T n_\infty$ is satisfied.

At the horizon, $(J^\mu)^{(\mathrm{scat})}$ and $(T^\mu{}_\nu)^{(\mathrm{scat})}$ vanish, and thus we only have the contributions from the absorbed particles. The particle and energy densities n_H and ρ_H and the radial and tangential pressures p_{rad} and p_{tan} are determined by $J^\mu = n_H u_H^\mu$ ($g_{\mu\nu}u_H^\mu u_H^\nu = -1$) and the decomposition (68) which, for a kinetic gas, is guaranteed to exist [10, 63]. Evaluating the expressions in equations (61)–(63) at $\xi = 2$ and noting that $U_\lambda(2) = 0$ one finds

$$\begin{pmatrix} J^\tau \\ J^r \end{pmatrix}\Big|_{\xi=2} = \frac{1}{4}\pi\alpha m^4 \int_1^\infty \frac{\lambda_c(\varepsilon)^2}{\varepsilon}\begin{pmatrix} v^\tau \\ v^r \end{pmatrix} \mathrm{e}^{-z\varepsilon}\mathrm{d}\varepsilon, \tag{80}$$

$$\begin{pmatrix} T^\tau{}_\tau & T^\tau{}_r \\ T^r{}_\tau & T^r{}_r \end{pmatrix}\Big|_{\xi=2} = \frac{1}{4}\pi\alpha m^5 \int_1^\infty \frac{\lambda_c(\varepsilon)^2}{\varepsilon}\begin{pmatrix} v^\tau v_\tau & v^\tau v_r + W \\ v^r v_\tau & v^r v_r \end{pmatrix} \mathrm{e}^{-z\varepsilon}\mathrm{d}\varepsilon, \qquad W = \frac{1}{3\varepsilon^2}\left(\frac{\lambda_c(\varepsilon)}{4}\right)^4, \tag{81}$$

$$T^\vartheta{}_\vartheta\Big|_{\xi=2} = \frac{1}{64}\pi\alpha m^5 \int_1^\infty \frac{\lambda_c(\varepsilon)^4}{\varepsilon}\mathrm{e}^{-z\varepsilon}\mathrm{d}\varepsilon, \tag{82}$$

with

$$\begin{pmatrix} v^\tau \\ v^r \end{pmatrix} = \varepsilon\begin{pmatrix} 1 + \dfrac{1}{2\varepsilon^2}\left(1 + \dfrac{\lambda_c(\varepsilon)^2}{8}\right) \\ -1 \end{pmatrix}, \qquad \begin{pmatrix} v_\tau \\ v_r \end{pmatrix} = -\varepsilon\begin{pmatrix} 1 \\ 1 - \dfrac{1}{2\varepsilon^2}\left(1 + \dfrac{\lambda_c(\varepsilon)^2}{8}\right) \end{pmatrix}.$$

These are still rather complicated expressions. To obtain simpler expressions which are easier to interprete, we take the limit $z \to \infty$ (remember that for typical astrophysical applications z is very large) and obtain (see appendix C for details)

$$\frac{\rho_H}{n_H} = \frac{mc^2}{2\sqrt{3}}\left(3 + \sqrt{\frac{31}{3}}\right) \approx 1.79 mc^2, \tag{83}$$

$$\frac{p_{\mathrm{rad}}}{n_H} = \frac{mc^2}{2\sqrt{3}}\left(-3 + \sqrt{\frac{31}{3}}\right) \approx 0.0619 mc^2, \tag{84}$$

$$\frac{p_{\mathrm{tan}}}{n_H} = \frac{mc^2}{\sqrt{3}} \approx 0.577 mc^2. \tag{85}$$

We note that the tangential pressure is almost an order of magnitude larger than the radial one, showing that the collisionless kinetic gas behaves very differently than an isotropic perfect fluid near the horizon. This difference is probably due to the fact that most gas particles have nonvanishing angular momenta and do not collide. Moreover, the four-velocity and timelike eigenvector e_0 of $(T^\mu{}_\nu)$ are

$$u_H = \frac{1}{\sqrt{3}}\left[\frac{5}{2}\frac{\partial}{\partial\tau} - \frac{\partial}{\partial r}\right], \qquad e_0 = \left(\frac{31}{3}\right)^{-1/4}\left[\left(1+\frac{1}{2}\sqrt{\frac{31}{3}}\right)\frac{\partial}{\partial\tau} - \frac{\partial}{\partial r}\right]. \tag{86}$$

Although the value of $1+\sqrt{31/3}/2 \simeq 2.61$ is quite close to 5/2, this calculation shows that u and e_0 are not parallel, and thus condition (i) in section 4.4 for the observables to be fluid-like is violated.

Finally, we compute the mass accretion rate $\dot{M} := mj_n$ and compression ratio n_H/n_∞ of the gas. For large z we find (see appendix C)

$$\lim_{z\to\infty}\frac{1}{\sqrt{2\pi z}}\frac{\dot{M}}{n_\infty} = -4mcr_H^2, \qquad \lim_{z\to\infty}\frac{1}{\sqrt{2\pi z}}\frac{n_H}{n_\infty} = \frac{\sqrt{3}}{\pi}, \tag{87}$$

where $r_H = 2GM_H/c^2$ is the Schwarzschild radius of the black hole. Therefore, both the accretion rate and the compression ratio scale like $z^{1/2}$ for large values of z, and hence they are smaller by a factor of z compared to the corresponding quantities in the Michel model [48, 49, 51, 52], describing the spherical steady-state accretion of a polytropic perfect fluid.

A more detailed analysis regarding the behavior and physical properties of the observables of the spherical steady-state model as a function of radius and the asymptotic temperature is given in [62].

5.2. Stability of the flow

The main goal of this section is to study the stability of the spherical, steady-state accretion flows discussed in the previous section. To this end, we consider time-dependent, possibly nonspherical and nonlinear perturbations of the distribution function arising from fairly general initial data on the initial time slice $\tau = 0$. According to the results in the previous sections, such initial data can be parametrized by two functions $\mathcal{F}_i^{(abs)}(G, Q^2, Q^3, \varepsilon, \lambda_z, \lambda)$ and $\mathcal{F}_i^{(\mathrm{scat})}(G, Q^2, Q^3, \varepsilon, \lambda_z, \lambda)$ of the six variables G, Q^2, Q^3, ε, λ_z and λ, see equations (41)–(43) for the definitions of G, Q^2, Q^3 as functions of (x,p).[11] Here, we recall that the range of these variables is:

$$R^{(abs)} := \{(G, Q^2, Q^3, \varepsilon, \lambda_z, \lambda) \in \mathbb{R}^6 : -\infty < G \leqslant 0, 1 < \varepsilon < \infty, |\lambda_z| < \lambda, 0 \leqslant \lambda < \lambda_c(\varepsilon)\}$$

and

$$R^{(\mathrm{scat})} := \{(G, Q^2, Q^3, \varepsilon, \lambda_z, \lambda) \in \mathbb{R}^6 : -\infty < G \leqslant \infty, 1 < \varepsilon < \infty, |\lambda_z| < \lambda, \lambda > \lambda_c(\varepsilon)\},$$

respectively. Therefore, $\mathcal{F}_i^{(abs)} : R^{(abs)} \to \mathbb{R}$ and $\mathcal{F}_i^{(\mathrm{scat})} : R^{(\mathrm{scat})} \to \mathbb{R}$ are non-negative functions which, in addition, are 2π-periodic in Q^2 and Q^3.

The solution generated by this data is:

$$f(x,p) = \begin{cases} \mathcal{F}_i^{(abs)}(G_{\varepsilon,\lambda}(\xi,\pi_\xi) - \tau, Q^2, Q^3, \varepsilon, \lambda_z, \lambda), & \text{if } \lambda < \lambda_c(\varepsilon) \\ \mathcal{F}_i^{(\mathrm{scat})}(G_{\varepsilon,\lambda}(\xi,\pi_\xi) - \tau, Q^2, Q^3, \varepsilon, \lambda_z, \lambda), & \text{if } \lambda > \lambda_c(\varepsilon) \end{cases}, \tag{88}$$

where the function $G_{\varepsilon,\lambda}(\xi,\pi_\xi)$ is given in equation (44). Note that the solution is stationary if and only if the functions $\mathcal{F}_i^{(abs)}$ and $\mathcal{F}_i^{(\mathrm{scat})}$ are independent of G. The observables are given

[11] For simplicity, we assume that all the gas particles have the same positive rest mass $m > 0$. For solutions describing particles with different masses, one simply replaces the distribution function with the appropriate mass momenta, see equation (53).

by fibre integrals over this distribution function, as explained and worked out in the previous section. Here, we analyze the asymptotic behavior of these observables along certain future-directed timelike curves.

We assume that the initial functions $\mathcal{F}_i^{(abs)}$ and $\mathcal{F}_i^{(\mathrm{scat})}$ satisfy the following conditions:

(i) $\mathcal{F}_i^{(abs)} : R^{(abs)} \to \mathbb{R}$ and $\mathcal{F}_i^{(\mathrm{scat})} : R^{(\mathrm{scat})} \to \mathbb{R}$ are non-negative, measurable functions which are 2π-periodic in Q^2 and Q^3. Furthermore, we require these functions to be uniformly bounded from above by an equilibrium distribution function, that is, there exist positive constants α and β such that

$$0 \leqslant \mathcal{F}_i^{(abs,\mathrm{scat})}(G, Q^2, Q^3, \varepsilon, \lambda_z, \lambda) \leqslant \alpha \mathrm{e}^{-\beta\varepsilon}$$

for all $(G, Q^2, Q^3, \varepsilon, \lambda_z, \lambda) \in R^{(abs,\mathrm{scat})}$.

(ii) There exists a function $f_{-\infty} : (1, \infty) \to \mathbb{R}$ such that

$$\lim_{G\to-\infty} \mathcal{F}_i^{(abs)}(G, Q^2, Q^3, \varepsilon, \lambda_z, \lambda) = f_{-\infty}(\varepsilon)$$

for all $0 \leqslant Q^2, Q^3 \leqslant 2\pi$, $\varepsilon > 1$, and $|\lambda_z| < \lambda < \lambda_c(\varepsilon)$.

(iii) There exists a function $f_{+\infty} : (1, \infty) \to \mathbb{R}$ such that in the limits $G \to \pm\infty$ the function $\mathcal{F}_i^{(\mathrm{scat})}$ converges uniformly in $(Q^2, Q^3, \lambda_z, \lambda)$ to the functions $f_{\pm\infty}$:

$$\lim_{G\to-\infty} \sup_{\substack{Q^2,Q^3\in[0,2\pi] \\ |\lambda_z|<\lambda,\lambda>\lambda_c(\varepsilon)}} |\mathcal{F}_i^{(\mathrm{scat})}(G, Q^2, Q^3, \varepsilon, \lambda_z, \lambda) - f_{-\infty}(\varepsilon)| = 0, \tag{89}$$

$$\lim_{G\to+\infty} \sup_{\substack{Q^2,Q^3\in[0,2\pi] \\ |\lambda_z|<\lambda,\lambda>\lambda_c(\varepsilon)}} |\mathcal{F}_i^{(\mathrm{scat})}(G, Q^2, Q^3, \varepsilon, \lambda_z, \lambda) - f_{+\infty}(\varepsilon)| = 0, \tag{90}$$

for all $\varepsilon > 1$.

Condition (i) guarantees the existence of the fibre integrals defining the particle current density J_μ and the stress energy-momentum tensor $T_{\mu\nu}$, as follows from the analysis in the last section. Conditions (ii) and (iii) imply that in the asymptotic region $\xi \to \infty$, where $G \to \pm\infty$, the initial distribution function converges to distribution functions $f_{\pm\infty}(\varepsilon)$ which only depend on the energy ε. Here, the plus (minus) signs refer to particles which, at $\tau = 0$, have positive (negative) radial velocity. For an equilibrium distribution function which does not discriminate between infalling and outgoing particles, one chooses $f_{-\infty} = f_{+\infty}$, but for generality we shall not necessarily impose this condition.

In the following, we analyze the behavior of the observables J_μ and $T_{\mu\nu}$ associated with the solution (88) of the Liouville equation. These observables are given by integrals of the form given in equations (51) and (52). The main results of this section are described in the following two theorems.

Theorem 2. *Consider the solution $f : \Gamma_{\mathrm{accr}} \to \mathbb{R}$ of the Liouville equation belonging to initial data satisfying the conditions (i),(ii), and (iii) above. Then, along the world line of a future-directed static observer $\gamma(t)$,*

$$\lim_{t\to\infty} J_\alpha(\gamma(t)) = J_\alpha[f_{-\infty}], \qquad \lim_{t\to\infty} T_{\alpha\beta}(\gamma(t)) = T_{\alpha\beta}[f_{-\infty}], \tag{91}$$

where J_α and $T_{\alpha\beta}$ are the components of the current density and stress energy-momentum tensor with respect to the non-rotating frame $\{e_0, e_1, e_2, e_3\}$ defined in equations (69)–(72), and

$J_\alpha[f_{-\infty}] = J^{(abs)}_\alpha + J^{(\mathrm{scat})}_\alpha$ and $T_{\alpha\beta}[f_{-\infty}] = T^{(abs)}_{\alpha\beta} + T^{(\mathrm{scat})}_{\alpha\beta}$ are the corresponding quantities for a steady-state, spherical configurations as in equations (61)–(66) with f_∞ replaced with $f_{-\infty}$.

Theorem 3. *Consider the solution $f : \Gamma_{\mathrm{accr}} \to \mathbb{R}$ of the Liouville equation belonging to initial data satisfying the conditions (i), (ii), and (iii) above. Let $\gamma(t)$ be the world line of a future-directed timelike observer with constant asymptotic radial velocity with respect to static observers,*

$$v_{obs,\infty} := \lim_{t\to\infty} \frac{\mathrm{d}r}{\mathrm{d}t}(t) = \lim_{\tau\to\infty} \frac{\mathrm{d}\xi}{\mathrm{d}\tau}(\tau)$$

satisfying $0 < v_{obs,\infty} < 1$ meaning that at large times, the observer moves away from the black hole with constant radial velocity.

Then, with respect to the static frame $\{e_0, e_1, e_2, e_3\}$ defined in equations (69)–(72), we have

$$\lim_{t\to\infty}\begin{pmatrix} J^0 \\ J^1 \end{pmatrix}(\gamma(t)) = 4\pi m^4 \int_1^\infty \begin{pmatrix} 1 \\ 0 \end{pmatrix} \varepsilon\sqrt{\varepsilon^2-1} f_{-\infty}(\varepsilon)\mathrm{d}\varepsilon + \pi m^4 \int_1^{\varepsilon_{obs,\infty}} \begin{pmatrix} 2\varepsilon\left[\sqrt{\varepsilon^2-1} - a(\varepsilon)\right] \\ \varepsilon^2 - 1 - a(\varepsilon)^2 \end{pmatrix} \Delta f_\infty(\varepsilon)\mathrm{d}\varepsilon, \tag{92}$$

$$\begin{aligned}\lim_{t\to\infty}\begin{pmatrix} T^0{}_0 & T^0{}_1 \\ T^1{}_0 & T^1{}_1 \end{pmatrix}(\gamma(t)) = {} & 4\pi m^5 \int_1^\infty \begin{pmatrix} -\varepsilon^2 & 0 \\ 0 & \frac{1}{3}(\varepsilon^2-1) \end{pmatrix} \sqrt{\varepsilon^2-1} f_{-\infty}(\varepsilon)\mathrm{d}\varepsilon \\ & + \pi m^5 \int_1^{\varepsilon_{obs,\infty}} \begin{pmatrix} 2\varepsilon^2\left[a(\varepsilon) - \sqrt{\varepsilon^2-1}\right] & \varepsilon\,[\varepsilon^2 - 1 - a(\varepsilon)^2] \\ -\varepsilon\,[\varepsilon^2 - 1 - a(\varepsilon)^2] & -\frac{2}{3}\,[a(\varepsilon)^3 - (\varepsilon^2-1)^{3/2}] \end{pmatrix} \Delta f_\infty(\varepsilon)\mathrm{d}\varepsilon,\end{aligned} \tag{93}$$

$$\begin{aligned}\lim_{t\to\infty} T^2{}_2(\gamma(t)) = \lim_{t\to\infty} T^3{}_3(\gamma(t)) = {} & \frac{4\pi m^5}{3} \int_1^\infty (\varepsilon^2-1)^{3/2} f_{-\infty}(\varepsilon)\mathrm{d}\varepsilon \\ & + \frac{\pi m^5}{3} \int_1^{\varepsilon_{obs,\infty}} [a(\varepsilon) - \sqrt{\varepsilon^2-1}\,]^2 [a(\varepsilon) + 2\sqrt{\varepsilon^2-1}\,] \Delta f_\infty(\varepsilon)\mathrm{d}\varepsilon,\end{aligned} \tag{94}$$

where $\varepsilon_{obs,\infty} := (1 - v^2_{obs,\infty})^{-1/2}$, $a(\varepsilon) := (\varepsilon^2 - 1)/(\varepsilon v_{obs,\infty})$, and where we have defined the difference

$$\Delta f_\infty := f_{+\infty} - f_{-\infty}.$$

The limits of the remaining components vanish.

Remarks.

1. Therefore, in the limit $t \to \infty$, the tetrad components of the observables J_α and $T_{\alpha\beta}$ converge pointwise to the sum of two expressions, the first one being independent of the observer's radial velocity and thus identical to the ones obtained from spherically symmetric stationary accretion with boundary condition $f_{-\infty}(\varepsilon)$. The other expression depends on the observer's asymptotic radial velocity and the difference Δf_∞ between the in- and outgoing distribution functions at infinity. For the particular case where

$f_{+\infty} = f_{-\infty}$ this second expression vanishes, and the pointwise limit of the observables J_α and $T_{\alpha\beta}$ is independent of the observer.

2. From the moving observer's point of view, it makes sense to ask how the results given in theorem 3 change if instead of the static frame $\{e_0, e_1, e_2, e_3\}$ defined in equations (69)–(72), a non-rotating (Fermi-propagated) frame $\{\hat{e}_0, \hat{e}_1, \hat{e}_2, \hat{e}_3\}$ along the observer is considered. The relation between the two frames is given by a Lorentz transformation of the form

$$\hat{e}_\alpha(t) = \Lambda(t)^\delta{}_\alpha e_\delta(t), \qquad \Lambda(t)^\delta{}_\alpha := [\Lambda_{\mathrm{rot}}(t)]^\beta{}_\alpha [\Lambda_{\mathrm{boost}}(t)]^\delta{}_\beta,$$

where $\Lambda_{\mathrm{rot}}(t)$ is an appropriate rotation and $\Lambda_{\mathrm{boost}}(t)$ a boost such that $u = [\Lambda_{\mathrm{boost}}(t)]^\delta{}_0 e_\delta(t)$ is the observer's four-velocity. Under such a transformation, the tetrad components of the observables change according to

$$J^\alpha = \Lambda^\alpha{}_\beta \hat{J}^\beta, \qquad T^\alpha{}_\beta = \Lambda^\alpha{}_\gamma \Lambda_\beta{}^\delta \hat{T}^\gamma{}_\delta,$$

where $\Lambda_\beta{}^\delta$ denotes the components of the inverse transposed of the matrix Λ. Hence, the limits of $\hat{J}^\alpha$ and $\hat{T}^\alpha{}_\beta$ as $t \to \infty$ exist if and only if $\Lambda(t)^\alpha{}_\beta$ has a well-defined limit for $t \to \infty$. This will be the case, for example, if the observer has an asymptotic constant velocity in the radial direction, in which case

$$\lim_{t\to\infty} (\Lambda_{\mathrm{boost}}(t)^\alpha{}_\beta) = \begin{pmatrix} \varepsilon_{obs,\infty} & \varepsilon_{obs,\infty} v_{obs,\infty} & 0 & 0 \\ \varepsilon_{obs,\infty} v_{obs,\infty} & \varepsilon_{obs,\infty} & 0 & 0 \\ 0 & 0 & 1 & 0 \\ 0 & 0 & 0 & 1 \end{pmatrix}.$$

3. The proofs of our stability theorems require the understanding of two key issues. The first one is the behavior of the distribution function $f(x,p)$ for large values of τ. This involves analyzing the function $G_{\varepsilon,\lambda}(\xi, \pi_\xi) - \tau$ along the world line of the observer, where $G_{\varepsilon,\lambda}(\xi, \pi_\xi)$ is given by the line integral in equation (44). For static observers this issue is trivial since $G_{\varepsilon,\lambda}(\xi, \pi_\xi)$ is constant in ξ (for fixed values of the energy ε and angular momentum λ). However, for moving observers the two terms $G_{\varepsilon,\lambda}(\xi, \pi_\xi)$ and τ compete against each other, and thus this issue requires a detailed analysis.

   The second issue is about the validity of passing the limit $\tau \to \infty$ under the integrals over the momentum p. In order to handle this issue, we use Lebesgue's dominated convergence theorem[12]. This issue is also much more delicate for moving observers than for static ones, since in the former case the fibre and the volume form on it are not fixed, so that it is more difficult to find a uniform bound.

Proof of theorem 2. In the static case, the function $G_{\varepsilon,\lambda}(\xi, \pi_\xi)$ is constant along the world line of the observer (for each fixed values of the energy ε and the angular momentum λ). Therefore, it follows from our assumptions that

$$\lim_{\tau\to\infty} \mathcal{F}_i^{(abs,\mathrm{scat})}(G_{\varepsilon,\lambda}(\xi, \pi_\xi) - \tau, Q^2, Q^3, \varepsilon, \lambda_z, \lambda) = f_{-\infty}(\varepsilon)$$

for any values of $\xi > 2$, $\varepsilon > 1$, $Q^2, Q^3 \in [0, 2\pi]$, and $|\lambda_z| < \lambda$ and π_ξ given by one of the two expressions $\pi_{\xi\pm}(\xi)$ defined in equation (46).

[12] See, for instance [64].

The observables J_α and $T_{\alpha\beta}$ are given by expressions of the same form as defined in equations (51) and (52) with the additional weights p_α and $p_\alpha p_\beta$, respectively. With respect to the non-rotating frame $\{e_0, e_1, e_2, e_3\}$ defined in equations (69)–(72), the components of the momentum are:

$$p_0 = \frac{-m\varepsilon}{\sqrt{1-\frac{2}{\xi}}}, \tag{95}$$

$$p_1 = \frac{m}{\sqrt{1-\frac{2}{\xi}}}\left[-\frac{2\varepsilon}{\xi} + \left(1-\frac{2}{\xi}\right)\pi_\xi\right], \tag{96}$$

$$p_2 = \frac{m\pi_\vartheta}{\xi} = \frac{m\lambda}{\xi}\cos\chi, \tag{97}$$

$$p_3 = \frac{m\lambda_z}{\xi\sin\vartheta} = \frac{m\lambda}{\xi}\sin\chi. \tag{98}$$

From these expressions and equation (46) it follows the existence of positive constants c_1 and c_2 (depending on $\xi > 2$) such that

$$|p_\alpha| \leqslant m\,[c_1\varepsilon + c_2\lambda]$$

for all $\alpha = 0, 1, 2, 3$. Therefore, the integrands in J_α and $T_{\alpha\beta}$ are bounded by the functions

$$H_s(\varepsilon, \lambda) := \alpha m^{3+s}(c_1\varepsilon + c_2\lambda)^s \mathrm{e}^{-\beta\varepsilon}\frac{\lambda}{\xi^2\sqrt{\varepsilon^2 - U_\lambda(\xi)}}$$

with $s = 1$ and $s = 2$ for J_α and $T_{\alpha\beta}$, respectively. These functions are Lebesgue-integrable on the desired ranges, for

$$\int_1^\infty\int_0^{2\pi}\int_0^{\lambda_c(\varepsilon)} H_s(\varepsilon,\lambda)\mathrm{d}\lambda\mathrm{d}\chi\mathrm{d}\varepsilon \leqslant 2\pi\alpha m^{3+s}\int_1^\infty\left(\int_0^{\lambda_c(\varepsilon)}\frac{\lambda\mathrm{d}\lambda}{\xi^2\sqrt{\varepsilon^2-U_\lambda(\xi)}}\right)(c_1\varepsilon + c_2\lambda_c(\varepsilon))^s\mathrm{e}^{-\beta\varepsilon}\mathrm{d}\varepsilon.$$

According to appendix B the integral over λ gives

$$\frac{1}{1-\frac{2}{\xi}}\left[\sqrt{\varepsilon^2 - U_0(\xi)} - \sqrt{\varepsilon^2 - U_c(\xi)}\right] \leqslant c_3\varepsilon.$$

Since $\lambda_c(\varepsilon) \leqslant c_4\varepsilon$ (see appendix A), it follows that H_s is integrable over the range corresponding to case (I). A similar argument shows that H_s is also integrable over the range associated with the scattered particles (case (II)).

Now we can use Lebesgue's dominated convergence theorem in order to pass the limit below the integral, and we conclude that J_α and $T_{\alpha\beta}$ converge to the corresponding stationary expressions computed in section 4.3 with f_∞ replaced with $f_{-\infty}$. □

Proof of theorem 3. As mentioned before, the proof for moving observers is more complicated than in the static case due to two issues. The first issue is that $G_{\varepsilon,\lambda}(\xi,\pi_\xi)$ is not constant anymore, since the assumption implies that $\xi\to\infty$ along the observer's world line. Hence, depending on the values of the constants ε and λ the expression

$$G_{\varepsilon,\lambda}(\xi,\pi_{\xi+})-\tau$$

might converge to $-\infty$ or ∞ along the world line of the observer (see lemma 3). The second issue is the fact that the fibre and the volume element change in time. As a consequence, the measure (see equation (49))

$$\frac{\lambda\mathrm{d}\lambda\mathrm{d}\varepsilon\mathrm{d}\chi}{\xi^2\sqrt{\varepsilon^2-U_\lambda(\xi)}}$$

appearing in the definition of the observables is not constant anymore, and the application of Lebesgue's theorem would require finding a uniform (ξ-independent) Lebesgue-integrable upper bound for the integrand. To bypass this problem, we change the integration variable λ to the new variable

$$v:=\sqrt{\varepsilon^2-U_\lambda(\xi)}\,,$$

which represents the radial velocity of the particles. In terms of this new variable,

$$\frac{\lambda\mathrm{d}\lambda\mathrm{d}\varepsilon\mathrm{d}\chi}{\xi^2\sqrt{\varepsilon^2-U_\lambda(\xi)}}=-\frac{\mathrm{d}v\mathrm{d}\varepsilon\mathrm{d}\chi}{1-\frac{2}{\xi}},$$

so the measure becomes trivial, up to the factor $1-2/\xi$ which converges to 1 along the observer's world line. The expressions for the current density have the form (see (51) and (52))[13]

$$J^{(abs)}_\delta(x)=\frac{m^3}{1-\frac{2}{\xi}}\int_0^{2\pi}\int_1^\infty\int_0^\infty p_{\delta-}\mathcal{F}^{(abs)}_-\mathbf{1}_{\left(v_c(\varepsilon,\xi),\sqrt{\varepsilon^2-1+\frac{2}{\xi}}\right)}(v)\mathrm{d}v\mathrm{d}\varepsilon\mathrm{d}\chi,$$

$$J^{(scat)}_\delta(x)=\frac{m^3}{1-\frac{2}{\xi}}\int_0^{2\pi}\int_1^\infty\int_0^\infty\left[p_{\delta-}\mathcal{F}^{(scat)}_-+p_{\delta+}\mathcal{F}^{(scat)}_+\right]\mathbf{1}_{(0,v_c(\varepsilon,\xi))}(v)\mathrm{d}v\mathrm{d}\varepsilon\mathrm{d}\chi,$$

where we have abbreviated $\mathcal{F}^{(abs)}_-:=\mathcal{F}^{(abs)}_i(G_{\varepsilon,\lambda}(\xi,\pi_{\xi-}(\xi))-\tau,Q^2,Q^3,\varepsilon,\lambda\sin\chi\sin\vartheta,\lambda)$ and $\mathcal{F}^{(scat)}_\pm:=\mathcal{F}^{(scat)}_i(G_{\varepsilon,\lambda}(\xi,\pi_{\xi\pm}(\xi))-\tau,Q^2,Q^3,\varepsilon,\lambda,\lambda\sin\chi\sin\vartheta)$, where we have defined $v_c(\varepsilon,\xi):=\sqrt{\varepsilon^2-U_{\lambda_c(\varepsilon)}(\xi)}$, and where λ should be substituted by the expression

$$\lambda(v,\xi):=\xi\sqrt{\frac{\varepsilon^2-v^2}{1-\frac{2}{\xi}}-1}\,. \tag{99}$$

[13] Note that the lower limit $\varepsilon_{\min}(\xi)$ in the ε-integral in $J^{(scat)}_\delta$ can be replaced by 1 since $\xi\to\infty$.

Finally, in order to work on a fixed integration domain, we have introduced the indicator function $\mathbf{1}_{(a,b)}$ with respect to the interval (a,b), which is defined by:

$$\mathbf{1}_{(a,b)}(v) = \begin{cases} 1 & \text{if} \quad v \in (a,b), \\ 0 & \text{if} \quad v \notin (a,b). \end{cases}$$

According to the hypothesis, both integrands are bounded by a constant times

$$|p_\delta| \mathrm{e}^{-\beta\varepsilon} \mathbf{1}_{(0,\varepsilon)}(v).$$

Here, the components of the momentum, p_δ, with respect to the static frame defined in equations (69)–(72) can be bounded using the explicit expressions given in equations (95)–(98), where we notice that (see equation (99))

$$\left| \frac{\lambda}{\xi} \right| \leqslant c_5 \varepsilon$$

and

$$|\pi_{\xi\pm}| = \left| \frac{\frac{2}{\xi}\varepsilon \pm v}{1 - \frac{2}{\xi}} \right| \leqslant c_6 \varepsilon + c_7 v$$

for some positive constants c_5, c_6 and c_7 which are independent of ε, v and ξ. Consequently, both integrands are bounded by a constant times

$$\varepsilon \mathrm{e}^{-\beta\varepsilon} \mathbf{1}_{(0,\varepsilon)}(v),$$

which is integrable. Therefore, we can apply Lebesgue's dominated convergence theorem and pass the limit $\tau \to \infty$ below the integral. In the following, we analyze these limits.

Let us start with the contribution from the absorbed particles, $J_\delta^{(abs)}$. In this case, both endpoints of the interval $(v_c(\varepsilon,\xi), \sqrt{\varepsilon^2 - 1 + \frac{2}{\xi}})$ converge to $\sqrt{\varepsilon^2 - 1}$ when $\xi \to \infty$. Consequently, in the limit $\xi \to \infty$, the integrand converges pointwise to zero almost everywhere and hence

$$\lim_{t \to \infty} J_\delta^{(abs)}(\gamma(t)) = 0.$$

Next, we analyze the limit of the integrand of $J_\delta^{(\mathrm{scat})}$. For this, we first notice that $v_c(\varepsilon,\xi) \to \sqrt{\varepsilon^2 - 1}$ as $\xi \to \infty$, and hence

$$\lim_{t \to \infty} \mathbf{1}_{(0, v_c(\varepsilon,\xi))}(v) = \begin{cases} 1 & \text{if} \quad 0 < v < \sqrt{\varepsilon^2 - 1}, \\ 0 & \text{if} \quad v > \sqrt{\varepsilon^2 - 1} \end{cases},$$

Therefore, the limit is zero in the region $v > \sqrt{\varepsilon^2 - 1}$ (see figure 5). Consequently, in what follows, we may focus our attention on the complementary region $v^2 < \varepsilon^2 - 1$. The next step consists in determining the limit values of $\mathcal{F}_\pm^{(\mathrm{scat})}$. For this, we need to understand the limit

$$\lim_{\tau \to \infty} \left[G_{\varepsilon, \lambda(v,\xi(\tau))}(\xi(\tau), \pi_{\xi\pm}(\tau)) - \tau \right], \qquad \pi_{\xi\pm}(\tau) := \pi_{\xi\pm}(\xi(\tau)).$$

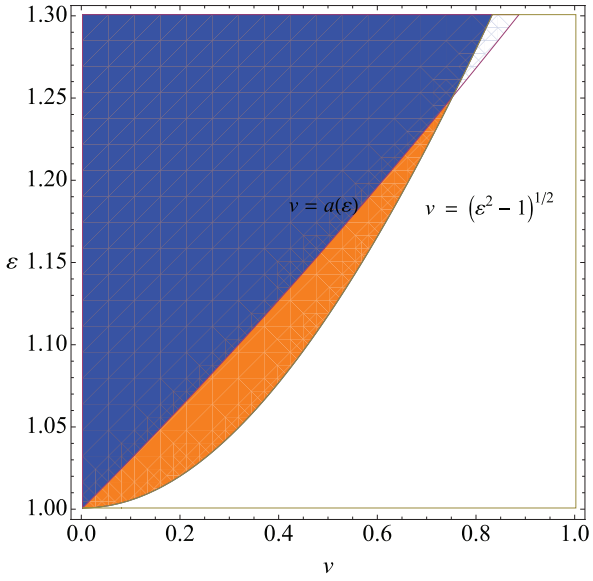

Figure 5. The three regions in the (ε, v) diagram which are delimited by the two curves $v = \sqrt{\varepsilon^2 - 1}$ and $v = a(\varepsilon) = (\varepsilon^2 - 1)/(\varepsilon v_{obs,\infty})$. In the white region, the integrand defining the observables converges to zero. In the orange region the expression $G_{\varepsilon,\lambda(v,\xi(\tau))}(\xi(\tau), \pi_{\xi+}(\tau)) - \tau$ tends to $+\infty$, and in the blue region it tends to $-\infty$.

The result is given in the following

Lemma 5 (see figure 5). *Let $\varepsilon > 1$ and $0 < v < \sqrt{\varepsilon^2 - 1}$. Then,*

$$\lim_{\tau\to\infty} [G_{\varepsilon,\lambda(v,\xi(\tau))}(\xi(\tau), \pi_{\xi-}(\tau)) - \tau] = -\infty,$$

$$\lim_{\tau\to\infty} [G_{\varepsilon,\lambda(v,\xi(\tau))}(\xi(\tau), \pi_{\xi+}(\tau)) - \tau] = \begin{cases} -\infty & \text{if } v < a(\varepsilon), \\ +\infty & \text{if } v > a(\varepsilon), \end{cases}$$

where we recall that $a(\varepsilon) = (\varepsilon^2 - 1)/(\varepsilon v_{obs,\infty})$.

Proof. We defer the proof of this technical lemma to appendix D. □

With the help of lemma 5 it is now straightforward to complete the computation of the asymptotic limit of $J^{(\mathrm{scat})}_\delta$ along the observer's path. Using assumption (iii) of the theorem we obtain

$$\lim_{t\to\infty} J^{(\mathrm{scat})}_\delta(\gamma(t)) = m^3 \int_0^{2\pi}\int_1^\infty\int_0^{\sqrt{\varepsilon^2-1}} \left\{ \lim_{\tau\to\infty} p_{\delta-} f_{-\infty}(\varepsilon) + \lim_{\tau\to\infty} p_{\delta+} \left[f_{-\infty}(\varepsilon) + \Delta f_\infty(\varepsilon) \mathbf{1}_{(a(\varepsilon),\infty)}(v) \right] \right\} \mathrm{d}v\mathrm{d}\varepsilon\mathrm{d}\chi,$$

where we recall that $\Delta f_\infty := f_{+\infty} - f_{-\infty}$. The limits of the components of the momentum can be obtained using equations (95)–(99):

$$\lim_{\tau\to\infty} p_{0\pm} = -m\varepsilon, \quad \lim_{\tau\to\infty} p_{1\pm} = \pm mv, \quad \lim_{\tau\to\infty} p_{2\pm} = m\cos\chi\sqrt{\varepsilon^2 - v^2 - 1},$$

$$\lim_{\tau\to\infty} p_{3\pm} = m\sin\chi\sqrt{\varepsilon^2 - v^2 - 1}.$$

From this, it is simple to obtain the result given in equation (92). The proof for the convergence of the stress energy-momentum tensor proceeds in a similar way. □

6. Conclusions

In this work, we have considered a relativistic, collisionless kinetic gas propagating on the curved spacetime describing a Schwarzschild black hole. First, we provided a brief review for the formal structure of the theory needed in this article, including the symplectic structure, the Hamiltonian formulation of the Liouville vector field, and the lift of Killing vector fields on the cotangent bundle associated with the spacetime manifold. Next, using standard tools from the theory of Hamiltonian mechanics, we derived the most general distribution function describing the accretion of a collisionless gas into a Schwarzschild black hole (see theorem 1). Unlike the previous derivation in [12] where the same problem was solved in the Kerr case, here we directly exploited the integrability of the Hamiltonian system and defined the generating function leading to the new symplectic coordinates in which the Liouville vector field is trivialized through an integral over the Poincaré one-form. Furthermore, we provided explicit expressions for the relevant physical observables on the spacetime manifold, including the particle current density and the stress energy-momentum tensor.

After these general remarks on the structure of the general solution of the Liouville equation on a Schwarzschild background, we turned our attention to applications for the accretion problem. We started with the simple case in which the gas flow is assumed to be spherically symmetric and steady-state, and showed that these assumptions yield a one-particle distribution function which depends only on the mass m, the energy E and the total angular momentum ℓ of the particle. The value of ℓ plays an important role in distinguishing those particle that fall into the black hole from those that are reflected at the centrifugal barrier. As we exhibited, the former particles contribute to the accretion rate but not to the particle density n_∞ at infinity, while the reflected particles yield a positive n_∞ but do not contribute to the accretion rate. Next, we provided an explicit example in which the distribution function describes a gas in thermodynamic equilibrium at some temperature T at infinity, and computed the observables as a function of the inverse temperature $\beta = 1/(k_B T)$. In the low temperature limit $\beta \to \infty$ we verified that our results coincide with those in [48, 49] for the accretion rate that were obtained based on Newtonian calculations. Additionally, we computed the energy density and radial and tangential pressures p_{rad} and p_{tan} at the horizon for $\beta \to \infty$ and showed that p_{tan} is almost an order of magnitude larger than p_{rad}. This provides a partial explanation for the fact that the accretion is much less intense than in the Bondi–Michel case of a perfect, polytropic fluid case where $p_{\mathrm{tan}} = p_{\mathrm{rad}}$.

In the final part of this work, we studied the nonlinear stability of the steady-state, spherically symmetric accretion flows. To this end, we specified initial conditions for the distribution function on a constant time slice satisfying the following properties: first, the initial distribution function $\mathcal{F}_i$ is non-negative and bounded from above by an equilibrium distribution function. Second, in the asymptotic region $\mathcal{F}_i$ converges (in a suitable sense) to a function $f_\infty(E)$ depending only on the energy of the particles. Under these assumptions, we proved that outside of the horizon the observables, including the current density and the stress energy-momentum tensor, converge pointwise to the corresponding observables associated with the stationary, spherical flow described by $f_\infty(E)$ along the world lines of static observers (see theorem 2). Similar results hold for the convergence along the world lines of timelike, nonstatic observers with asymptotic constant and positive radial velocity (see theorem 3). This proves an

asymptotic stability result for the steady, spherical flows of collisionless matter. We emphasize that the initial data is not required to be spherically symmetric for our result to hold. Of course, the physical explanation for this result is that almost all the gas particles either disperse or fall into the black hole, so that after infinite time only those particles emanating from the reservoir in the asymptotic region with distribution $f_\infty(E)$ are 'seen' by the observer.

There are several important questions that have been left unanswered in this work and we would like to conclude this article by mentioning some of these points. First, although our stability result shows that (under the hypotheses made in this article) the kinetic gas relaxes in time to a stationary spherical configuration, a physically relevant problem is to determine the time scale associated with this relaxation process. Here, the distribution of the gas particles moving on or near the trajectories corresponding to the critical value of the angular momentum $\ell_c(E)$ (i.e. the value of ℓ below which the particle falls into the black hole and above which the particle is scattered at the potential barrier) should play a critical role. Indeed, a 'fine-tuned' distribution of particles whose angular momenta is precisely $\ell = \ell_c(E)$ will not decay in time since the particles take an infinite time to reach the unstable equilibrium point, corresponding to the unstable circular orbit. Of course, this example does not contradict our stability result since the corresponding distribution function f has the form of a Dirac-delta-distribution in momentum space; hence it does not satisfy our assumptions. However, an interesting question is to consider a smooth distribution function (satisfying our assumptions) which is strongly peaked about the critical value $\ell = \ell_c(E)$. The instability of the equilibrium point implies that the peak will disperse in time, and it is precisely this dispersion process that should be responsible for the decay and dictate its rate.

Next, we emphasize that we have restricted ourselves to the invariant submanifold Γ_{accr} of the relativistic phase space corresponding to unbounded trajectories. Thus, the results derived so far in this article apply to distribution functions which have their support in the region of phase space corresponding to such unbounded trajectories. Due to the linearity of the Liouville equation, the complementary case of bounded trajectories can be analyzed separately; hence, as long as the self-gravity and collisions between the gas particles can be neglected, our main results will not be influenced by the contributions from the bounded trajectories. In particular, these contributions affect neither the accretion rate nor the expressions for the particle and energy densities and pressures at the horizon or at infinity, and hence our results for the accretion and compression rates persist. Likewise, our stability results in theorems 2 and 3 will not be altered if a contribution due to gas particles moving on bounded trajectories is added, as long as the observables J_α and $T_{\alpha\beta}$ in these theorems are restricted to the contributions from the unbounded trajectories. However, an interesting question is whether or not the full observables including the contributions from gas particles on bounded orbits still relax to a stationary configuration along the world lines of static observers. This question is much more difficult to answer since in this case the gas particles do not disperse.

Finally, it should be interesting to explore the situation where collisions are taken into account and see how they affect the accretion rate. The analysis of this case is much more demanding than the one considered in the present article, since it requires solving the relativistic Boltzmann equation including the collision term on the curved Schwarzschild background geometry. Furthermore, in the collisional case, it is not possible to analyze the different cases (absorbed versus scattered versus bounded trajectories) separately since collisions might mix trajectories of different types. Nevertheless, it is our hope that the new symplectic coordinates introduced in the this article should simplify the analysis since they trivialize the transport part of the Boltzmann equation. We hope to address some of these issues in future work.

Acknowledgments

It is our pleasure to thank Håkan Andréasson, Francisco Astorga, Darío Núñez, Gerhard Rein, Manuel Tiglio, and Thomas Zannias for fruitful and stimulating discussions. We also thank Aftab Ahmad, James Edwards, and Thomas Zannias for reading a previous version of the manuscript and making suggestions. This research was supported in part by CONACyT Grants No. 577742 and No. 271904, and by a CIC Grant to Universidad Michoacana.

Appendix A. Properties of the effective potential

In this appendix, we briefly discuss the qualitative properties of the effective potential $V_{m,\ell}$ defined in equation (27) describing the geodesics in the Schwarzschild spacetime. Since this is discussed in standard textbooks on general relativity (see for example [65]) here we focus on the properties needed for the analysis in this article.

In terms of dimensionless variables, we have $V_{m,\ell}(r) = m^2 U_\lambda(\xi)$ with

$$U_\lambda(\xi) := \left(1 - \frac{2}{\xi}\right)\left(1 + \frac{\lambda^2}{\xi^2}\right) = 1 - \frac{2}{\xi} + \frac{\lambda^2}{\xi^2} - \frac{2\lambda^2}{\xi^3}, \qquad \xi = \frac{r}{M_H}. \tag{A.1}$$

For $\lambda^2 \leqslant 12$ the function $U_\lambda : [2,\infty) \to \mathbb{R}$ is a strictly monotonically increasing function from 0 to 1. When $\lambda^2 > 12$ this function has a local maximum (describing the potential barrier), which is given by

$$\xi_{\max} = \frac{\lambda^2}{2}\left[1 - \sqrt{1 - \frac{12}{\lambda^2}}\right], \qquad U_\lambda(\xi_{\max}) = \frac{8}{9} + \frac{\lambda^2 - 12}{9\xi_{\max}}, \tag{A.2}$$

and a local minimum (describing a potential well) given by

$$\xi_{\min} = \frac{\lambda^2}{2}\left[1 + \sqrt{1 - \frac{12}{\lambda^2}}\right], \qquad U_\lambda(\xi_{\min}) = \frac{8}{9} + \frac{\lambda^2 - 12}{9\xi_{\min}}, \tag{A.3}$$

see figure A1. As λ^2 grows from 12 to ∞, $\xi_{\max}$ decreases monotonically from 6 to 3 (the radius of the photon sphere) while $\xi_{\min}$ increases monotonically from 6 (the innermost stable circular orbit) to ∞. Accordingly, $U_\lambda(\xi_{\max})$ grows monotonically from 8/9 to ∞ while $U_\lambda(\xi_{\min})$ grows monotonically from 8/9 to 1.

Given $\varepsilon > \sqrt{8/9}$, the critical value $\lambda_c(\varepsilon) > \sqrt{12}$ for the total angular momentum for which the maximum of the potential barrier is exactly equal to ε^2 is given by

$$\lambda_c(\varepsilon)^2 = \frac{12}{1 - 4\alpha - 8\alpha^2 + 8\alpha\sqrt{\alpha^2 + \alpha}}, \qquad \alpha := \frac{9}{8}\varepsilon^2 - 1 > 0.$$

As ε increases from $\sqrt{8/9}$ to ∞, $\lambda_c(\varepsilon)$ increases monotonically from $\sqrt{12}$ to ∞. For large α we have $\lambda_c(\varepsilon)^2 = 24\alpha[1 + \mathcal{O}(\alpha^{-1})]$. For the particular value $\varepsilon = 1$, corresponding to the case of particles with vanishing radial velocity at infinity, we have $\lambda_c(\varepsilon) = 4$ and the maximum is located at $\xi_{\max} = 4$.

Likewise, given $\varepsilon \in (\sqrt{8/9}, 1)$, there is an upper bound for the angular momentum $\lambda_{ub}(\varepsilon)$ corresponding to the case where the minimum of the potential well is equal to ε^2, which is given by

$$\lambda_{ub}(\varepsilon)^2 = \frac{12}{1 - 4\alpha - 8\alpha^2 - 8\alpha\sqrt{\alpha^2 + \alpha}}.$$

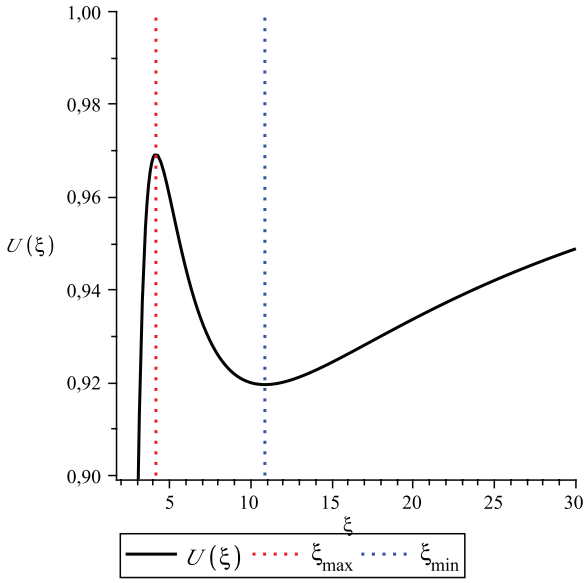

Figure A1. The effective potential $U(\xi) = U_\lambda(\xi)$ as a function of ξ for $\lambda = \sqrt{15}$.

As ε increases from $\sqrt{8/9}$ to 1, $\lambda_{ub}(\varepsilon)$ increases monotonically from $\sqrt{12}$ to ∞.

With these observations we can classify the orbits in the following way. For $\sqrt{8/9} < \varepsilon < 1$ the particles are scattered at the effective potential and fall into the black hole when $\lambda < \lambda_c(\varepsilon)$, while the orbits are bounded when $\lambda_c(\varepsilon) < \lambda < \lambda_{ub}(\varepsilon)$. For $\varepsilon > 1$ the particles are falling into the black hole when $\lambda < \lambda_c(\varepsilon)$ while they are scattered at the potential when $\lambda > \lambda_c(\varepsilon)$.

Appendix B. Some useful integral identities

In this appendix, we summarize some of the integral identities used in the derivation of equations (61)–(66). Introducing the shorthand notation $s_{1,2} := \sqrt{\varepsilon^2 - U_{\lambda_{1,2}}(\xi)}$ we have, for any $0 \leqslant \lambda_1 < \lambda_2 \leqslant \lambda_{\max}$,

$$\int_{\lambda_1}^{\lambda_2} \frac{\lambda \mathrm{d}\lambda}{\sqrt{\varepsilon^2 - U_\lambda(\xi)}} = -\frac{\xi^2}{1-\frac{2}{\xi}}(s_2 - s_1) = \frac{\lambda_2^2 - \lambda_1^2}{s_1 + s_2},$$

$$\int_{\lambda_1}^{\lambda_2} \pi_{\xi\pm}(\xi) \frac{\lambda \mathrm{d}\lambda}{\sqrt{\varepsilon^2 - U_\lambda(\xi)}} = \frac{\lambda_2^2 - \lambda_1^2}{1-\frac{2}{\xi}} \left[\frac{2\varepsilon}{\xi} \frac{1}{s_1 + s_2} \pm \frac{1}{2} \right],$$

$$\int_{\lambda_1}^{\lambda_2} \pi_{\xi\pm}^2(\xi) \frac{\lambda \mathrm{d}\lambda}{\sqrt{\varepsilon^2 - U_\lambda(\xi)}} = \frac{\lambda_2^2 - \lambda_1^2}{s_1 + s_2} \left[\left(\frac{\frac{2\varepsilon}{\xi} \pm s_1}{1-\frac{2}{\xi}} \right) \left(\frac{\frac{2\varepsilon}{\xi} \pm s_2}{1-\frac{2}{\xi}} \right) + \frac{1}{3} \left(\frac{s_2 - s_1}{1-\frac{2}{\xi}} \right)^2 \right],$$

$$\int_{\lambda_1}^{\lambda_2} \lambda^2 \frac{\lambda \mathrm{d}\lambda}{\sqrt{\varepsilon^2 - U_\lambda(\xi)}} = \frac{1}{3} \frac{\lambda_2^2 - \lambda_1^2}{(s_1 + s_2)^2} \left[\lambda_1^2 (s_1 + 2s_2) + \lambda_2^2 (s_2 + 2s_1) \right].$$

For the particular in which $\pi_\xi = \pi_{\xi_-}(\xi)$, the second and third identities can also be rewritten as

$$\int_{\lambda_1}^{\lambda_2} \pi_{\xi_-}(\xi) \frac{\lambda \mathrm{d}\lambda}{\sqrt{\varepsilon^2 - U_\lambda(\xi)}} = -\frac{\lambda_2^2 - \lambda_1^2}{s_1 + s_2}\left[\varepsilon - \frac{1}{2}\frac{1 + \frac{\lambda_1^2}{\xi^2}}{\varepsilon + s_1} - \frac{1}{2}\frac{1 + \frac{\lambda_2^2}{\xi^2}}{\varepsilon + s_2}\right],$$

$$\int_{\lambda_1}^{\lambda_2} \pi_{\xi_-}^2(\xi) \frac{\lambda \mathrm{d}\lambda}{\sqrt{\varepsilon^2 - U_\lambda(\xi)}} = \frac{\lambda_2^2 - \lambda_1^2}{s_1 + s_2}\left[\left(\varepsilon - \frac{1 + \frac{\lambda_1^2}{\varepsilon^2}}{\varepsilon + s_1}\right)\left(\varepsilon - \frac{1 + \frac{\lambda_2^2}{\varepsilon^2}}{\varepsilon + s_2}\right) + \frac{1}{3\xi^4}\left(\frac{\lambda_2^2 - \lambda_1^2}{s_1 + s_2}\right)^2\right],$$

which shows that the corresponding expressions are regular on the horizon $\xi = 2$.

Appendix C. Explicit expressions in the low temperature limit

In this appendix, we provide some details about the calculations required for understanding the low temperature limit $z = m\beta \to \infty$ in section 5.1. We start with the computation of the ratio between the mass accretion rate and the energy density at infinity, that is,

$$\frac{\dot{M}}{n_\infty} = \frac{m j_n}{n_\infty}.$$

Using equations (76) and (78) for the particle density at infinity, which we rewrite as

$$n_\infty = 4\pi\alpha m^4 \int_1^\infty \mathrm{e}^{-z\varepsilon}\sqrt{\varepsilon^2 - 1}\,\varepsilon \mathrm{d}\varepsilon,$$

we obtain

$$\frac{m j_n}{n_\infty} = -\pi m M_H^2 \frac{\int_1^\infty \mathrm{e}^{-z(\varepsilon-1)}\lambda_c(\varepsilon)^2 \mathrm{d}\varepsilon}{\int_1^\infty \mathrm{e}^{-z(\varepsilon-1)}\sqrt{\varepsilon^2 - 1}\,\varepsilon \mathrm{d}\varepsilon} = -\pi m M_H^2 \sqrt{z} \frac{\int_0^\infty \mathrm{e}^{-x}\lambda_c(1 + \frac{x}{z})^2 \mathrm{d}x}{\int_0^\infty \mathrm{e}^{-x}\sqrt{2x + \frac{x^2}{z}}\left(1 + \frac{x}{z}\right)\mathrm{d}x},$$

where we have applied the variable substitution $\varepsilon \mapsto x = z(\varepsilon - 1)$ in the last step. Dividing both sides of the equation by $\sqrt{z}$, taking the limit $z \to \infty$ and recalling that $\lambda_c(1) = 4$ we obtain

$$\lim_{z\to\infty} \frac{1}{\sqrt{z}}\frac{\dot{M}}{n_\infty} = -16\pi m M_H^2 \frac{\int_0^\infty \mathrm{e}^{-x}\mathrm{d}x}{\int_0^\infty \mathrm{e}^{-x}\sqrt{2x}\,\mathrm{d}x} = -16\sqrt{2\pi}\, m M_H^2.$$

Next, to determine the particle density at the horizon, we use a similar computation to find from equation (80),

$$\lim_{z\to\infty} \frac{1}{\sqrt{z}}\frac{J^\tau}{n_\infty} = \frac{5}{\sqrt{2\pi}}, \qquad \lim_{z\to\infty} \frac{1}{\sqrt{z}}\frac{J^r}{n_\infty} = -\sqrt{\frac{2}{\pi}}.$$

Using $n_H = \sqrt{-g_{\mu\nu} J^\mu J^\nu}\Big|_{\xi=2}$ we find

$$\lim_{z\to\infty} \frac{1}{\sqrt{z}}\frac{n_H}{n_\infty} = \sqrt{\frac{6}{\pi}}. \tag{C.1}$$

Finally, in order to compute the energy density and principle pressures at the horizon, we rewrite equation (81) in the form

$$T^{\tau}{}_{\tau} = -A - B, \quad T^{\tau}{}_{r} = -A + H, \quad T^{r}{}_{\tau} = A, \quad T^{r}{}_{r} = A - B, \quad T^{\vartheta}{}_{\vartheta} = T^{\varphi}{}_{\varphi} = D,$$

with

$$A = \frac{1}{4}\pi\alpha m^5 \int_1^\infty \lambda_c(\varepsilon)^2 \varepsilon \mathrm{e}^{-z\varepsilon} \mathrm{d}\varepsilon, \tag{C.2}$$

$$B = \frac{1}{4}\pi\alpha m^5 \int_1^\infty \frac{\lambda_c(\varepsilon)^2}{2\varepsilon}\left(1 + \frac{\lambda_c^2(\varepsilon)}{8}\right)\mathrm{e}^{-z\varepsilon} \mathrm{d}\varepsilon, \tag{C.3}$$

$$H = \frac{1}{4}\pi\alpha m^5 \int_1^\infty \frac{\lambda_c(\varepsilon)^2}{4\varepsilon^3}\left(1 + \frac{\lambda_c^2(\varepsilon)}{4} + \frac{\lambda_c^4(\varepsilon)}{48}\right)\mathrm{e}^{-z\varepsilon} \mathrm{d}\varepsilon, \tag{C.4}$$

$$D = \frac{1}{64}\pi\alpha m^5 \int_1^\infty \frac{\lambda_c(\varepsilon)^4}{\varepsilon}\mathrm{e}^{-z\varepsilon} \mathrm{d}\varepsilon. \tag{C.5}$$

In terms of these quantities, the eigenvalues of the matrix $T^{\mu}{}_{\nu}$ are

$$\lambda_{\pm} = -B \pm \sqrt{AH}, \qquad D.$$

Dividing the expressions for A, B, H and D by $\sqrt{z}\, n_\infty$ and taking the limit $z \to \infty$ we obtain

$$\lim_{z\to\infty} \frac{1}{\sqrt{z}} \frac{A}{n_\infty} = \lim_{z\to\infty} \frac{1}{\sqrt{z}} \frac{D}{n_\infty} = \sqrt{\frac{2}{\pi}}\, m, \qquad \lim_{z\to\infty} \frac{1}{\sqrt{z}} \frac{B}{n_\infty} = \frac{3}{\sqrt{2\pi}} m,$$
$$\lim_{z\to\infty} \frac{1}{\sqrt{z}} \frac{H}{n_\infty} = \frac{31}{12}\sqrt{\frac{2}{\pi}}\, m,$$

from which

$$\lim_{z\to\infty} \frac{1}{\sqrt{z}} \frac{\rho_H}{n_\infty} = \lim_{z\to\infty} \frac{1}{\sqrt{z}} \frac{-\lambda_-}{n_\infty} = \frac{1}{\sqrt{2\pi}}\left(3 + \sqrt{\frac{31}{3}}\right) m,$$
$$\lim_{z\to\infty} \frac{1}{\sqrt{z}} \frac{p_{\mathrm{rad}}}{n_\infty} = \lim_{z\to\infty} \frac{1}{\sqrt{z}} \frac{\lambda_+}{n_\infty} = \frac{1}{\sqrt{2\pi}}\left(-3 + \sqrt{\frac{31}{3}}\right) m,$$
$$\lim_{z\to\infty} \frac{1}{\sqrt{z}} \frac{p_{\mathrm{tan}}}{n_\infty} = \lim_{z\to\infty} \frac{1}{\sqrt{z}} \frac{D}{n_\infty} = \sqrt{\frac{2}{\pi}}\, m.$$

Together with equation (C.1) this yields the results given in equations (83)–(85).

Appendix D. Proof of lemma 5

To prove lemma 5 we need to determine the limits

$$\lim_{\tau\to\infty} \left[G_{\varepsilon,\lambda(\nu,\xi(\tau))}(\xi(\tau), \pi_{\xi\pm}(\tau)) - \tau\right]$$

for fixed $0 < v < \sqrt{\varepsilon^2 - 1}$, where the function $G_{\varepsilon,\lambda} : \mathcal{C} \to \mathbb{R}$ is defined in lemma 3, and where $\lambda(v, \xi)$ is defined in equation (99). For the lower sign, $\pi_{\xi-}(\tau)$, the limit is $-\infty$ since in this case $G_{\varepsilon,\lambda(v,\xi(\tau))}(\xi(\tau), \pi_{\xi-}(\tau)) \leqslant 0$. This proves the first statement of the lemma.

The other case is more delicate since here $G_{\varepsilon,\lambda(v,\xi(\tau))}(\xi(\tau), \pi_{\xi+}(\tau))$ is positive and thus this term may dominate $-\tau$ as $\tau \to \infty$. To analyze this case we write

$$G_{\varepsilon,\lambda(v,\xi(\tau))}(\xi(\tau), \pi_{\xi+}(\tau)) - \tau = \tau \left[\frac{\xi(\tau)}{\tau} \frac{1}{\xi(\tau)} \int_{\xi_0}^{\xi(\tau)} \frac{\frac{2}{x}\sqrt{\varepsilon^2 - U_\lambda(x)} + \varepsilon}{\left(1 - \frac{2}{x}\right)\sqrt{\varepsilon^2 - U_\lambda(x)}} \mathrm{d}x - 1 \right]_{\lambda = \lambda(v,\xi(\tau))}, \tag{D.1}$$

with ξ_0 the radius of the turning point, where $\sqrt{\varepsilon^2 - U_\lambda(\xi_0)}$ vanishes. In order to understand the behavior of the integral in equation (D.1) for large τ, it is convenient to change the integration variable x to the new variable $\bar{v} := \sqrt{\varepsilon^2 - U_\lambda(x)}$ which ranges from 0 to v. More precisely, we consider for fixed $\xi = \xi(\tau) > \xi_0$ and $\lambda = \lambda(v, \xi)$ the auxiliary function

$$\begin{aligned} H_\lambda : (\xi_0, \xi_{\min}) &\to (0, \sqrt{\varepsilon^2 - U_\lambda(\xi_{\min})}) \\ x &\mapsto \sqrt{\varepsilon^2 - U_\lambda(x)}, \end{aligned}$$

where $\xi_{\min}$ is the location of the minimum of the effective potential U_λ, see equation (A.3) in appendix A. Since by definition of ξ_0 and $\xi_{\min}$ the function H_λ is monotonously increasing, it is invertible. Its derivative is

$$\frac{\mathrm{d}H_\lambda}{\mathrm{d}x}(x) = -\frac{1}{2H_\lambda(x)} \frac{\mathrm{d}U_\lambda}{\mathrm{d}x}(x) > 0, \qquad \xi_0 < x < \xi_{\min}.$$

In order to use the variable substitution $\bar{v} := H_\lambda(x)$ in the integral on the right-hand side of equation (D.1) we need to make sure that $\xi = \xi(\tau)$ lies in the required interval $(\xi_0, \xi_{\min})$. In order to see that this condition is satisfied for large enough ξ, recall equation (A.3) which shows that for large values of λ we have $\xi_{\min} = \xi_{\min}(\lambda) \simeq \lambda^2$. Furthermore, it follows immediately from equation (99) that

$$\lim_{\xi \to \infty} \frac{\lambda(v, \xi)}{\xi} = \sqrt{\varepsilon^2 - v^2 - 1}\,. \tag{D.2}$$

Hence,

$$\lim_{\xi \to \infty} \frac{\xi_{\min}(\lambda(v, \xi))}{\xi^2} = \lim_{\xi \to \infty} \frac{\lambda(v, \xi)^2}{\xi^2} \frac{\xi_{\min}(\lambda(v, \xi))}{\lambda(v, \xi)^2} = \varepsilon^2 - v^2 - 1 > 0,$$

which guarantees that for large enough ξ we have $\xi < \xi_{\min}$. Therefore, for such large ξ the variable substitution $\bar{v} := H_\lambda(x)$ is allowed and we can write

$$\frac{1}{\xi} \int_{\xi_0}^{\xi} \frac{\frac{2}{x}\sqrt{\varepsilon^2 - U_\lambda(x)} + \varepsilon}{\left(1 - \frac{2}{x}\right)\sqrt{\varepsilon^2 - U_\lambda(x)}} \mathrm{d}x \Bigg|_{\lambda = \lambda(v,\xi)} = -\frac{2}{\xi} \int_0^v \frac{\frac{2}{x}\bar{v} + \varepsilon}{\left(1 - \frac{2}{x}\right)\frac{\mathrm{d}U_\lambda}{\mathrm{d}x}(x)} \Bigg|_{x = H_\lambda^{-1}(\bar{v}), \lambda = \lambda(v,\xi)} \mathrm{d}\bar{v}. \tag{D.3}$$

In order to compute the required limit for $\xi \to \infty$ we use:

Lemma 6. *Let $\varepsilon > 1$ and $0 < v < \sqrt{\varepsilon^2 - 1}$. Then,*

$$\lim_{\lambda\to\infty} \frac{H_\lambda^{-1}(\bar{v})}{\lambda} = \frac{1}{\sqrt{\varepsilon^2 - \bar{v}^2 - 1}} \tag{D.4}$$

for all $0 \leqslant \bar{v} \leqslant v$. □

Proof. Set $x := H_\lambda^{-1}(\bar{v})$. By definition, $x > \xi_0 > 3$, and hence

$$\varepsilon^2 - \bar{v}^2 = U_\lambda(x) = \left(1 - \frac{2}{x}\right)\left(1 + \frac{\lambda^2}{x^2}\right) \geqslant \frac{1}{3}\left(1 + \frac{\lambda^2}{x^2}\right).$$

This implies that λ/x is bounded as $\lambda \to \infty$, which in turn implies that $x \to \infty$ as $\lambda \to \infty$. Consequently,

$$\lim_{\lambda\to\infty} \frac{\lambda^2}{x^2} = \lim_{\lambda\to\infty} \frac{\varepsilon^2 - \bar{v}^2}{1 - \frac{2}{x}} - 1 = \varepsilon^2 - \bar{v}^2 - 1$$

which proves the lemma. □

With the help of the limits given in equations (D.2) and (D.4) we find

$$\lim_{\xi\to\infty} \xi \frac{\mathrm{d}U_\lambda}{\mathrm{d}x}(x)\bigg|_{x=H_\lambda^{-1}(\bar{v}),\lambda=\lambda(v,\xi)} = \lim_{\xi\to\infty} \frac{\xi}{\lambda(v,\xi)}\left[-\frac{2\lambda^3}{x^3} + \frac{2\lambda}{x^2} + \frac{6\lambda^3}{x^4}\right]_{x=H_\lambda^{-1}(\bar{v}),\lambda=\lambda(v,\xi)}$$
$$= -2\frac{(\varepsilon^2 - \bar{v}^2 - 1)^{3/2}}{(\varepsilon^2 - v^2 - 1)^{1/2}}.$$

Hence, it follows from equation (D.3) that

$$\lim_{\xi\to\infty} \frac{1}{\xi} \int_{\xi_0}^{\xi} \frac{\frac{2}{x}\sqrt{\varepsilon^2 - U_\lambda(x)} + \varepsilon}{\left(1 - \frac{2}{x}\right)\sqrt{\varepsilon^2 - U_\lambda(x)}} \mathrm{d}x \bigg|_{\lambda=\lambda(v,\xi)} = \varepsilon \int_0^v \frac{(\varepsilon^2 - v^2 - 1)^{1/2}}{(\varepsilon^2 - \bar{v}^2 - 1)^{3/2}} \mathrm{d}\bar{v} = \varepsilon \frac{v}{\varepsilon^2 - 1}.$$

Therefore, using equation (D.1) we obtain

$$\lim_{\tau\to\infty} \frac{1}{\tau}\left[G_{\varepsilon,\lambda(v,\xi(\tau))}(\xi(\tau), \pi_{\xi+}(\tau)) - \tau\right] = \lim_{\tau\to\infty}\left[\frac{\xi(\tau)}{\tau}\frac{1}{\xi(\tau)} \int_{\xi_0}^{\xi(\tau)} \frac{\frac{2}{x}\sqrt{\varepsilon^2 - U_\lambda(x)} + \varepsilon}{\left(1 - \frac{2}{x}\right)\sqrt{\varepsilon^2 - U_\lambda(x)}} \mathrm{d}x - 1\right]_{\lambda=\lambda(v,\xi(\tau))}$$
$$= v_{obs,\infty}\frac{\varepsilon v}{\varepsilon^2 - 1} - 1 = \frac{v}{a(\varepsilon)} - 1$$

for all $0 < v < \sqrt{\varepsilon^2 - 1}$. This implies the second statement of lemma 5. □

References

[1] Jüttner F 1911 Maxwell's law of speed distribution in the theory of relativity *Ann. Phys.* **34** 856–82
[2] Jüttner F 1911 The dynamics of an inert gas in the theory of relativity *Ann. Phys.* **35** 145–61
[3] Synge J L 1934 The energy tensor of a continuous medium *Trans. R. Soc. Can.* **28** 127–71
[4] Tauber G E and Weinberg J W 1961 Internal state of a gravitating gas *Phys. Rev.* **122** 1342–65

[5] Israel W 1963 Relativistic kinetic theory of a simple gas *J. Math. Phys.* **4** 1163–81
[6] Cercignani C and Kremer G M 2002 *The Relativistic Boltzmann Equation and Applications* (Basel: Birkhäuser)
[7] Lindquist R W 1966 Relativistic transport theory *Ann. Phys., NY* **37** 487–518
[8] Ehlers J 1971 General relativity and kinetic theory *General Relativity and Cosmology* ed R K Sachs (New York: Acedemic) pp 1–70
[9] Ehlers J 1973 Survey of general relativity theory *Relativity, Astrophysics and Cosmology* ed W J Israel (Dordrecht: D. Reidel) pp 1–125
[10] Sarbach O and Zannias T 2013 Relativistic kinetic theory: an introduction *AIP Conf. Proc.* 1548 134–55
[11] Sarbach O and Zannias T 2014 Tangent bundle formulation of a charged gas *AIP Conf. Proc.* 1577 192–207
[12] Sarbach O and Zannias T 2014 The geometry of the tangent bundle and the relativistic kinetic theory of gases *Class. Quantum Grav.* **31** 085013
[13] Andréasson H 2011 The Einstein–Vlasov system/kinetic theory *Living Rev. Relativ.* **14** 4
[14] Rein G and Rendall A D 1992 Global existence of solutions of the spherically symmetric Vlasov–Einstein system with small initial data *Commun. Math. Phys.* **150** 561–83
[15] Dafermos M 2006 A note on the collapse of small data self-gravitating massless collisionless matter *J. Hypermedia Diff. Equ.* **3** 589
[16] Fajman D, Joudioux J and Smulevici J 2015 A vector field method for relativistic transport equations with applications (arXiv:1510.04939)
[17] Taylor M 2016 The global nonlinear stability of Minkowski space for the massless Einstein–Vlasov system (arXiv:1602.02611)
[18] Ringström H 2013 *On the Topology and Future Stability of the Universe* (Oxford: Oxford University Press)
[19] Andréasson H and Ringström H 2016 Proof of the cosmic no-hair conjecture in the $\mathbb{T}^3$-Gowdy symmetric Einstein–Vlasov setting *J. Eur. Math. Soc.* **18** 1565–650
[20] Fajman D 2016 Future asymptotic behavior of three-dimensional spacetimes with massive particles *Class. Quantum Grav.* **33** 11LT01
[21] Rendall A D and Velazquez J J L 2011 A class of dust-like self-similar solutions of the massless Einstein–Vlasov system *Ann. Henri Poincare* **12** 919–64
[22] Andréasson H 2012 Black hole formation from a complete regular past for collisionless matter *Ann. Henri Poincaré* **13** 1511–36
[23] Andréasson H 2014 On gravitational collapse and cosmic censorship for collisionless matter *Int. J. Geom. Meth. Mod. Phys.* **11** 1460002
[24] Akbarian A and Choptuik M W 2014 Critical collapse in the spherically-symmetric Einstein–Vlasov model *Phys. Rev.* D **90** 104023
[25] Eardley D M and Smarr L 1979 Time functions in numerical relativity: marginally bound dust collapse *Phys. Rev.* D **19** 2239–59
[26] Christodoulou D 1984 Violation of cosmic censorship in the gravitational collapse of a dust cloud *Commun. Math. Phys.* **93** 171–95
[27] Ortiz N and Sarbach O 2011 Conformal diagrams for the gravitational collapse of a spherical dust cloud *Class. Quantum Grav.* **28** 235001
[28] Rein G 1994 Static solutions of the spherically symmetric Vlasov–Einstein system *Math. Proc. Camb. Phil. Soc.* 115 559–70
[29] Andréasson H and Rein G 2007 On the steady states of the spherically symmetric Einstein–Vlasov system *Class. Quantum Grav.* **24** 1809–32
[30] Andréasson H, Fajman D and Thaller M 2015 Static solutions to the Einstein–Vlasov system with non-vanishing cosmological constant *SIAM J. Math. Anal.* **47** 2657–88
[31] Andréasson H, Eklund M and Rein G 2009 A numerical investigation of the steady states of the spherically symmetric Einstein–Vlasov–Maxwell system *Class. Quantum Grav.* **26** 145003
[32] Andréasson H, Kunze M and Rein G 2011 Existence of axially symmetric static solutions of the Einstein–Vlasov system *Commun. Math. Phys.* **308** 23–47
[33] Andréasson H, Kunze M and Rein G 2014 Rotating, stationary, axially symmetric spacetimes with collisionless matter *Commun. Math. Phys.* **329** 787–808
[34] Ames E, Andréasson H and Logg A 2016 On axisymmetric and stationary solutions of the self-gravitating Vlasov system *Class. Quantum Grav.* **33** 155008

[35] Andréasson H and Rein G 2006 A numerical investigation of the stability of steady states and critical phenomena for the spherically symmetric Einstein–Vlasov system *Class. Quantum Grav.* **23** 3659–78
[36] Bancel D and Choquet-Bruhat Y 1973 Existence, uniqueness, and local stability for the Einstein–Maxwell–Boltzman system *Commun. Math. Phys.* **33** 83–96
[37] Noundjeu P, Noutchegueme N and Rendall A D 2004 Existence of initial data satisfying the constraints for the spherically symmetric Einstein–Vlasov–Maxwell system *J. Math. Phys.* **45** 668–76
[38] Lee H and Rendall A D 2013 The spatially homogeneous relativistic Boltzmann equation with a hard potential *Commun. PDE* **12** 2238–62
[39] Event horizon telescope www.eventhorizontelescope.org
[40] Peebles P J E 1972 Star distribution near a collapsed object *Astrophys. J.* **178** 371–5
[41] Bahcall J N and Wolf R A 1976 Star distribution around a massive black hole in a globular cluster *Astrophys. J.* **209** 214–32
[42] Shapiro S L and Teukolsky S A 1986 Relativistic stellar dynamics on the computer. IV—Collapse of a star cluster to a black hole *Astrophys. J.* **307** 575–92
[43] Colombi S, Sousbie T, Peirani S, Plum G and Suto Y 2015 Vlasov versus N-body: the Hénon sphere *Mon. Not. R. Astron. Soc.* **450** 3724–41
[44] Ma C P and Bertschinger E 1995 Cosmological perturbation theory in the synchronous and conformal Newtonian gauges *Astrophys. J.* **455** 7–25
[45] Bazow D, Denicol G, Heinz U, Martinez M and Noronha J 2016 Analytic solution of the Boltzmann equation in an expanding system *Phys. Rev. Lett.* **116** 022301
[46] Bazow D, Denicol G, Heinz U, Martinez M and Noronha J 2016 Nonlinear dynamics from the relativistic Boltzmann equation in the Friedmann–Lemaître–Robertson–Walker spacetime *Phys. Rev.* D **94** 125006
[47] Chruściel P T, Costa J L and Heusler M 2012 Stationary black holes: uniqueness and beyond *Living Rev. Relativ.* **15** 7
[48] Zel'dovich Y B and Novikov I D 1971 *Stars and Relativity* (New York: Dover)
[49] Shapiro S L and Teukolsky S A 1983 *Black Holes, White Dwarfs and Neutron Stars* (New York: Wiley)
[50] Bondi H 1952 On spherically symmetrical accretion *Mon. Not. R. Astron. Soc.* **112** 195–204
[51] Michel F C 1972 Accretion of matter by condensed objects *Astrophys. Space Sci.* **15** 153–60
[52] Chaverra E and Sarbach O 2015 Radial accretion flows on static, spherically symmetric black holes *Class. Quantum Grav.* **32** 155006
[53] do Carmo M P 1992 *Riemannian Geometry* (Boston: Birkhäuser)
[54] Arnold V I 1989 *Mathematical Methods of Classical Mechanics* (New York: Springer)
[55] Misner C W, Thorne K S and Wheeler W J A 1973 *Gravitation* (San Francisco, CA: W. H. Freeman)
[56] Faraoni V 2015 *Cosmological and Black Hole Apparent Horizons* (Cham: Springer)
[57] Dennison K A and Baumgarte T W 2014 A simple family of analytical trumpet slices of the Schwarzschild spacetime *Class. Quantum Grav.* **31** 17001
[58] Rioseco P, Sarbach O and Zannias T in preparation
[59] Goldstein H, Poole C and Safko J 2002 *Classical Mechanics* (San Francisco, CA: Addison-Wesley)
[60] Batt J, Faltenbacher W and Horst E 1986 Stationary spherically symmetric models in stellar dynamics *E. Arch. Ration. Mech. Anal.* **93** 159–83
[61] Schaeffer J 1999 A class of counterexamples to Jeans' theorem for the Vlasov–Einstein system *J. Commun. Math. Phys.* **204** 313–27
[62] Rioseco P and Sarbach O 2017 Spherical steady-state accretion of a relativistic collisionless gas into a Schwarzschild black hole (arXiv:1701.07104)
[63] Synge J L 1956 *Relativity: the Special Theory* (Amsterdam: Elsevier)
[64] Royden H L 1989 *Real Analysis* (New York: Macmillan)
[65] Straumann N 2013 *General Relativity* (Berlin: Springer)

Part III

Appended Paper II:

Phase space mixing in the equatorial plane of a Kerr black hole.

Phase space mixing in the equatorial plane of a Kerr black hole

Paola Rioseco and Olivier Sarbach

Instituto de Física y Matemáticas, Universidad Michoacana de San Nicolás de Hidalgo, Edificio C-3, Ciudad Universitaria, 58040 Morelia, Michoacán, México

(Received 2 August 2018; published 19 December 2018)

It is shown that a collisionless, relativistic kinetic gas configuration propagating in the equatorial plane of a Kerr black hole undergoes a relaxation process and eventually settles down to a stationary, axisymmetric configuration surrounding the black hole. The underlying mechanism for this relaxation process is due to phase space mixing, which implies that although the one-particle distribution function f satisfying the collisionless Boltzmann equation is quasiperiodic in time, the associated macroscopic observables computed from averages over f possess well-defined limits as time goes to infinity. The final state of the gas is described by an effective distribution function depending only upon the constants of motion, and it can be determined by an appropriate average of the initial distribution function.

DOI: 10.1103/PhysRevD.98.124024

I. INTRODUCTION

Phase space mixing plays an important role in a wide range of areas in physics, including galactic dynamics, plasma physics and quantum physics. Roughly speaking, this phenomenon can be understood as the relaxation of the observables associated with a distribution function which is transported along an anharmonic Hamiltonian flow and hence spreads all over phase space due to different orbits having different angular frequencies.

In the context of galactic dynamics, groundbreaking work by Lynden-Bell [1,2] has shown that phase space mixing might be one of the fundamental mechanisms responsible for driving the one-particle distribution function describing the stellar distribution in a galaxy to an equilibrium configuration, although collisions or the exchange of energy between individual stars are negligible. For further important discussions on these topics, see for instance Refs. [3–6].

In plasma physics, phase mixing has been argued to be the driving mechanism for Landau damping, the relaxation of a charged collisionless gas to a homogeneous configuration. Recently, this explanation has been put on a rigorous basis by the work of Mouhot and Villani [7] who established that for the case of a finite box with periodic boundary conditions the known phase-mixing property for the linearized Vlasov-Poisson also occurs in the full Vlasov-Poisson system, without linearization. For generalization of this work to the special-relativistic setting, see [8,9].

At the quantum level, phase space mixing has recently been applied [10] to quenches in Bose-Einstein condensates in order to understand the behavior of the condensate in the vicinity of the saddle point in a double-well potential. Again, it was found that the system relaxes to a steady state due to phase-space mixing. For field-theoretical applications of the mixing phenomenon, see for example [11,12].

In the present work, we analyze the effects of phase mixing and its associated relaxation process in a general relativistic scenario. More specifically, we consider a collisionless, relativistic gas configuration that is trapped by the gravitational field of a rotating black hole. We restrict ourselves to the simplest case in which the gas configuration is sufficiently thin such that its self-gravity can be neglected and in which the gas is confined to the equatorial plane of the black hole, leaving the discussion of more realistic configurations to future work [13]. As a consequence of our assumptions, each individual gas particle follows a bound geodesic trajectory in the equatorial plane of a Kerr black hole background, and an explicit solution representation for the one-particle distribution function can be obtained by representing the geodesic flow in terms of action-anglelike variables, see Sec. II.

Based on this solution representation, we compute the particle current density four-vector and provide some examples in Sec. III showing that the particle density measured by a stationary observer outside the event horizon, although fluctuating in time, undergoes damped oscillations and eventually settles down to a constant value. An intuitive explanation for this convergence is given by exhibiting snapshots of the distribution function in the momentum space of the observer at different times which clearly illustrate the mixing in phase space.

To provide a precise mathematical formulation for the mixing property, in Sec. IV we consider an observable $N[\varphi]$ which is obtained by integrating the one-particle distribution function over a given test function φ on relativistic phase space. The time evolution of this observable is obtained by transporting the test function along the vector field generating the time translation symmetry. Denoting this transported test function by φ_t, we formulate and prove

a theorem which shows that, provided a certain determinant condition holds on the support of φ, $N[\varphi_t]$ converges for $t \to \infty$ to the same observable $N[\varphi]$ with the distribution function replaced by its average over the angle variables. Therefore, apart from providing a rigorous formulation for the mixing property, our theorem allows to predict the final state of the gas configuration by considering the average of the initial distribution function. Finally, we show that the determinant condition is satisfied almost everywhere in phase space, and discuss the applicability of our theorem to the examples in Sec. III.

In Sec. V we present the conclusions and main implications of our results, and also give an outlook to future work. Technical details and relevant analytic expressions required for this article are listed in an Appendix. Throughout this work we use geometrized units in which the gravitational constant and the speed of light are one.

II. COLLISIONLESS DISTRIBUTION FUNCTION IN TERMS OF ACTION-ANGLE VARIABLES

The geodesic flow describing the motion of free falling, massive particles following (spatially) bound trajectories on a Kerr spacetime may be represented analytically in terms of action-anglelike variables [14–16]. For the purpose of this work, it is sufficient to consider the 3-dimensional spacetime $(\mathcal{M}, g)$ describing the induced geometry on the equatorial plane of a Kerr black hole exterior of mass $M > 0$ and rotational parameter a satisfying $|a| \leq M$. In terms of Boyer-Lindquist coordinates (t, r, φ), the metric has the following representation:

$$g = -dt^2 + \frac{2M}{r}(dt - a d\varphi)^2 + (r^2 + a^2)d\varphi^2 + \frac{r^2}{\Delta}dr^2, \quad r > r_H \tag{1}$$

with $\Delta := r^2 - 2Mr + a^2$ and $r_H := M + \sqrt{M^2 - a^2}$ the radius of the event horizon. Due to the time-translation and axial symmetry of $(\mathcal{M}, g)$, the geodesic equations form an integrable Hamiltonian system which is characterized by the free-particle Hamiltonian $\mathcal{H}$ and the constants of motion $\mathcal{E}$ and $\mathcal{L}$, given by the following functions on the co-tangent bundle $T^*\mathcal{M}$ associated with $\mathcal{M}$:

$$\mathcal{H}(x,p) := \frac{1}{2}g^{\mu\nu}(x)p_\mu p_\nu, \qquad \mathcal{E}(x,p) := -p_t,$$
$$\mathcal{L}(x,p) := p_\varphi, \qquad (x,p) \in T^*\mathcal{M},$$

which Poisson-commute among themselves. The orbits are confined to the invariant subsets

$$\Gamma_{m,E,L} := \{(x,p) \in T^*\mathcal{M} : \mathcal{H}(x,p) = -\frac{m^2}{2},$$
$$\mathcal{E}(x,p) = E, \mathcal{L}(x,p) = L\},$$

with $m > 0$. Since only bound orbits are considered, the angular momentum L has to be large enough in magnitude such that $L^2 > L_{\rm ms}^2$, with $L_{\rm ms}$ the angular momentum corresponding to the marginally stable circular orbit [17], and the energy E has to lie inside a certain interval $E_{\rm min}(L) < E < E_{\rm max}(L)$ with $E_{\rm min}(L)$ the energy of the stable circular orbit with angular momentum L and $E_{\rm max}(L) \leq m$ the maximum of the potential well. In this range, it can be verified that the invariant sets $\Gamma_{m,E,L}$ are smooth 3-dimensional submanifolds of $T^*\mathcal{M}$ having topology $\mathbb{R} \times S^1 \times S^1$. For the following, we focus on the phase space of bound trajectories $\Gamma_{\rm bound}$, the union of all these invariant submanifolds.

Using standard tools from Hamiltonian mechanics [18] one can introduce action-angle variables (Q^α, J_α) on $\Gamma_{\rm bound}$, see for instance [14,15]. The action variables are defined as[1]

$$J_0 := -\frac{1}{T}\int_0^T p_t dt = \mathcal{E}, \qquad J_1 := \frac{1}{2\pi}\oint p_\varphi d\varphi = \mathcal{L},$$
$$J_2 := \frac{1}{2\pi}\oint p_r dr = \frac{1}{\pi}\int_{r_1}^{r_2}\frac{\sqrt{R(r)}}{\Delta}dr, \tag{2}$$

where here the first integral defining J_0 is performed along an integral curve of the vector field ∂_t (t being the parameter along this curve), the second integral defining J_1 is similarly performed over the closed curve along the vector field ∂_φ,[2] and the third integral over the closed curve in the (r, p_r)-plane described by the radial equation $(\Delta p_r)^2 = R(r)$ with

$$R(r) := (Er^2 - a\hat{L})^2 - \Delta(m^2r^2 + \hat{L}^2), \qquad \hat{L} := L - aE, \tag{3}$$

and with $r_1 < r_2$ the turning points. The angle variables $Q^\alpha := \frac{\partial \mathcal{S}}{\partial J_\alpha}$ are obtained from the generating function

$$\mathcal{S}(x; J_0, J_1, J_2) = -Et + L\varphi + \int_{(r,p_r)} p_r dr, \tag{4}$$

where the integral on the right-hand side should be interpreted as a line integral along the curve $(\Delta p_r)^2 = R(r)$ connecting the reference point $(r_1, 0)$ to the given point (r, p_r) on this curve. $\mathcal{S}$, Q^α, and J_α admit explicit representations in terms of standard elliptic integrals (details of the derivation will be presented elsewhere [13]). In order to describe the result we denote the roots of the fourth-order polynomial $R(r)$ by $0 < r_0 < r_1 < r_2$ and introduce the dimensionless variables

$$\alpha := \frac{a}{M}, \quad \varepsilon := \frac{E}{m}, \quad \lambda := \frac{L}{Mm}, \quad \xi_j := \frac{r_j}{M}, \quad j = 0,1,2.$$

[1] Our definition of J_0 differs from the definition of J_t in [15] by a minus sign.

[2] More precisely, these integral curves are defined with respect to the complete lifts of the Killing vector fields ∂_t and ∂_φ on $T^*\mathcal{M}$, see for example Refs. [19,20] for the most important properties of the complete lift in the context of relativistic kinetic theory.

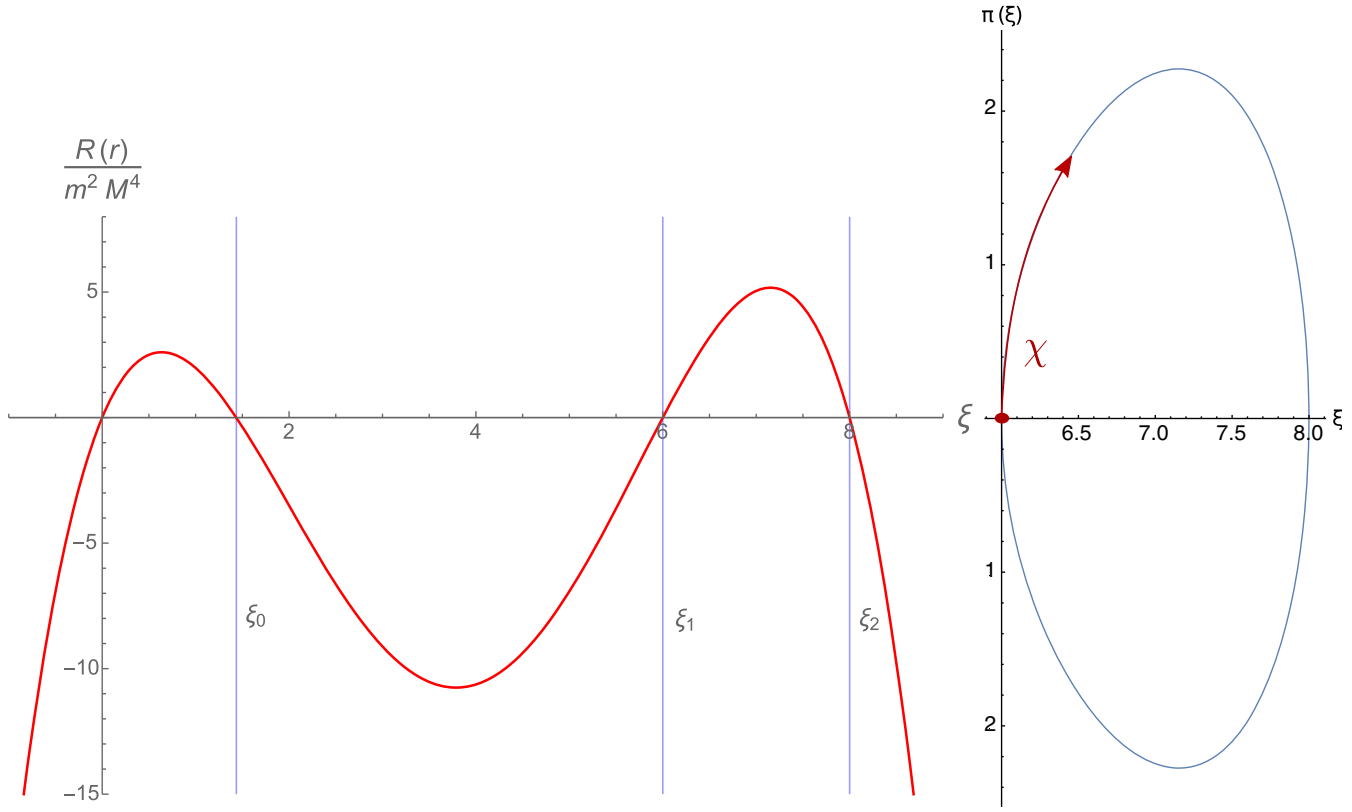

FIG. 1. Left panel: The function $R(r)/M^4m^2$ and its four roots $0 < \xi_0 < \xi_1 < \xi_2$ for the parameter values $\alpha = 0.9$, $\varepsilon = 0.93297$ and $\lambda = 2.9528$. Only the nontrivial roots ξ_j, $j = 0, 1, 2$, which lie outside the event horizon are relevant in this work. Right panel: the projection of the set $\Gamma_{m,E,L}$ with the same parameter values onto the (r, p_r)-plane and the angle χ parametrizing this set. Here, $\xi := r/M$ and $\pi(\xi) := \Delta p_r/M^2m$.

The curve $(\Delta p_r)^2 = R(r)$ is parametrized by the π-periodic angle coordinate χ (see Fig. 1) defined by

$$\frac{r}{M} = \xi_0 + \frac{\xi_1 - \xi_0}{1 - b^2\sin^2\chi}, \tag{5}$$

$$\frac{\Delta p_r}{M^2 m} = \frac{1}{2}\sqrt{1-\varepsilon^2}(\xi_2-\xi_1)(\xi_1-\xi_0) \times \sqrt{\frac{\xi_1}{\xi_2-\xi_0}}\frac{\sqrt{1-k^2\sin^2\chi}}{(1-b^2\sin^2\chi)^2}\sin(2\chi), \tag{6}$$

with $b := \sqrt{(\xi_2-\xi_1)/(\xi_2-\xi_0)}$ and $k := \sqrt{\xi_0/\xi_1}b$, such that $0 < k < b < 1$. In terms of these quantities one finds

$$J_0 = m\varepsilon, \quad J_1 = Mm\lambda, \quad J_2 = \frac{Mm}{\pi}[(1-\varepsilon^2)\mathbb{H}_0 + \varepsilon\mathbb{H}_3], \tag{7}$$

$$Q^0 = -t + M\frac{\mathbb{H}_0\mathbb{H}_2(\chi) - \mathbb{H}_2\mathbb{H}_0(\chi)}{\mathbb{H}_0},$$
$$Q^1 = \varphi + \frac{\mathbb{H}_0\mathbb{H}_1(\chi) - \mathbb{H}_1\mathbb{H}_0(\chi)}{\mathbb{H}_0}, \qquad Q^2 = \pi\frac{\mathbb{H}_0(\chi)}{\mathbb{H}_0}, \tag{8}$$

where the functions $\mathbb{H}_j(\chi)$ and corresponding constants $\mathbb{H}_j := \mathbb{H}_j(\pi/2)$ are defined in the Appendix. The coordinates (Q^α, J_α) provide new symplectic coordinates on Γ_{bound}, the submanifold of $T^*\mathcal{M}$ corresponding to bound orbits. The action variables J_α label the invariant submanifolds $\Gamma_{m,E,L}$, the coordinates (Q^1, Q^2) are 2π-periodic functions providing angles on each S^1-factor of $\Gamma_{m,E,L} = \mathbb{R}\times S^1\times S^1$, while Q^0 parametrizes its $\mathbb{R}$-factor.

In terms of these action-anglelike variables, the collisionless Boltzmann equation $\{\mathcal{H}, f\} = 0$ for the one-particle distribution function f assumes the simple form

$$\left(\Omega^0\frac{\partial}{\partial Q^0} + \Omega^1\frac{\partial}{\partial Q^1} + \Omega^2\frac{\partial}{\partial Q^2}\right)f = 0, \qquad \Omega^\alpha := \frac{\partial\mathcal{H}}{\partial J_\alpha}. \tag{9}$$

Since $\mathcal{H}$ and Ω^α only depend on the action variables J_α, the most general solution of Eq. (9) has the form

$$f(x,p) = F(Q^1 - \omega^1 Q^0, Q^2 - \omega^2 Q^0, J_0, J_1, J_2), \tag{10}$$

with $F(Q^1, Q^2, J_0, J_1, J_2)$ an arbitrary function which is 2π-periodic in the Q variables and decays sufficiently fast in the J variables, such that the integrals defining the spacetime observables are well defined. Here the frequencies ω^1 and ω^2 are defined by

$$\omega^1 := \frac{\Omega^1}{\Omega^0} = \frac{1}{M}\frac{\mathbb{H}_1}{\mathbb{H}_2 - \varepsilon\mathbb{H}_0}, \qquad \omega^2 := \frac{\Omega^2}{\Omega^0} = -\frac{\pi}{\mathbb{H}_1}\omega^1. \tag{11}$$

Equations (7), (8), (10) provide an explicit solution representation for the distribution function f which will enable us to study the dynamical behavior of generic, time-dependent gas configurations in the next two sections. Note that according to Eq. (8) the distribution function f is axisymmetric if and only if F is independent of Q^1, and it is stationary and axisymmetric if and only if F is independent of Q^1 and Q^2 (in which case it depends only on the action variables J_α). In the remainder of this work, we demonstrate that any distribution function relaxes in time (in some sense made precise in Sec. IV) to such a stationary and axisymmetric configuration.

III. RELAXATION OF SPACETIME OBSERVABLES AND PHASE SPACE MIXING

In this section we analyze the behavior of spacetime observables along the world lines of observers located outside the event horizon. For simplicity and the sake of illustration, in this section we assume that the black hole is non-rotating (although we will come back to the rotating case in the next section). Furthermore, we focus on the particle current density four-vector (see for instance [21])

$$\mathcal{J}^\mu(x) = \int f(x,p)p^\mu \mathrm{dvol}_x(p),$$
$$\mathrm{dvol}_x(p) := \sqrt{-\det(g^{\mu\nu}(x))}dp_t dp_r dp_\vartheta dp_\varphi,$$

measured by a static observer in the equatorial plane with fixed spatial coordinates $(r,\vartheta,\varphi) = (r_{\mathrm{obs}}, \pi/2, \varphi_{\mathrm{obs}})$, $r_{\mathrm{obs}} > 2M$, with respect to its rest frame

$$e_0 = \frac{1}{\sqrt{1-\frac{2M}{r}}}\frac{\partial}{\partial t}, \qquad e_1 = \sqrt{1-\frac{2M}{r}}\frac{\partial}{\partial r},$$
$$e_2 = \frac{1}{r}\frac{\partial}{\partial\vartheta}, \qquad e_3 = \frac{1}{r}\frac{\partial}{\partial\varphi}.$$

In order to perform the integral over the momentum we first reexpress the volume form $\mathrm{dvol}_x(p)$ in terms of the conserved quantities m, E, ℓ and ℓ_z, where ℓ and ℓ_z are, respectively, the total and the azimuthal component of the angular momentum. For points x located in the equatorial plane, one obtains

$$\mathrm{dvol}_x(p) = \frac{1}{r^2}dE dp_r dp_\vartheta d\ell_z = \frac{dE(mdm)(\ell d\ell)d\sigma}{\sqrt{R(r)}},$$

where we have defined σ by $\sin\sigma = \ell_z/\ell$ and the function $R(r)$ is given in Eq. (3). Assuming a kinetic gas distribution of identical particles of positive rest mass m which are confined to the equatorial plane (such that $\sigma = \pm\pi/2$ and $\ell_z = L$), one obtains the following orthonormal components of the current density:

$$\mathcal{J}^\alpha := m^3 \int \left.\frac{[f(x,p_+)p_+^\alpha + f(x,p_-)p_-^\alpha]|\lambda| d\varepsilon d\lambda}{\sqrt{(1-\varepsilon^2)\xi(\xi-\xi_0)(\xi-\xi_1)(\xi_2-\xi)}}\right|_{\xi=r_{\mathrm{obs}}/M}, \tag{12}$$

with $p_\pm^0 := m\varepsilon/\sqrt{1-\frac{2}{\xi}}$, $p_\pm^1 := \sqrt{1-\frac{2}{\xi}}p_{r\pm}$, $p_\pm^2 := 0$ and $p_\pm^3 := m\lambda/\xi$, and where $p_\pm$ denote the two possible values for the four-momentum $p = p^\alpha e_\alpha$ corresponding to the two solutions of equation $(\Delta p_r)^2 = R(r)$. To make further progress, we use the relations (A1) to reexpress the integral in terms of the turning points ξ_1 and ξ_2. Instead of ξ_1 and ξ_2, it is convenient to use the generalized Keplerian variables (P, e) as in Ref. [22], which are defined by

$$\xi_1 = \frac{P}{1+e}, \qquad \xi_2 = \frac{P}{1-e},$$

such that $\xi_0 = 2P/(P-4)$. Here, the eccentricity e is restricted to the interval $0 < e < 1$, the limit $e \to 0$ representing circular trajectories, and the semi-latus rectum P is restricted to $P > 6 + 2e$, the limits $P \to \infty$ and $P \to 6 + 2e$ (with fixed e) corresponding, respectively, to the Newtonian limit and the innermost stable orbits (ISO) which separate the bound orbits from those that plunge into the black hole. Note that there is a one-to-two correspondence between the parameters (P, e) and the constants of motion $(\varepsilon, \pm\lambda)$. Note also that given $\xi_{\mathrm{obs}} = r_{\mathrm{obs}}/M$, the parameters (P, e) are restricted by the conditions $\xi_0 < \xi_1 < \xi_{\mathrm{obs}} < \xi_2$, which yield

$$P_{\min}(e) := \max\{6+2e, (1-e)\xi_{\mathrm{obs}}\} < P < (1+e)\xi_{\mathrm{obs}} =: P_{\max}(e). \tag{13}$$

Based on these observations, Eq. (12) can be rewritten as the sum $\mathcal{J}^\alpha = \mathcal{J}^\alpha_{\lambda>0} + \mathcal{J}^\alpha_{\lambda<0}$ over the contributions corresponding to gas particles with positive/negative angular momentum λ, where

$$\mathcal{J}^\alpha_{\lambda>0} = \frac{m^3}{2}\sum_\pm \int_0^1 de \int_{P_{\min}(e)}^{P_{\max}(e)} dP \times \frac{F(Q^1_\pm - \omega^1 Q^0_\pm, Q^2_\pm - \omega^2 Q^0_\pm, J_0, J_1, J_2)p^\alpha_\pm}{\sqrt{(1-\varepsilon^2)\xi(\xi-\xi_0)(\xi-\xi_1)(\xi_2-\xi)}} \times \left.\frac{e\sqrt{P}[(P-6)^2-4e^2]}{\sqrt{(P-3-e^2)^5[(P-2)^2-4e^2]}}\right|_{\xi=\xi_{\mathrm{obs}}}. \tag{14}$$

Here, it is understood that all the relevant quantities are expressed in terms of (P, e) which determine the locations of the roots ξ_0, ξ_1, ξ_2 and the conserved quantities (ε, λ) taking the positive sign of λ (and similarly for $\mathcal{J}^0_{\lambda<0}$ where one takes the negative sign of λ). The sum over the $\pm$ signs refers to the two possible choices for $p_\pm$ which, in turn correspond to the two possible values for the angle variables $Q^\alpha_\pm$. Note that $Q^\alpha_+ + Q^\alpha_- = 2\pi$.

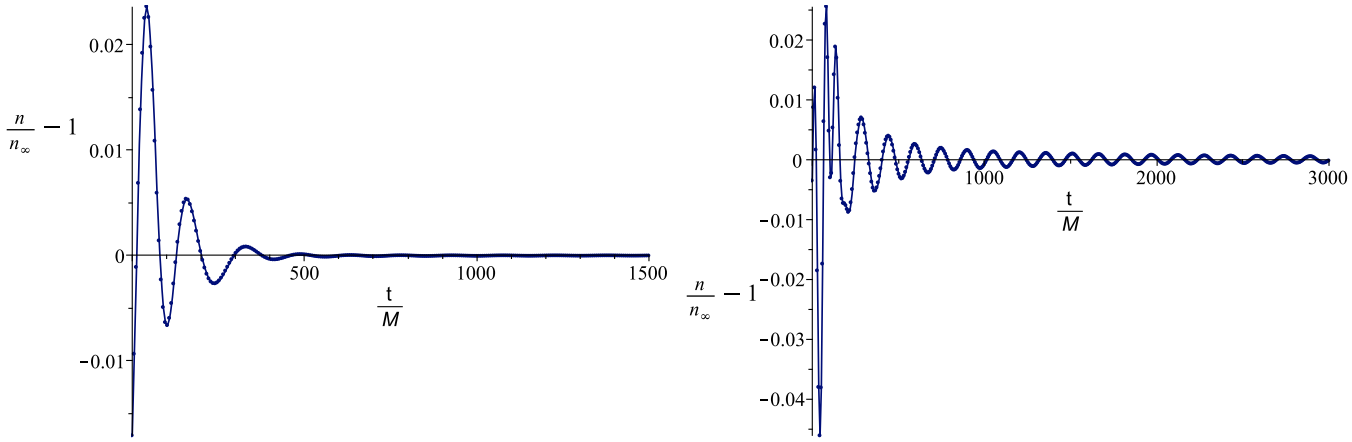

FIG. 2. Particle density as a function of time measured by a static observer located at $r_{\rm obs} = 6M$ and $\varphi_{\rm obs} = 0$ in a Schwarzschild spacetime for case A (left panel) and case B (right panel). As is visible from these plots, the initial decay is much faster in case A, although the log − log plots below indicate that in both cases the final decay is of the inverse power-law type.

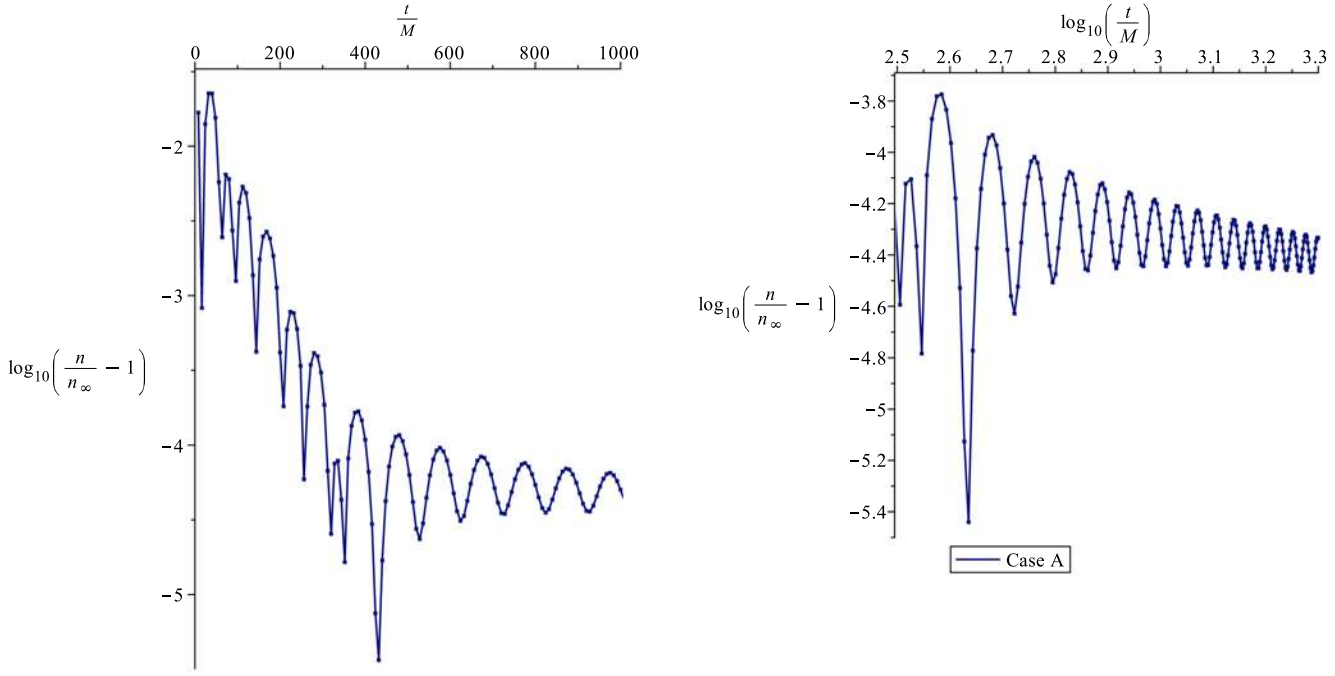

FIG. 3. This plot shows the decay of the particle density towards its asymptotic value n_∞ for case A. Left panel: log plot of the relative error $|n/n_\infty - 1|$, indicating an initial exponential decay for the initial period until $t \simeq 400M$. Right panel: log − log plot of the relative error, indicating that for times larger than $\simeq 700M$ the decay is slower (apparently of the inverse power-law type).

In Figs. 2, 3 and 4 we display the time behavior of the particle density $n := \mathcal{J}^0_{\lambda>0}$ measured by the observer for the case of an initial distribution function of the form $F(q^1, q^2, J_0, J_1, J_2) = F_Q(q^1, q^2) F_J(P, e)$, where

$$F_Q(q^1, q^2) := \frac{1}{N} \exp\left[-\frac{\cos^2(q^1)}{\eta_1^2} - \frac{\cos^2(q^2)}{\eta_2^2}\right],$$
$$F_J(P, e) := \exp\left[-\frac{(P - 2e - P_0 + 2e_0)^2}{(\Delta P)^2} - \frac{(e - e_0)^2}{(\Delta e)^2}\right], \tag{15}$$

N is a positive normalization factor chosen such that $\int_0^{2\pi} dq^1 \int_0^{2\pi} dq^2 F_Q(q^1, q^2) = 1$, and η_1, η_2, P_0, e_0, ΔP, Δe are positive constants whose values are given in Table I. Notice that the function F_Q defined in Eq. (15) satisfies $F_Q(q^1, q^2) = F_Q(2\pi - q^1, 2\pi - q^2)$, which implies that both terms in the sum $\sum_\pm$ yield the same contribution for $\mathcal{J}^\alpha_{\lambda>0}$ when $\alpha = 0, 3$, while $\mathcal{J}^1_{\lambda>0} = 0$. The observer is located at either $(r_{\rm obs}, \varphi_{\rm obs}) = (6M, 0)$ or $(9M, 0)$.

Even though the distribution function oscillates in time and does not have a (pointwise) limit, the results in the plots indicate that the observable n converges to a finite value

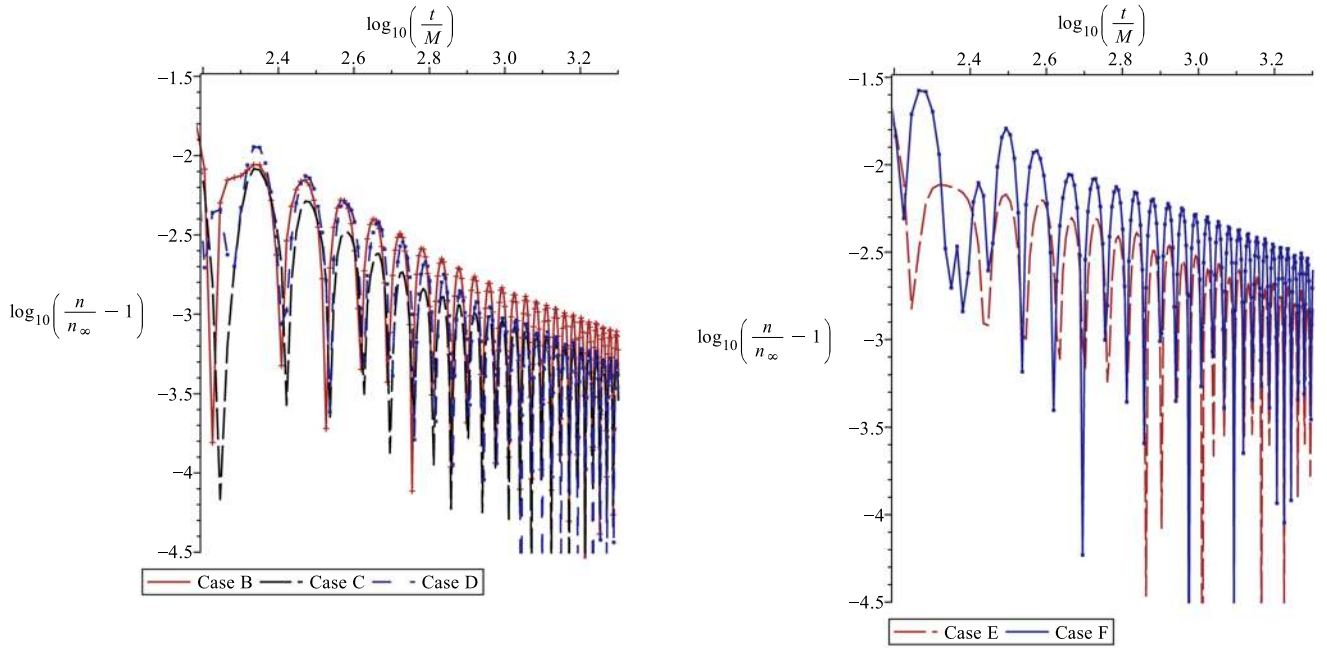

FIG. 4. log − log plots of the relative error $|n/n_\infty - 1|$ for cases $B - F$, showing the decay of the particle density towards its final value n_∞.

(denoted by n_∞ and computed from the averaged distribution function as will be explained in the third remark after Theorem 1) as $t \to \infty$. We note that in case A the convergence is rather fast (exponential decay during the initial period, with relative fluctuations below 0.001 after times larger than $300M$), while in the remaining cases the convergence appears to be slower (inverse power-law decay with relative fluctuations below 0.001 after a few thousand M). We have also computed the remaining nontrivial component $\mathcal{J}^3_{\lambda>0}$ and the contributions $\mathcal{J}^\alpha_{\lambda<0}$ belonging to negative angular momentum (assuming the same distribution $F_J(P, e)$) and verified that they exhibit a similar time behavior, with $\mathcal{J}^3 := \mathcal{J}^3_{\lambda>0} + \mathcal{J}^3_{\lambda<0} \to 0$.

As shown in the next section, the relaxation process displayed in Figs. 2–4 is due to phase space mixing. To get an intuitive idea about this phenomenon, in Fig. 5 we show snapshots of the function $F_Q(Q^1 - \omega^1 Q^0, Q^2 - \omega^2 Q^0)$ for an observer located at $r_{\rm obs} = 6M$ and $\varphi_{\rm obs} = 0$ at different times. As is visible from these plots, the geodesic flow (which is volume preserving according to Liouville's theorem) stretches the phase space elements and spreads them over large regions in phase space, inducing the mixing property. As a consequence, averaged (macroscopic) quantities computed from the distribution function, such as the components of the current density in Eq. (14), have the form of an integral over a smooth function multiplied by an oscillating function whose frequency increases unboundedly in time. In the limit $t \to \infty$ these oscillations cancel out, and hence one can replace the distribution function with its nonoscillatory part, that is, its average over the angle variables:

TABLE I. Parameter values for the initial distribution function F, describing a kinetic gas whose gas particles all move on bound orbits, and the location of the observer $\xi_{\rm obs}$. Note that cases $B - F$ contain circular orbits ($e = 0$) in their main support, while case A corresponds to a gas configuration whose distribution is peaked around highly eccentric orbits. Also shown is the estimated power κ obtained from fitting the envelope of the relative error $|n/n_\infty - 1|$ to an inverse power law of the form $t^{-\kappa}$, and the time $t_{<0.001}$ after which this error is estimated to lie below 0.001. In case A the decay is dominated by an initial exponential decaying phase, as indicated in the right panel of Fig. 2, after which the error is already very small, which makes it difficult to determine the power κ. In all other cases the values for κ and $t_{<0.001}$ have been estimated to about 10% accuracy.

Case	η_1	η_2	P_0	e_0	ΔP	Δe	$\xi_{\rm obs}$	κ	$t_{<0.001}$
A	3	5	9.2	0.6	0.632	0.316	6	⋯	$300M$
B	3	5	6.68	0.14	0.5	0.387	6	0.9	$1500M$
C	3	5	6.3	0.12	0.5	0.447	6	0.9	$900M$
D	3	5	6.383	0.092	0.5	0.316	6	0.9	$900M$
E	3	5	9.2	0.1	1.10	0.548	9	0.8	$3500M$
F	3	5	9.2	0.1	0.632	0.316	9	0.8	$7000M$

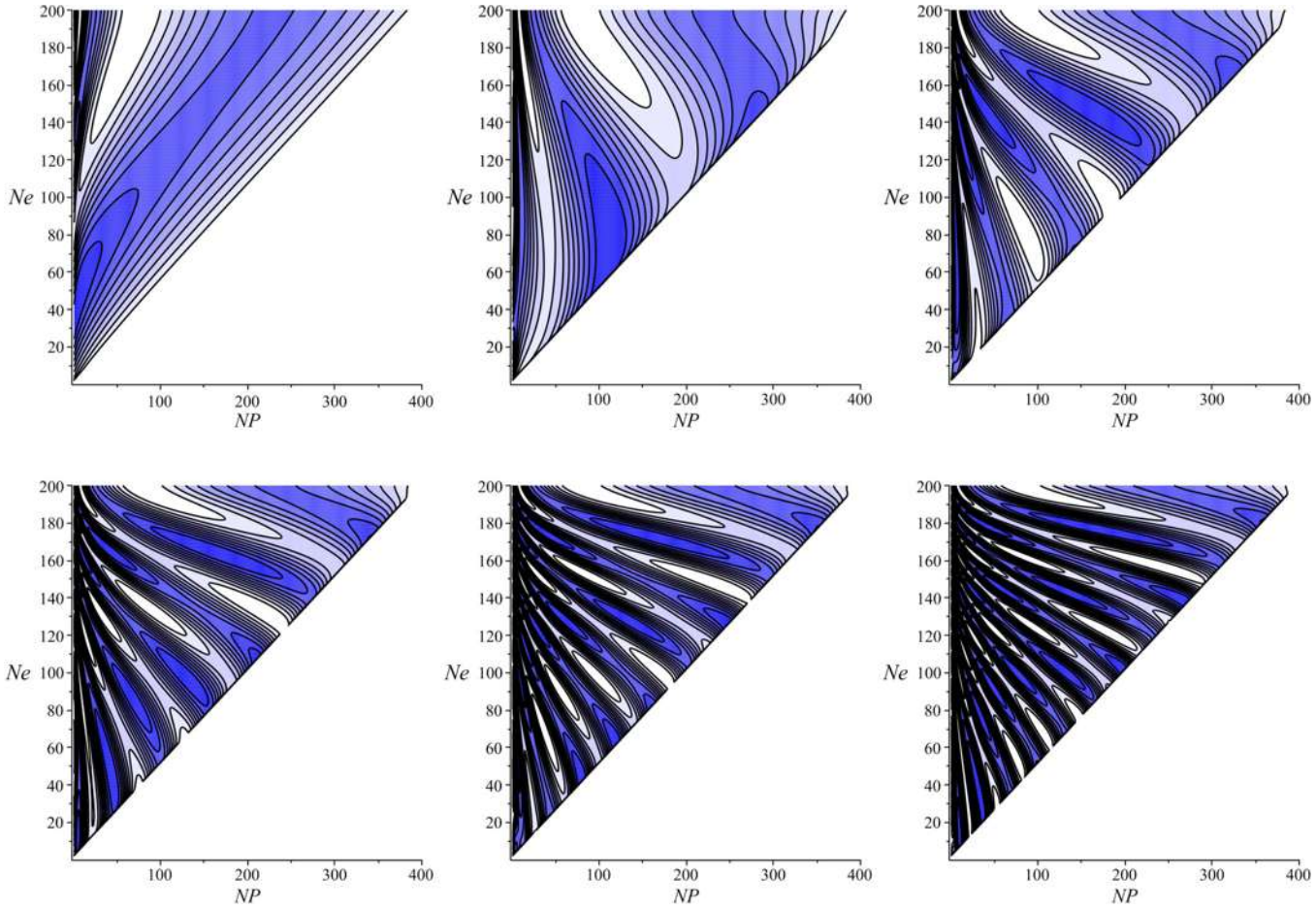

FIG. 5. Level sets for the distribution function $F_Q(Q^1 - \omega^1 Q^0, Q^2 - \omega^2 Q^0)$ as a function of the parameters ($P' \coloneqq P - 6 - 2e$, e) as seen by a static observer located at $r_{\text{obs}} = 6M$ and $\varphi_{\text{obs}} = 0$ for different times: $t = 0M$, $t = 100M$, $t = 200M$, $t = 300M$, $t = 400M$, and $t = 500M$ (from top left to right bottom). In these plots, the values of NP and Ne are related to (P', e) through the formulas $P' = 0.01 \times NP$ and $e = 0.005 \times Ne$, respectively, and the inequalities (13) translate into $0 \leq NP \leq 2Ne$. The colors indicate different intervals in the range of F_Q, with dark blue corresponding to values of F_Q lying close to its maximum and white corresponding to values of F_Q close to its minimum.

$$F(Q^1 - \omega^1 Q^0, Q^2 - \omega^2 Q^0, J_0, J_1, J_2) \rightharpoonup \bar{F}(J_0, J_1, J_2) \coloneqq \frac{1}{(2\pi)^2} \int_0^{2\pi} \int_0^{2\pi} F(Q^1, Q^2, J_0, J_1, J_2) dQ^1 dQ^2 \tag{16}$$

The precise sense in which this convergence is valid will be explained in the next section.

IV. MATHEMATICAL FORMULATION OF THE MIXING PROPERTY

After discussing the intuitive picture behind the mixing phenomenon and the corresponding relaxation process of the spacetime observables, in this section we provide a precise mathematical formulation of this effect which provides a rigorous explanation for the convergence of certain macroscopic observables. Here, a macroscopic observable is described by a test function $\varphi \in C_0^\infty(\Gamma_{\text{bound}})$ on the relativistic phase space Γ_{bound}, and its associated value is defined by the quantity

$$N[\varphi] \coloneqq \int_{\Gamma_{\text{bound}}} f(x,p)\varphi(x,p)\text{dvol}_\Gamma, \tag{17}$$

with $\text{dvol}_\Gamma = dtd\varphi dr dp_t dp_\varphi dp_r$ the canonical volume form on Γ_{bound} and $f(x,p)$ the one-particle distribution function describing the state of the kinetic gas. Note that our definition (17) is based on a fully covariant (i.e., independent of any choice of foliation or local coordinates) spacetime point of view which includes a time integral, such that $N[\varphi]$ does not dependent on time. Therefore, in order to understand the dynamical behavior, one needs to perform a translation of the test function φ along a time direction. Due to the many-fingered nature of time in general relativity there are no such preferred time directions in a general situation. In our case, the presence of the

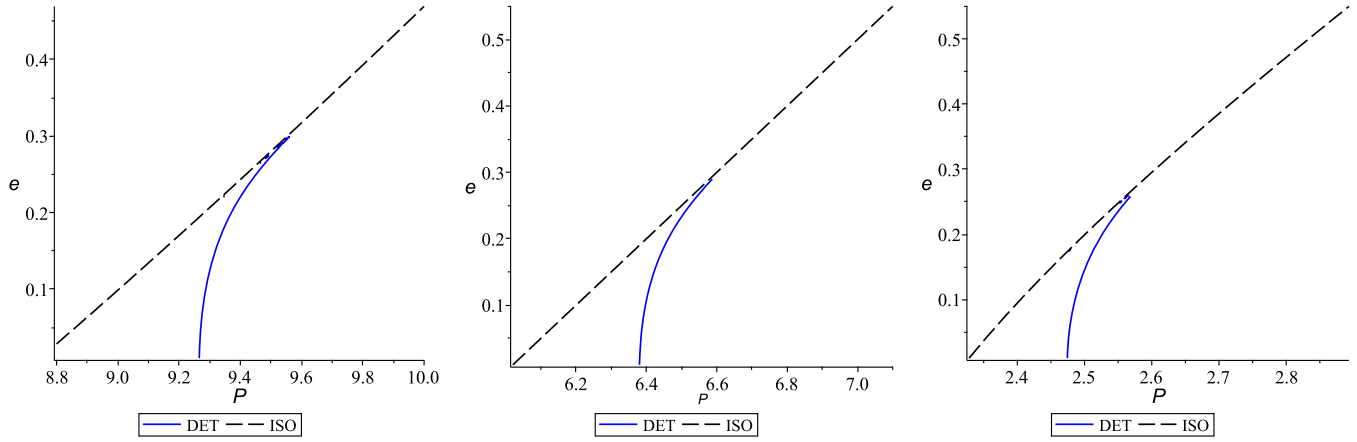

FIG. 6. The determinant condition in the (P, e)-space for a Schwarzschild black hole (middle panel) and a Kerr black hole with rotational parameter $a = 0.9M$ (prograde orbits in the left panel, retrograde orbits in the right panel). The black dashed line corresponds to innermost stable orbits (ISO), for which $\xi_0 = \xi_1$, while the blue solid line indicates the points for which the determinant condition (21) is violated. (Note that the Schwarzschild range $P > 6 + 2e$ for the semi-latus rectum changes in the rotating case, see for instance Appendix A in Ref. [22]).

Killing vector field ∂_t induces a natural vector field $\hat{k}$ on phase space Γ_{bound} defined as the complete lift of ∂_t (see Refs. [19,20] for details). This vector field, in turn, induces a flow ψ^t on Γ_{bound} with respect to which one may define the time-translated test function:[3]

$$\varphi_t(x, p) \coloneqq \varphi(\psi^{-t}(x, p)). \tag{18}$$

It is important to mention that in the rotating case, the Killing vector field ∂_t is spacelike and not timelike inside the ergoregion, meaning that (due to the dragging by rotation) stationary observers lying inside the ergoregion cannot follow the integral curves of ∂_t. In this case one might replace ∂_t with the linear combination $X \coloneqq \partial_t + \Omega\partial_\varphi$, with the constant angular velocity Ω chosen such that X is timelike in the vicinity of the observer, and define ψ^t as the flow with respect to the complete lift $\hat{X}$ of X. This provides a more sensible definition for the time-translated test function φ, if φ has its support in a region lying close to the event horizon which intersects the ergoregion. We stress that the theorem below holds for both (and probably more general) cases, the flow of ψ^t being defined with respect to the complete lift of either ∂_t or X.[4]

For the statement of the following theorem, the area function, defined by

$$A_m(E, L) \coloneqq \oint p_r dr = 2Mm[(1-\varepsilon^2)\mathbb{H}_0 + \varepsilon\mathbb{H}_3],$$
$$L^2 > L^2_{ms}, \qquad E_{\min}(L) < E < E_{\max}(L), \tag{19}$$

plays an important role. Note that this function determines the action variable $J_2 = \frac{A_m}{2\pi}$, and the frequencies ω^1 and ω^2 defined in Eq. (11) are determined by the gradient of A_m as follows:

$$\omega^1 = \frac{\partial A_m}{\partial L} \Big/ \frac{\partial A_m}{\partial E}, \qquad \omega^2 = -2\pi \Big/ \frac{\partial A_m}{\partial E}. \tag{20}$$

After these remarks, we are ready to formulate the main result of this article:

Theorem 1. Let $F \in L^1(S^1 \times S^1 \times (-\infty, \infty) \times (-\infty, \infty) \times (0, \infty))$ be a Lebesgue-integrable function which, according to Eq. (10), determines a solution $f(x, p)$ on Γ_{bound} of the collisionless Boltzmann equation on the equatorial plane of a Kerr black hole background. Let $\bar{F}$ and $\bar{f}$ be the corresponding distribution functions obtained by averaging over the angle variables. Let $\varphi \in C_0^\infty(\Gamma_{\text{bound}})$ be a test function, and denote by φ_t its time-translation as defined in Eq. (18).

Suppose further that on the support of φ the following nondegeneracy condition holds:

$$\det(D^2 A_m(E, L)) \neq 0, \tag{21}$$

where $D^2 A_m(E, L)$ denotes the Hessian matrix of the area function (19).

Then,

$$\lim_{t\to\infty} N[\varphi_t] = \int_{\Gamma_{\text{bound}}} \bar{f}(x, p)\varphi(x, p)\text{dvol}_\Gamma. \tag{22}$$

Remarks:

(1) The validity of the determinant condition (21) will be analyzed towards the end of this section, following the proof of the theorem. As will be verified

[3]Geometrically speaking, φ_t is the push-forward of φ with respect to ψ^t.

[4]As one can easily verify, the effect of replacing ∂_t by X is equivalent to replacing the frequency ω^1 by $\omega^1 + \Omega$ in the proof of Theorem 1.

numerically, it is satisfied everywhere except for points lying on a certain curve in (E, L)-space, see Fig. 6. However, we stress that the theorem does not require condition (21) to hold everywhere; it is sufficient to hold for points lying in the support of φ, that is, in the vicinity where the observer performs the measurement.

(2) Although the above formulation of the theorem requires the test function φ to be smooth, this assumption can be relaxed considerably. For example, it is possible to consider certain observables with test functions of the form

$$\varphi(x,p) = \delta(x - x_{\mathrm{obs}})\sqrt{-\det(g^{\mu\nu}(x))}\psi(p),$$

corresponding to spacetime observables at some given event x_{obs}, as the ones considered in the previous section, see [13,23].

(3) The quantity n_∞ in Figs. 2, 3 and 4 has been calculated by replacing F by its average $\bar{F}$ in Eq. (14).

(4) Note that the hypothesis of the theorem require φ to be supported on Γ_{bound}, which excludes circular orbits since the latter belong to the boundary of Γ_{bound}. However, the theorem can likely be generalized to the more realistic case in which the support of φ includes circular orbits (see also the remarks at the end of this section).

Proof of Theorem 1. In a first step, we rewrite the integral defining $N[\varphi]$ in terms of the action-angle variables (Q^α, J_α) as follows:

$$N[\varphi] = \int F(Q^1 - \omega^1 Q^0, Q^2 - \omega^2 Q^0, J_0, J_1, J_2) \times \Phi(Q^0, Q^1, Q^2, J_0, J_1, J_2) dQ^0 dQ^1 dQ^2 dJ_0 dJ_1 dJ_2,$$

where $\Phi(Q^0, Q^1, Q^2, J_0, J_1, J_2) = \varphi(x,p)$ is the representation of the test function φ in terms of (Q^α, J_α) and where we have used the fact that the transformation $(x,p) \mapsto (Q^\alpha, J_\alpha)$ is canonical. With respect to these variables, the flow associated with the vector field $\hat{k} = -\partial/\partial Q^0$ amounts to a translation of Q^0 by $-t$, keeping the other variables fixed, such that $\varphi_t(x,p) = \Phi(Q^0 + t, Q^1, Q^2, J_0, J_1, J_2)$. By means of the variable substitution $Q^0 = \Theta^0 - t$, $Q^A = \Theta^A + \omega^A \Theta^0$, $A = 1, 2$, one obtains

$$N[\varphi_t] = \int_0^\infty dm \int_0^{2\pi} d\Theta^1 \int_0^{2\pi} d\Theta^2 \int_{L^2 > L^2_{\mathrm{ms}}} dL \times \int_{E_{\min}(L)}^{E_{\max}(L)} dE F_m(\Theta^1 + \omega^1 t, \Theta^2 + \omega^2 t, E, L) \times \Phi_m(\Theta^1, \Theta^2, E, L),$$

where we have defined $F_m(\Theta^1, \Theta^2, E, L) := F(\Theta^1, \Theta^2, E, L, A_m(E,L)/2\pi)$ and

$$\Phi_m(\Theta^1, \Theta^2, E, L) := \frac{1}{2\pi}\frac{\partial A_m}{\partial m}(E,L) \int_{-\infty}^{\infty} \Phi\Big(\Theta^0, \Theta^1 + \omega^1\Theta^0, \Theta^2 + \omega^2\Theta^0, E, L, \frac{A_m(E,L)}{2\pi}\Big) d\Theta^0.$$

In a next step, we perform a variable substitution in order to replace the integral over (E, L) by an integral over (ω^1, ω^2). To this purpose, we denote by $W_m : (E,L) \mapsto (\omega^1, \omega^2)$ the map that defines (for fixed m) the angular frequencies (ω^1, ω^2) in terms of the constants of motion (E, L). Its Jacobian determinant is related to the determinant of the Hessian of the area function as follows:

$$\det(DW_m) = -\frac{(\omega^2)^3}{(2\pi)^2}\det(D^2 A_m(E,L)).$$

Therefore, due to condition (21) the map W_m is (at least) locally invertible on the support of φ. If not globally invertible, we may cover its domain with open subsets U_i on which W_m is invertible. Since Φ is compactly supported, only a finite number of these subsets are required. On each of these U_i's we define

$$G_{m,i}(\Theta^1, \Theta^2, \omega^1, \omega^2) := \begin{cases} \frac{F_m(\Theta^1, \Theta^2, E, L))}{|\det DW_m(E,L)|}, & (\omega^1, \omega^2) \in W_m(U_i), \\ 0, & \text{otherwise.} \end{cases}$$

Assuming first that Φ_m is supported in one of these sets U_i, we have

$$N[\varphi_t] = \int_0^\infty dm \int_0^{2\pi} d\Theta^1 \int_0^{2\pi} d\Theta^2 \times \int_{\mathbb{R}^2} d\omega^1 d\omega^2 g_{m,i}(t, \Theta^1, \Theta^2, \omega^1, \omega^2) \times \Phi_m(\Theta^1, \Theta^2, E, L), \tag{23}$$

where

$$g_{m,i}(t, \Theta^1, \Theta^2, \omega^1, \omega^2) := G_{m,i}(\Theta^1 + \omega^1 t, \Theta^2 + \omega^2 t, \omega^1, \omega^2). \tag{24}$$

After these initial steps, we encounter ourselves exactly in the same situation as a collisionless gas in a periodic box, and the mixing property is easily revealed by means of Fourier transformation (see section III in [7]): for this, define

$$\hat{G}_{m,i}(k_1, k_2, \eta_1, \eta_2) := \frac{1}{(2\pi)^2} \int_{-\infty}^{\infty} \int_{-\infty}^{\infty} \int_0^{2\pi} \int_0^{2\pi} G_{m,i}(\Theta^1, \Theta^2, \omega^1, \omega^2) \times e^{-i(k_1\Theta^1 + k_2\Theta^2)} e^{-i(\eta_1\omega^1 + \eta_2\omega^2)} d\Theta^1 d\Theta^2 d\omega^1 d\omega^2,$$

where $(k_1, k_2) \in \mathbb{Z}^2$ and $(\eta_1, \eta_2) \in \mathbb{R}^2$. Then,

$$\hat{g}_{m,i}(t, k_1, k_2, \eta_1, \eta_2) = \hat{G}_{m,i}(k_1, k_2, \eta_1 - k_1 t, \eta_2 - k_2 t),$$

hence the Fourier transform converts the rotations of the angle variables $(\Theta^1, \Theta^2) \mapsto (\Theta^1 + \omega^1 t, \Theta^2 + \omega^2 t)$ into a translation $(\eta_1, \eta_2) \mapsto (\eta_1 - k_1 t, \eta_2 - k_2 t)$ of the frequencies associated with the angular frequencies. According to the Riemann-Lebesgue lemma $\hat{g}_{m,i}(t, k_1, k_2, \eta_1, \eta_2)$ converges pointwise to 0 for all fixed $(k_1, k_2, \eta_1, \eta_2)$ with $(k_1, k_2) \neq (0, 0)$. Consequently,

$$\lim_{t\to\infty} \hat{g}_{m,i}(t, k_1, k_2, \eta_1, \eta_2) = \delta_{k_1 0}\delta_{k_2 0}\hat{G}_{m,i}(0, 0, \eta_1, \eta_2) =: \hat{g}^{\infty}_{m,i}(k_1, k_2, \eta_1, \eta_2),$$

for all $(k_1, k_2, \eta_1, \eta_2) \in \mathbb{Z}^2 \times \mathbb{R}^2$ with the convergence rate determined by the smoothness of $G_{m,i}(\Theta^1, \Theta^2, \omega^1, \omega^2)$ with respect to ω^1, ω^2. Here, $\hat{g}^{\infty}_{m,i}(k_1, k_2, \eta_1, \eta_2)$ is the Fourier transform of the function

$$g^{\infty}_{m,i}(\Theta^1, \Theta^2, \omega^1, \omega^2) = \frac{1}{(2\pi)^2}\int_0^{2\pi}\int_0^{2\pi} G_{m,i}(\Theta^1, \Theta^2, \omega^1, \omega^2) \times d\Theta^1 d\Theta^2 = \overline{G_{m,i}}(\Theta^1, \Theta^2, \omega^1, \omega^2),$$

which is the average of $G_{m,i}$ over the angle variables. Since Φ_m is smooth and has compact support, it follows that $N[\varphi_t]$ converges for $t \to \infty$ to the same expression as the one in the right-hand side of Eq. (23) with $g_{m,i}(t, \Theta^1, \Theta^2, \omega^1, \omega^2)$ replaced with $g^{\infty}_{m,i}(\Theta^1, \Theta^2, \omega^1, \omega^2)$. This proves the theorem for the case in which the support of Φ_m lies within one of the subsets U_i.

For the general case, a partition of unity can be used to write Φ_m as a finite sum of functions each of which is supported in only one of the subsets U_i. □

Now that the theorem has been proven, we discuss the validity of the nondegeneracy condition (21). Based on the explicit representation in Eq. (19), we have computed the determinant of the Hessian of the area function. As in the previous section, it is convenient to describe the result in terms of the generalized Keplerian variables (P, e) instead of (E, L). Interestingly, it turns out the determinant condition is satisfied everywhere except for points lying on the blue solid curves shown in Figs. 6 for different values of the rotational parameter.

To provide analytic support for the results shown in these figures we consider the particular case of quasicircular orbits on a Schwarzschild background, for which $\alpha = 0$ and $e \ll 1$. In this case, the expansion of the first derivatives of the area function in terms of the eccentricity e yield

$$A_E := \frac{\partial A_m}{\partial E} = M\frac{2\pi P^2}{\sqrt{P-6}}\left[1 + \frac{3}{4}\frac{2P^3 - 32P^2 + 165P - 266}{(P-2)(P-6)^2} \times e^2 + \mathcal{O}(e^4)\right], \tag{25}$$

$$A_L := \frac{\partial A_m}{\partial L} = -\frac{2\pi\sqrt{P}}{\sqrt{P-6}}\left[1 + \frac{3}{4}\frac{1}{(P-6)^2}e^2 + \mathcal{O}(e^4)\right], \tag{26}$$

giving

$$\det\begin{pmatrix} \frac{\partial A_E}{\partial P} & \frac{\partial A_E}{\partial e} \\ \frac{\partial A_L}{\partial P} & \frac{\partial A_L}{\partial e} \end{pmatrix} = MD(P)e + \mathcal{O}(e^3),$$

$$D(P) := -9\pi^2\frac{P^{3/2}(4P^2 - 39P + 86)}{(P-2)(P-6)^3}, \quad P > 6.$$

The function D is positive when P is slightly larger than 6 and negative for large P, and it has a single root at $P = P_* := (39 + \sqrt{145})/8 \simeq 6.38$, which corresponds to the limit point of the blue solid curve as $e \to 0$ in the middle panel of Fig. 6. From Eqs. (25) and (26) one can also conclude that (A_E, A_L) is a function of (P, e^2) which is locally invertible for small e^2 and P away from P_*.

We end this section by observing that the distribution functions considered in the previous section in cases A, E and F have their main support away from the blue solid curve in (P, e)-space where the determinant condition is violated, while in the remaining cases B, C and D the main support of the distribution function intersects this curve (compare the values given in Table I with the middle panel of Fig. 6). Although the determinant condition is violated in the latter cases, the plots in Figs. 3 and 4 suggest that the particle density still converges for $t \to \infty$, indicating that mixing is still sufficiently strong for the relaxation process to take place.

V. CONCLUSIONS

In this work, we have shown that a relativistic, collisionless kinetic gas propagating in the equatorial plane of a Kerr black hole spacetime settles down to a stationary, axisymmetric configuration. As we have demonstrated, this relaxation process is due to phase space mixing, an effect that plays a prominent role in a wide range of fields in physics including galactic dynamics and plasma physics. Here, we have exhibited the relevance of the mixing phenomenon for the dynamical behavior of spacetime observables within the fully general relativistic setting of a kinetic gas which is trapped in the strong gravitational field of a black hole.

The main implication of this work is that the one-particle distribution function f describing the state of the gas,

which in general is a function of the five coordinates $(Q^1, Q^2, J_0, J_1, J_2)$ parametrizing the relativistic phase space Γ_{bound} corresponding to bound trajectories, can be replaced by a much simpler distribution function $\bar{f}$ which is a function depending only of the constants of motion (J_0, J_1, J_2) and which can be computed by averaging the initial distribution function over the angle variables (Q^1, Q^2). Indeed, our main theorem in the previous section shows that, provided the determinant condition (21) is satisfied on the support of φ, the integral over f times any test function φ converges in time to the integral over $\bar{f}$ times the same test function φ. At the physical level, these integrals have the interpretation of macroscopic observables, where different choices for the test function correspond to different physical quantities being measured.

The determinant condition (21) means that the map $(E, L) \mapsto (\omega^1, \omega^2)$ which defines the angular frequencies in terms of the constants of motion E and L is locally invertible, a condition that is well known in perturbation theory of integrable Hamiltonian systems, see for example Sec. X. 51 in [18]. For geodesic motion in the equatorial plane of a Kerr black hole we have shown that the determinant condition holds everywhere with the exception of points in the (E, L)-plane lying on a curve (a zero-measure set) which connects a particular circular orbit to innermost stable orbits at large eccentricities. As the plots in Sec. III indicate, mixing still occurs in the vicinity of these exceptional points, suggesting that our theorem also holds under weaker assumptions. It should be interesting to relate the behavior of the gas in the vicinity of the exceptional points to Tremaine's analysis of stable singularities or catastrophes in galaxies [4] and the implications on the time scale in which the mixing occurs. In any case, for the specific examples we have analyzed in Sec. III, the damping of the oscillations in the particle density is rather fast, with relative amplitude lying below 0.001 after a few thousand light-crossing times corresponding to the gravitational radius of the black hole.

A further interesting problem consists in analyzing the effects of the self-gravity of the gas configuration (which have been neglected in the present work) on the mixing property. The inclusion of the self-gravity implies that the Kerr metric acquires correction terms due to the non-vanishing stress-energy tensor associated with the gas, which in turn leads to a perturbed Hamiltonian flow describing the geodesic motion for the gas particles. Based on general arguments from Kolmogorov-Arnold-Moser (KAM) theory, it has been argued [22,24] that such perturbations could trigger dynamical chaos in the vicinity of resonant orbits. Therefore, it should be particularly interesting to study the mixing phenomenon in the neighborhood of such orbits, and investigate whether or not the relaxation of the observables persists in the self-gravitating case.

The generalization of the mixing property to thick disk configurations, where individual gas particles are not necessarily confined to the equatorial plane, will be given in future work [13].

ACKNOWLEDGMENTS

We wish to thank Francisco Astorga, Michael Kiessling, Alexander Komech, Ulises Nucamendi, and Thomas Zannias for fruitful and stimulating discussions. We also thank Michael Kiessling, and Thomas Zannias for comments on a previous version of this manuscript. This research was supported in part by CONACyT Grants No. 577742, by the CONACyT Network Project No. 294625 "Agujeros Negros y Ondas Gravitatorias", and by a CIC Grant to Universidad Michoacana. We also thank the Erwin Schrödinger Institute for Theoretical Physics, where this work was initiated, for hospitality. P. R. also thanks Chalmers University of Technology and the University of Vienna for hospitality, where part of this work was completed.

APPENDIX: EXPLICIT EXPRESSIONS FOR THE FUNCTIONS $\mathbb{H}_j$

Using the definition of the function $R(r)$ in Eq. (3), the following relations between (ε, λ) and its roots (ξ_j) are obtained:

$$1-\varepsilon^2=\frac{2}{\xi_{012}},\qquad \hat{\lambda}^2=\frac{\xi_0\xi_1\xi_2}{\xi_{012}},$$
$$\hat{\lambda}^2+2\alpha\hat{\lambda}\varepsilon+\alpha^2=2\frac{\xi_0\xi_1+\xi_0\xi_2+\xi_1\xi_2}{\xi_{012}}, \tag{A1}$$

where we have abbreviated $\xi_{012} \coloneqq \xi_0+\xi_1+\xi_2$ and introduced $\hat{\lambda} \coloneqq \lambda - \alpha\varepsilon$. The functions $\mathbb{H}_j(\chi)$ and corresponding constants $\mathbb{H}_j \coloneqq \mathbb{H}_j(\pi/2)$ in terms of which the angle variables Q^α are expressed are defined as follows:

$$\mathbb{H}_0(\chi) \coloneqq -\frac{C}{2}\Big\{(\xi_0\xi_{012}-\xi_1\xi_2)\mathbb{F}(\chi,k)+\xi_1(\xi_2-\xi_0)\mathbb{E}(\chi,k) + (\xi_1-\xi_0)\xi_{012}\Pi(\chi,b^2,k)-\frac{1}{2}\xi_1(\xi_2-\xi_1) \times\frac{\sqrt{1-k^2\sin^2\chi}}{1-b^2\sin^2\chi}\sin(2\chi)\Big\}, \tag{A2}$$

$$\mathbb{H}_1(\chi) \coloneqq -C\Big\{\left(\hat{\lambda}+\alpha\frac{\varepsilon\xi_0^2-\alpha\hat{\lambda}}{(\xi_0-\xi_+)(\xi_0-\xi_-)}\right)\mathbb{F}(\chi,k) - \alpha\frac{\xi_1-\xi_0}{\xi_+-\xi_-}\left[\frac{\varepsilon\xi_+^2-\alpha\hat{\lambda}}{(\xi_0-\xi_+)(\xi_1-\xi_+)}\Pi(\chi,b_+^2,k) - (+\leftrightarrow-)\right]\Big\}, \tag{A3}$$

$$\mathbb{H}_2(\chi) := 2C\left\{\frac{\xi_0(\varepsilon\xi_0^2-\alpha\hat{\lambda})}{(\xi_0-\xi_+)(\xi_0-\xi_-)}\mathbb{F}(\chi,k)+\varepsilon(\xi_1-\xi_0)\Pi(\chi,b^2,k)-\frac{\xi_1-\xi_0}{\xi_+-\xi_-}\left[\frac{\xi_+(\varepsilon\xi_+^2-\alpha\hat{\lambda})}{(\xi_0-\xi_+)(\xi_1-\xi_+)}\Pi(\chi,b_+^2,k)-(+\leftrightarrow-)\right]\right\}, \tag{A4}$$

and

$$\mathbb{H}_3(\chi) := \mathbb{H}_2(\chi)+\frac{\lambda}{\varepsilon}\mathbb{H}_1(\chi) = \frac{2C}{\sqrt{\xi_{012}(\xi_{012}-2)}}\left\{\xi_0^2\mathbb{F}(\chi,k)+(\xi_1-\xi_0)(\xi_{012}-2)\Pi(\chi,b^2,k)\right.$$
$$\left.-\frac{\xi_1-\xi_0}{\xi_+-\xi_-}[\xi_+(\xi_2-\xi_+)\Pi(\chi,b_+^2,k)-(+\leftrightarrow-)]\right\}, \tag{A5}$$

with $b := \sqrt{(\xi_2-\xi_1)/(\xi_2-\xi_0)}$, $k := \sqrt{\xi_0/\xi_1}b$, $\xi_\pm := 1\pm\sqrt{1-\alpha^2}$, $b_\pm := \sqrt{\frac{\xi_0-\xi_\pm}{\xi_1-\xi_\pm}}b$ and $C := \sqrt{\frac{2\xi_{012}}{\xi_1(\xi_2-\xi_0)}}$, and where the functions $\mathbb{F}(\chi,k)$, $\mathbb{E}(\chi,k)$ and $\Pi(\chi,b^2,k)$ denote standard elliptic integrals as defined, for instance, in Ref. [25].

In terms of these functions one finds

$$\mathcal{S} = Mm\left[-\varepsilon\frac{t}{M}+\lambda\varphi+(1-\varepsilon^2)\mathbb{H}_0(\chi)+\varepsilon\mathbb{H}_3(\chi)\right], \tag{A6}$$

and

$$\frac{\partial\mathcal{S}}{\partial m} = M\mathbb{H}_0(\chi), \qquad \frac{\partial\mathcal{S}}{\partial L} = \varphi+\mathbb{H}_1(\chi), \qquad \frac{\partial\mathcal{S}}{\partial E} = -t+M\mathbb{H}_2(\chi)-E\mathbb{H}_0(\chi), \tag{A7}$$

from which the expressions (8) are easily derived.

[1] D. Lynden-Bell, The stability and vibrations of a gas of stars, Mon. Not. R. Astron. Soc. **124**, 279 (1962).
[2] D. Lynden-Bell, Statistical mechanics of violent relaxation in stellar systems, Mon. Not. R. Astron. Soc. **136**, 101 (1967).
[3] S. Tremaine, M. Hénon, and D. Lynden-Bell, H-functions and mixing in violent relaxation, Mon. Not. R. Astron. Soc. **219**, 285 (1986).
[4] S. Tremaine, The geometry of phase mixing, Mon. Not. R. Astron. Soc. **307**, 877 (1999).
[5] J. Binney and S. Tremaine, *Galactic Dynamics*, 2nd ed. (Princeton University Press, Princeton, New Jersey, 2008).
[6] G. N. Candlish, R. Smith, M. Fellhauer, B. K. Gibson, P. Kroupa, and P. Assmann, Phase mixing due to the galactic potential: Steps in the position and velocity distributions of popped star clusters, Mon. Not. R. Astron. Soc. **437**, 3702 (2014).
[7] C. Mouhot and C. Villani, On Landau damping, Acta Math. **207**, 29 (2011).
[8] B. Young, On linear Landau damping for relativistic plasmas via Gevrey regularity, J. Differ. Equations **259**, 3233 (2015).
[9] B. Young, Landau damping in relativistic plasmas, J. Math. Phys. (N.Y.) **57**, 021502 (2016).
[10] R. Mathew and E. Tiesinga, Phase-space mixing in dynamically unstable, integrable few-mode quantum systems, Phys. Rev. A **96**, 013604 (2017).
[11] T. V. Dudnikova, A. I. Komech, E. A. Kopylova, and Y. M. Suhov, On convergence to equilibrium distribution, I. The Klein–Gordon equation with mixing, Commun. Math. Phys. **225**, 1 (2002).
[12] T. V. Dudnikova, A. I. Komech, N. E. Ratanov, and Y. M. Suhov, On convergence to equilibrium distribution, II. The wave equation in odd dimensions, with mixing, J. Stat. Phys. **108**, 1219 (2002).
[13] P. Rioseco and O. Sarbach, Dynamics of collisionless thick discs around a Kerr black hole (to be published).
[14] W. Schmidt, Celestial mechanics in Kerr space-time, Classical Quantum Gravity **19**, 2743 (2002).
[15] T. Hinderer and E. E. Flanagan, Two timescale analysis of extreme mass ratio inspirals in Kerr. I. Orbital motion, Phys. Rev. D **78**, 064028 (2008).
[16] R. Fujita and W. Hikida, Analytical solutions of bound timelike geodesic orbits in Kerr spacetime, Classical Quantum Gravity **26**, 135002 (2009).
[17] J. Bardeen, W. Press, and S. Teukolsky, Rotating black holes: Locally nonrotating frames, energy extraction, and scalar synchrotron radiation, Astrophys. J. **178**, 347 (1972).

[18] V. I. Arnold, *Mathematical Methods of Classical Mechanics* (Springer-Verlag, New York, 1989).
[19] O. Sarbach and T. Zannias, The geometry of the tangent bundle and the relativistic kinetic theory of gases, Classical Quantum Gravity **31**, 085013 (2014).
[20] P. Rioseco and O. Sarbach, Accretion of a relativistic, collisionless kinetic gas into a Schwarzschild black hole, Classical Quantum Gravity **34**, 095007 (2017).
[21] J. Ehlers, General relativity and kinetic theory, in *General Relativity and Cosmology*, edited by R. K. Sachs (Academic, New York, 1971), pp. 1–70.
[22] J. Brink, M. Geyer, and T. Hinderer, Astrophysics of resonant orbits in the Kerr metric, Phys. Rev. D **91**, 083001 (2015).
[23] P. Rioseco and O. Sarbach, Phase space mixing in external gravitational potentials (to be published).
[24] J. Brink, M. Geyer, and T. Hinderer, Orbital Resonances Around Black Holes, Phys. Rev. Lett. **114**, 081102 (2015).
[25] Digital library of mathematical functions, http://dlmf.nist.gov/.

Part IV

Conclusions

In this thesis, we considered a collisionless relativistic kinetic gas propagating on a curved spacetime geometry, for two physical scenarios (i) for a description of particles falling into a Schwarzschild black hole and (ii) in the case where the particles form a thin disk in the equatorial plane of a Kerr black hole.

To describe the relativistic kinetic gas, we started our discussion in Chapter 3 with a review of the mathematical description of the theory based on the cotangent bundle, which plays the role of the relativistic phase space, and as we discuss, it admits two natural important structures: a symplectic structure and the metric (called the Sasaki metric). The symplectic structure allows one to formulate a Hamiltonian framework on phase space, and to introduce the Liouville vector field which describes the transport part of the relativistic Boltzmann equation. The Sasaki metric yields a natural volume form on phase space, which is important for the physical interpretation of the distribution function. In particular, we defined the observables of the theory as integrals over the distribution function multiplied by a suitable test function. Particularly relevant examples are the conserved quantities, namely the current density and the energy-momentum tensor. Secondly, a perturbative description of the Einstein-Liouville system is presented in Chapter 3.1, which allows us to fix the background geometry and solve the Liouville equation independently of the Einstein equations. In this work, we have also assumed that the gas is sufficiently diluted such that collisions can be neglected. We derived the equation that we want to solve and from which we can obtain information of the observables.

Next, we find the most general solution for a distribution that describes the relativistic kinetic gas particles over fixed spacetime that represents a black hole. To achieve this, we used standard tools from the theory of integrable Hamiltonian systems, as summarized in the Chapter 5, and described the Liouville vector field in terms of new symplectic coordinates which trivializes it. Moreover, in both cases the explicit expressions for the relevant observables were given, in case (i) in terms of explicit integrals, and in case (ii) in terms of elliptic functions over spacetime.

The main results in this thesis for the two cases studied can be summarized as follows. In case (i) we assumed that the gas flow is spherically symmetric and steady-state, and showed that this implies that the one-particle distribution function depends only on the conserved quantities (m, E, ℓ) (mass, energy and total angular momentum) associated to the particle. Here, the total angular momentum ℓ allows one to distinguish between the particles that fall into the black hole from those that are reflected by the potential barrier. We show that at the horizon, the infalling particles contribute to the accretion rate, but not to the particle density at infinity while the reflected particles do not contribute to the total accretion rate but do contribute to n_∞. We give an explicit example in which the distribution function describes a gas in thermodynamic equilibrium i.e the gas configuration has a temperature T associated to it at infinity. We computed the observables as a function of $z = mc^2/k_B T$ (which is proportional

to inverse temperature). In the low temperature limit, we verified that our results coincide with the previous results in [16], whose values were obtained through a Newtonian approximation. Besides, we calculated the principal pressures p_{rad} and p_{tan} and the energy density at the horizon for low temperatures, finding that p_{rad} is around 10 times smaller than the tangential pressure p_{tan}. This gives a partial explanation about the fact that the accretion is much less intense than in the Bondi-Michel case of a perfect polytropic fluid $p_{rad} = p_{tan}$. In this work, we have also obtained an asymptotic stability result, where we relaxed the symmetry assumptions on the distribution function, and specified the initial distribution function $\mathcal{F}_i$ consists only of unbound trajectories, and we assumed that in the asymptotic region $\mathcal{F}_i$ the distribution converges to a function $f_\infty(E)$ depending only on the energy. Under these assumptions, we proved that outside the horizon, the observables converge pointwise along the world lines of static observers to the corresponding observables associated with the stationary, spherical flow described by $f_\infty(E)$. We found similar results along the world lines of timelike, non static observers with asymptotic constant radial velocity. These results show that the gas configuration relaxes in time to a static, spherically symmetric one, no matter the details of the initial data.

We extended these results in Sec. 6.1 where we analyze the behavior of the gas as a function of its temperature at infinity and the radial coordinate. With this, and fixing the value of the black hole mass M and the particle density number in the asymptotic region, we computed the energy accretion rate that diverges when the temperature goes to zero ($z \to \infty$) and when the temperare goes to infinity ($z \to 0$) having a minimum when $z = mc^2/k_BT \simeq 1$. The explanation of this fact is the competition between a smaller fraction of particles being accreted by the black hole versus the increase of the internal energy of each of them when the temperature increases. Additionally, we analyzed the principal differences between a collisionless flow to those of an isotropic perfect fluid (Bondi-Michel model). This difference can be observed in the value for the accretion rate (also named too Bondi formula) in the low temperature limit. In the relativistic kinetic gas the mass accretion rate is proportional to $\sqrt{z}$, in contrast with the polytropic perfect fluid where it is proportional to $z^{3/2}$. On the other hand, in the collisionless case the radial and tangential pressures differ from each other at finite radius implying that the gas is anisotropic, although their principal pressures are identical in the asymptotic region. Finally, we give an explanation for the fact that a collisionless relativistic kinetic gas does not behave as an isotropic perfect fluid for finites radius. It turns out this occurs because we discriminate between the particle trajectories that end in the black hole and those that emanate from a white hole (in the collisionless case, the latter should not be occupied). The idea for future work is to extend this analysis to the case where we include the effects of collisions, which may change the occupancy of the trajectories in time. It should be interesting to compare such results.

Regarding the analysis of case (ii), we presented a detailed description of the

mixing idea in the one dimensional case and a step by step proof of the mixing theorem that is shown in Sec. 6.2. The main result that we found in (ii) is that a relativistic, collisionless kinetic gas propagating in the equatorial plane of a Kerr black hole settles down to a stationary, axisymmetric configuration. This relaxation process is due to phase space mixing which plays an important role in several areas of physics. In particular, we showed the relevance of the mixing in the dynamical behavior of observables in the context of a fully relativistic system, where the particles feel the strong gravitational potential. The main implication of this work is that a general solution of the Liouville equation that describes the state of the gas particles which in general is a complicated function of the coordinates that parametrizes the bound trajectories on the phase space, can be replaced with a much simpler distribution $\bar{f}$ which only depends on the constants of motion (E, m, ℓ) and that can be calculated averaging the initial distribution over the angle variables. We should mention that our proof so far requires the satisfaction of some determinant condition (in the one-dimensional case this condition is the invertibility condition on the frequency function, in the Kerr case this means that the frequency map $(E, \ell) \mapsto (\omega^1, \omega^2)$, which defines the angular frequencies in terms of the constants of motion E and ℓ is locally invertible). For geodesic motion in equatorial plane of Kerr black hole we have shown that the determinant condition holds everywhere with the exception of a zero measure set that connects certain circular orbits with the innermost stable orbits in the $E-\ell$ plane. However, it turns out that distributions with compact support in the vicinity of these points, also present mixing as shown in Sec. III of Paper II through explicit numerical examples, suggesting that the mixing also holds under weaker assumptions.

Some natural extensions of this work include the analysis of collisions to better understand the transition between a relativistic kinetic gas to hydrodynamics, as well as the implications this might have on the behavior of observables such as the accretion rate and principal pressures. Besides, we are interested in extending the analysis of the mixing phenomenon to cases where the effects of self-gravity are considered. In particular, it should be interesting to check whether or not the relaxation of observables is maintained, or if instabilities could be triggered by resonances due to the self gravity [49, 50]. Further, we are planning on analyzing if the mixing occurs in case where the particles are not necessarily confined to the equatorial plane but rather form a thick disk around a Kerr black hole geometry.

Bibliography

[1] K. Huang. *Statistical Mechanics*. John Wiley & Sons, New York, USA, 1987.

[2] Ch. van Weert S. Groot, W. van Leeuwen. *Relativistic kinetic theory: principles and applications*. North-Holland, 1980.

[3] C. Cercignani. *Ludwig Boltzmann, The Man Who Trusted Atoms*. Oxford University Press, Oxford, 2010.

[4] J. Binney and S. Tremaine. *Galactic Dynamics (Second Edition)*. Princeton University Press, Princeton, New Jersey, 2008.

[5] E. Ames, H. Andréasson, and A. Logg. On axisymmetric and stationary solutions of the self-gravitating Vlasov system. *Class. Quantum Grav.*, 32:155008, 2016.

[6] W. Israel. Relativistic kinetic theory of a simple gas. *J. Math. Phys.*, 4:1163–1181, 1963.

[7] J. Ehlers, P. Geren, and R.K. Sachs. Isotropic solutions of the Einstein-Liouville equations. *J. Math. Phys.*, 9:1344–1349, 1968.

[8] A. Akbarian and M.W. Choptuik. Critical collapse in the spherically-symmetric Einstein-Vlasov model. *Phys. Rev.*, D90(10):104023, 2014.

[9] H. Andréasson. The Einstein-Vlasov system/kinetic theory. *Living Reviews in Relativity*, 14(4), 2011.

[10] G. Rein. Static solutions of the spherically symmetric Vlasov-Einstein system. *Math. Proc. Cambridge Phil. Soc.*, 115:559–570, 1994.

[11] G. Rein and A.D. Rendall. Global existence of solutions of the spherically symmetric Vlasov–Einstein system with small initial data. *Comm. Math. Phys.*, 150:561–583, 1992.

[12] H. Andréasson, M. Kunze, and G. Rein. Existence of axially symmetric static solutions of the Einstein-Vlasov system. *Commun. Math. Phys.*, 308:23–47, 2011.

[13] H. Andréasson, M. Kunze, and G. Rein. Rotating, stationary, axially symmetric spacetimes with collisionless matter. *Commun. Math. Phys.*, 329:787–808, 2014.

[14] H. Andréasson, M. Eklund, and G. Rein. A numerical investigation of the steady states of the spherically symmetric Einstein-Vlasov-Maxwell system. *Class. Quantum Grav.*, 26:145003, 2009.

[15] Event horizon telescope. `http://www.eventhorizontelescope.org`.

[16] S.L. Shapiro and S.A. Teukolsky. *Black Holes, White Dwarfs, and Neutron Stars*. John Wiley & Sons, New York, 1983.

[17] M.A. Abramowicz and P.C. Fragile. Foundations of black hole accretion disk theory. *Living Rev. Rel.*, 16:1, 2013.

[18] J.N. Bahcall and R.A. Wolf. Star distribution around a massive black hole in a globular cluster. *Astrophys. J.*, 209:214–232, 1976.

[19] S. Colombi, T. Sousbie, S. Peirani, G. Plum, and Y. Suto. Vlasov versus n-body: the hénon sphere. *Monthly Notices of the Royal Astronomical Society*, 450(4):3724–3741, 2015.

[20] P. Domínguez, E. Jiménez, M. Alcubierre, E. Montoya, and D. Núñez. Description of the evolution of inhomogeneities on a dark matter halo with the vlasov equation. *Gen.Rel.Grav.*, 49:123, 2017.

[21] Piotr T. Chruściel, João Lopes Costa, and Markus Heusler. Stationary black holes: Uniqueness and beyond. *Liv. Rev. Relativ.*, 15(7), 2012.

[22] P. Rioseco and O. Sarbach. Phase space mixing in the equatorial plane of a Kerr black hole. *arXiv:1807.10794*, 2018.

[23] D. Lynden-Bell. Statistical mechanics of violent relaxation in stellar systems. *Monthly Notices Roy Astronom. Soc.*, 136:101–121, 1967.

[24] D. Lynden-Bell. The stability and vibrations of a gas of stars. *Monthly Notices Roy Astronom. Soc.*, 124:279–296, 1962.

[25] G. N. Candlish, R. Smith, Fellhauer, B. K. Gibson, P. Kroupa, and P. Assmann. Phase mixing due to the galactic potential: steps in the position and velocity distributions of popped star clusters. *Monthly Notices Roy Astronom. Soc.*, 437:3702–3717, 2014.

[26] S. Tremaine, M. Hénon, and D. Lynden-Bell. H-functions and mixing in violent relaxation. *Monthly Notices Roy Astronom. Soc.*, 219:285–297, 1986.

[27] S. Tremaine. The geometry of phase mixing. *Monthly Notices Roy Astronom. Soc.*, 307:877–883, 1999.

[28] C. Mouhot and C. Villani. On Landau damping. *Acta Math.*, 207:29–201, 2011.

[29] B. Young. On linear Landau damping for relativistic plasmas via Gevrey regularity. *J. Diff. Eqns.*, 259:3233 – 3273, 2015.

[30] B. Young. Landau damping in relativistic plasmas. *J. Math. Phys.*, 57:021502, 2016.

[31] R. Mathew and E. Tiesinga. Phase-space mixing in dynamically unstable, integrable few-mode quantum systems. *Phys. Rev. A*, 96:013604, 2017.

[32] O. Sarbach and T. Zannias. Relativistic kinetic theory: An introduction. *AIP Conf. Proc.*, 1548:134–155, 2013.

[33] O. Sarbach and T. Zannias. The geometry of the tangent bundle and the relativistic kinetic theory of gases. *Class. Quantum Grav.*, 31:085013, 2014.

[34] S. Sasaki. On the differential geometry of tangent bundles of Riemannian manifolds. *Tohoku Math. J.*, 10:338–354, 1958.

[35] R.W. Lindquist. Relativistic transport theory. *Ann. Phys. (N.Y.)*, 37:487–518, 1966.

[36] S. Sasaki. On the differential geometry of tangent bundles of Riemannian manifolds, II. *Tohoku Math. J.*, 14:135–232, 1962.

[37] V.I. Arnold. *Mathematical Methods of Classical Mechanics*. Springer-Verlag, New York, 1989.

[38] H. Goldstein, C. Poole, and J. Safko. *Classical Mechanics*. Addison-Wesley, San Francisco, CA, 2002.

[39] M. Dunajski. Notes about integrable systems. `http://www.damtp.cam.ac.uk/user/md327/`.

[40] T. Hinderer and E.E. Flanagan. Two timescale analysis of extreme mass ratio inspirals in Kerr. I. Orbital Motion. *Phys. Rev. D*, 78:064028, 2008.

[41] P. Rioseco and O. Sarbach. Spherical steady-state accretion of a relativistic collisionless gas into a Schwarzschild black hole. *J. Phys. Conf. Ser.*, 831(1):012009, 2017.

[42] Digital library of mathematical functions. `http://dlmf.nist.gov/`.

[43] P. Rioseco and O. Sarbach. Accretion of a relativistic, collisionless kinetic gas into a Schwarzschild black hole. *Class. Quantum Grav.*, 34(9):095007, 2017.

[44] J.M. Stewart. *Non-Equilibrium Relativistic Kinetic Theory*. Springer-Verlag, Berlin, 1971.

[45] C. Cercignani and G.M. Kremer. *The Relativistic Boltzmann Equation: Theory and Applications*. Birkhäuser, Basel, 2002.

[46] S. Bochner and K. Chandrasekharan. *Fourier Transforms*. Princeton University Press, 1950.

[47] H. L. Royden. *Real Analysis*. Macmillan Publishing Company, New York, 1989.

[48] P. Rioseco and O. Sarbach. Phase space mixing in external gravitational potentials. *in preparation*, 2018.

[49] J. Brink, M. Geyer, and T. Hinderer. Orbital resonances around black holes. *Phys. Rev. Lett.*, 114:081102, 2015.

[50] J. Brink, M. Geyer, and T. Hinderer. Astrophysics of resonant orbits in the Kerr metric. *Phys. Rev. D*, 91(8):083001, 2015.